ANTIFOULING SURFACE MODIFICATIONS FOR MULTIPLE MATERIALS

BY COLLEEN CHAU, BASC.

A Thesis Submitted to The School of Graduate Studies
in Partial Fulfillment of the Requirements for
the Degree Master of Applied Science

McMaster University

MASTER OF APPLIED SCIENCES (2021)	McMaster University
School of Biomedical Engineering	Hamilton, Ontario
TITLE:	Antifouling Surface Modifications for Multiple Materials
AUTHOR:	Colleen Chau BASc. (University of British Columbia)
SUPERVISORS:	Dr. Qiyin Fang Dr. John L. Brash
NUMBER OF PAGES:	vii, 88

Abstract

Biomaterials used in biomedical implants, diagnostic devices, and in-situ sensors, all face the issue of biofouling. Surface modification of biomaterial surfaces with antifouling polymers can prevent non-specific adsorption of proteins and other bio-foulants onto these surfaces. Although there are many antifouling polymers to chose from, getting the polymers onto different materials is challenging as the surface modification process is dependent on the substrate's surface chemistry. This limits the kinds of materials that are able to be modified, especially in devices made with several materials that must be modified as a single unit. Therefore, the goal of this research is to develop an effective antifouling surface modification that is compatible with different types and classes of biomaterials. A three-step modification approach was taken to form dense antifouling polymer brushes. The surfaces were first activated using oxygen plasma to increase the density of surface hydroxyl groups. Next, a silane coupling agent with an Atom Transfer Radical Polymerization (ATRP) initiator was attached to the activated surfaces. Finally, an antifouling zwitterionic monomer was polymerized on the surface using an aqueous controlled living radical polymerization technique, Surface Initiated - Activators Regenerated by Electron Transfer – Atom Transfer Radical Polymerization (SI-ARGET-ATRP). Two zwitterionic antifouling polymers, poly(carboxybetaine methacrylate) (pCBMA), and poly(sulfobetaine methacrylate) (pSBMA) were investigated.

Clinically- and environmentally-relevant materials were studied and include poly(dimethylsiloxane) (PDMS), poly(ether ether ketone) (PEEK), titanium, silicon, and 3D printed stainless steel. Water contact angle (WCA) analysis showed that surfaces modified with zwitterionic polymers became more hydrophilic. WCA analysis may not be suitable for evaluating non-modified 3D printed surfaces due to their poor surface finish, and this material requires further surface topography characterization. Atomic force microscopy (AFM) and ellipsometry showed that the zwitterionic polymer layers did not necessarily have to be thick to produce their hydrophilic effect. AFM also revealed that each step of the surface modification process produced different roughness effects on all of the different surfaces. The zwitterionic layer with the smoother surface tended to better resist bovine serum albumin (BSA) adsorption. Radiolabelled BSA experiments showed reduced fouling on all 2D samples but to different degrees. The pCBMA modification was not successful in preventing BSA fouling on 3D printed 316L stainless steel. Full or partial BSA fouling may be due to the hydrolytic instability of the silane coupling agent, used to form covalent bonds between the antifouling polymers and the different surfaces, although further investigation is required to validate this hypothesis. Improving the long-term stability of silanes or research with other multi-surface compatible coupling agents that have better long-term stability in aqueous solutions should be pursued.

Acknowledgements

There are many people who I owe gratitude and thanks to during my graduate studies at McMaster University. First, I'd like to thank my supervisors, Dr. Fang and Dr. Brash, for their support and guidance. Dr. Fang, thank you for providing me and all of your students with different opportunities for collaboration and professional development. I appreciate your professional and life advice and mentorship. Dr. Brash, your energy and expertise in the biomedical field is truly inspiring. I am honoured to have worked with you and thank you for being so patient with me throughout this degree. I hope you will now be able to fully enjoy your retirement. Second, I'd like to thank Dr. Chen and her lab group at Suzhou University for making me feel welcomed and helping me with my work. I'd also like to thank Dr. Sask who is on my thesis committee for her time and comments.

To my friends and lab mates, I would have not made it without your help in the lab and the emotional support. A big thank you to Lena for training and providing me with all the resources for radiolabelling. I'd like to thank Dr. Darko Ljubic and Dr. Zhu for their lab space and their expertise in polymer chemistry. Amanda and Devon, thank you for being my friends, co-workers, and the best housemates a grad student could have. Thank you Jess, Eric, Ian, Bo, and Morgan for our life talks and always having a spare key for me. Sharon, thank you for passing on your surface modification knowledge to me and helping me with proof-reading and editing.

To Dr. Geng, thank you for the opportunity to work with you on your "Flipped-Lab" initiative.

Last, but not least, I would like to thank my family and my dearest Kelvin. Although my family is over 4,000 km away, I would like to thank them for still cheering me on even though they would rather I stay closer to home. Kelvin Pun, you have been there for me for almost all of my time here in Ontario. Thank you for driving to Hamilton from Kingston and back every weekend for the first year I was in Hamilton, learning to cook so that you can feed me when I was working on my thesis, and taking the load off my shoulders. I guess I should keep you.

Table of Contents

List of Figures

List of Tables

1.0 Introduction

Biofouling on surfaces is problematic for *in-situ* devices used for environmental monitoring, and for health care related devices. Environmental monitoring devices such as pH and dissolved oxygen probes (Hsu, 2014) provide real-time data and warnings of deviations from normal conditions so that corrections can be made. Devices used in health care include diagnostic and therapeutic devices which may be implanted or used outside the body. Monitoring and diagnostic devices are used to identify issues by detecting low concentrations of target molecules or markers in complex natural environments that include multiple species such as proteins, bacteria, and other cells. Non-target biomolecules can adsorb to the device and cause biofouling that reduces device sensitivity and performance, leading to device failure including the incidence of false positives (Lichtenberg, 2019; Jiang, 2020). Implantable medical devices such as prosthetic hip joints, vascular stents, and catheters are also prone to biofouling with severe consequences including bacterial infection and blood coagulation leading to device failure (Harding, 2014). Thus, strategies for the prevention of biofouling are widely sought after.

Proteins are a common bio-foulant that are present in many bio-fluids and have a strong tendency to adsorb to all types of surface (Choi, 2010). Removal of unwanted proteins from a device can be achieved using physical cleaning methods such as wiping or flushing with water (Lehaitre, 2008). For many in-situ devices, however, physical cleaning methods are not suitable. Surface modification that changes the surface physical and/or chemical properties of a material can provide longer lasting resistance to (ideally prevention of) protein fouling without interfering with the integrity and application of the device.

Among the different approaches to antifouling, modification of surfaces with hydrophilic polymers to prevent non-specific protein adsorption has been shown to be versatile for enhancing the accuracy and sensitivity of sensors (Liu, 2016), and directing cell adhesion and growth in cell patterned devices (Sun, 2018). There are many methods to attach the polymers to the surface. “Grafting-from” methods (i.e. surface-initiated polymerization of suitable monomers) allow thick polymer brushes to grow directly from initiator sites on the surface. However, grafting-from techniques often require contact of the surface with dangerous solvents and require strict environmental controls that hinder large scale production.

A surface-initiated polymerization technique that eliminates the need for such strict environmental conditions is Activators Regenerated by Electron Transfer – Atom Transfer Radical Polymerization (ARGET-ATRP) (Matyjaszewski, 2007; Simakova, 2012). ARGET-ATRP is an equilibrium controlled living radical polymerization that is catalyzed by very small amounts of copper so that the resultant polymers can be used for biological

applications without further purification. A reducing agent such as ascorbic acid is used to regenerate the copper catalyst complex to be continuously reused in the polymerization reaction. ARGET-ATRP can be used with a variety of monomers to create densely packed, uniform length polymer brushes on a surface.

Polyethylene glycol (PEG) has been widely used and has been considered to be the gold standard among antifouling polymers. However, questions on the oxidative stability of PEG (Damodaran, 2016) and its poor performance as an antifoulant in multi-protein environments, has limited PEG's use for long-term applications in biofluids. Polyzwitterions are a new class of polymers that have been shown to overcome these problems. Zwitterions are compounds that have both a positive and negative charge which allows stronger ionic bonds with water molecules; hence, a more tightly bound hydration layer is present that can resist protein adsorption in complex fluids containing multiple proteins and other biological materials. Typical zwitterions include phosphocholines (Ishihara, 1992; Feng, 2005), carboxybetaines (Zhu, 2014; Jesmer, 2020), and sulfobetaines (Zhang, 2006; Sin, 2013).

Devices are often constructed using multiple materials, thereby creating a challenge for surface modification of the device as a whole. Surface modification protocols are typically tailored for application to a specific material and may only be effective for that particular material. Other materials in the device may not be compatible with that method, resulting in the need for several modification steps to cover all materials in the device, and making the process costly and time consuming (Lee, 2007). In addition, some devices are constructed using highly specialized materials and manufacturing processes and need to be handled with the utmost care when applying surface treatments. There is therefore a need for methods that can be applied to many materials, and which are gentle, environmentally friendly, and scalable.

Surface modification with hydroxylated silanes is a simple and versatile method that has been used on a variety of oxide surfaces. Silanes are often used as coupling agents to form strong covalent bonds linking materials with differing chemistries (Kutz, 2011). Silanes contain a silicon atom, hydrolysable groups (e.g ethoxy groups) that bond to the substrate, and an organofunctional group that is customizable for the intended application. The hydrolytic mechanism for covalent silane surface modification of an oxide surface is shown in Figure 1-1.

In addition, silanes are widely available commercially. Although only oxide surfaces are suitable fundamentally for use with silane coupling agents, thus apparently limiting their usefulness, surface oxygen can be introduced into other substrates by oxygen plasma treatment. In this process the surface is bombarded and activated with high energy oxygen radicals (Bogaerts, 2001). Silanes can then be attached to the surface to form an ad-layer to which different modifying molecules can be linked. However, high energy

oxygen plasma has been shown to cause damage to some surfaces under certain processing conditions (Adly, 2017; Inagaki, 1998), which may destroy the integrity of the material and/or, in our case, adversely affect subsequent surface-initiated polymerization.

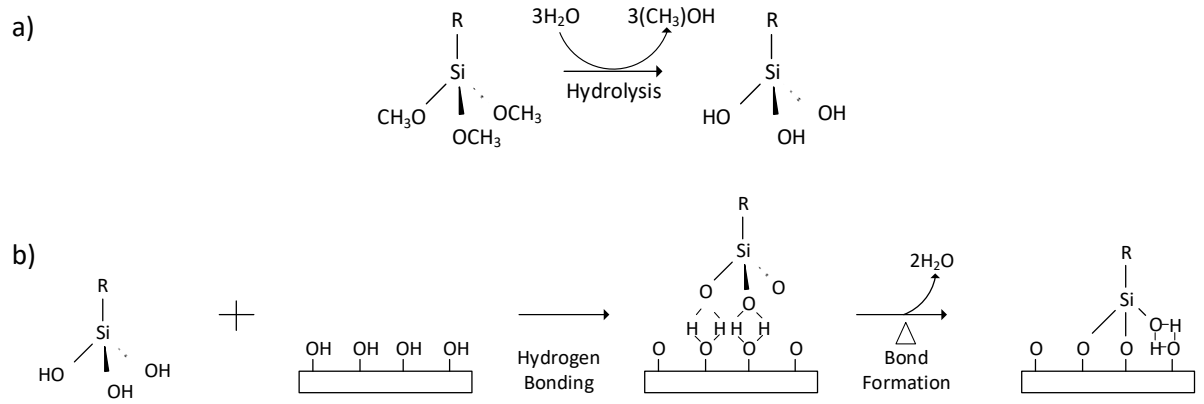

Figure 1-1: a) Hydrolysis of OCH_3 groups on trimethoxysilane in aqueous solution; b) Hydrolyzed silane bonding to oxide surface via intermediate hydrogen bond formation. Dehydration creates strong covalent bonds with the oxide surface. Adapted from (Arkles, 1977).

The overall goal of this study was to develop a surface modification method to confer antifouling properties that could be applied to multiple materials. This requires the selection of a multiple-material surface modifier and optimization of the modification process to achieve the best antifouling performance on all surfaces. The effectiveness of the modification process is assessed by determining grafting density, surface wetting properties, surface roughness, thickness of the modification layer (film), and surface chemistry.

Non-specific protein adsorption is recognized as the first step in biofouling in many situations; their relatively small size allows proteins to diffuse faster to the surface than the much bigger bacteria and other cells (Delauney, 2008; Xie, 2018; Lopez-Mila, 2018). Therefore, testing for anti-biofouling behavior often begins with evaluating protein adsorption using solutions of single proteins such as albumin (Lee, 2019; Ghaleh, 2018; Hecker, 2018; Zhang, 2015), lysozyme (Ettelt, 2018; Holmlin, 2001; Wang, 2013), or fibrinogen (Zhang, 2006; Yu, 2014). Adhesion of bacteria that can cause infections such as *E. coli* and *S. aureus,* is commonly used to evaluate anti-bacterial effectiveness (Zhang, 2015). Real life working fluids such as urine (Lopez-Mila, 2018), blood serum (Yang, 2009; Krause, 2011), and marine waters (Ventura, 2017) are used to evaluate the full spectrum of the resistance of the modified surface to biofouling. Following completion of these in-vitro tests, the final step is *in-situ* or *in-vivo* testing of the modified surface.

The work reported in this thesis comprises development of a potentially "universal" surface modification method applicable to materials typically found in biosensing and biomedical devices. Oxygen plasma was used to activate the substrates. A silane containing an ARGET-ATRP polymerization initiator residue was then attached to the activated surface and zwitterionic polymers of carboxybetaine methacrylate (CBMA) and sulfobetaine methacrylate (SBMA) were formed to give polymeric surface "brushes". Antifouling properties were assessed by resistance to protein adsorption.

Chapter 2 reviews the current state of the art of antifouling surfaces including surfaces modified with poly(ethylene glycol) and zwitterionic polymers. Also discussed are "slippery liquid-infused porous surfaces" (SLIPS). Other multi-material modification strategies such as modification with silanes, polydopamine, and polyphenols, are also explored.

Chapter 3 describes experiments conducted in this work using oxygen plasma treatment, silanes, and zwitterionic polymers to modify multiple substrates: i.e. PDMS, silicon, titanium, and poly(etheretherketone) PEEK. Data on adsorption of bovine serum albumin (BSA) to evaluate the antifouling capability of the modified surfaces are presented and discussed in detail.

Chapter 4 describes the application of these surface modification methods to additively manufactured stainless steel. Additive manufacturing (also referred to as 3D printing) is gaining in popularity for the preparation of customized implants and as a tool for prototyping.

Chapter 5 presents the overall conclusions of this project and gives suggestions for future work.

The contributions of this work include:

(1) Synthesis of a polymerizable CBMA monomer using acrylic acid and DMAEMA as reactants.
(2) A procedure for activation of the surfaces of PDMS, silicon, titanium and PEEK with oxygen plasma so that (3-trimethoxysilyl) propyl-2-bromo-2-methypropionate could be subsequently attached as a polymerization initiator.
(3) Methods for surface-initiated polymerization (SI-ARGET-ATRP) of CBMA and SBMA monomers to form polymer brushes of the corresponding antifouling polymers on the above-mentioned substrates.
(4) Comparison of the properties of the virgin and modified surfaces using water contact angle analysis for water wettability, atomic force microscopy (AFM) to evaluate surface roughness, ellipsometry to estimate polymer film thickness and polymer grafting density, and X-ray photoelectron spectroscopy to characterize surface chemistry.

(5) Evaluation of resistance to non-specific protein adsorption on the modified surfaces using radiolabeled bovine serum albumin (BSA) as a model protein.
(6) Use of the methods indicated above to modify 3D-printed stainless-steel surface with a view in demonstrating the suitability of the methods for devices manufactured with newly developed fabrication techniques.

2.0 Literature Review

2.1 Biofouling

Biofouling is the undesired adsorption of proteins, cells, and other materials in the contacting environment on wetted materials and surfaces. Surfaces that are in contact with fluids such as water, blood, or air are prone to biofouling which can cause the surfaces to deteriorate and lose their function. Three areas that face the challenges of biofouling include environmental devices (Chapman, 2012; Xie, 2019; Hsu, 2014), medical devices (Jaffer, 2019), and biomedical diagnostic devices (Jiang, 2020). The fouling of surfaces is complex and is dependent on the wetting environment which can be complex aqueous solution, fresh water, human- or animal-associated fluids. Despite the diversity of environments, the biofouling mechanism can be seen as occurring in four stages, as shown in Fig 2-1 (Xie, 2019):

- Adsorption of organic and inorganic macromolecules forming a primary film.
- Transport to and immobilization of bacteria and other microbial cells on the surface.
- Attachment of bacteria to the surface via extracellular biopolymer production.
- Development of a complex community of multicellular species and cellular debris on the surface.

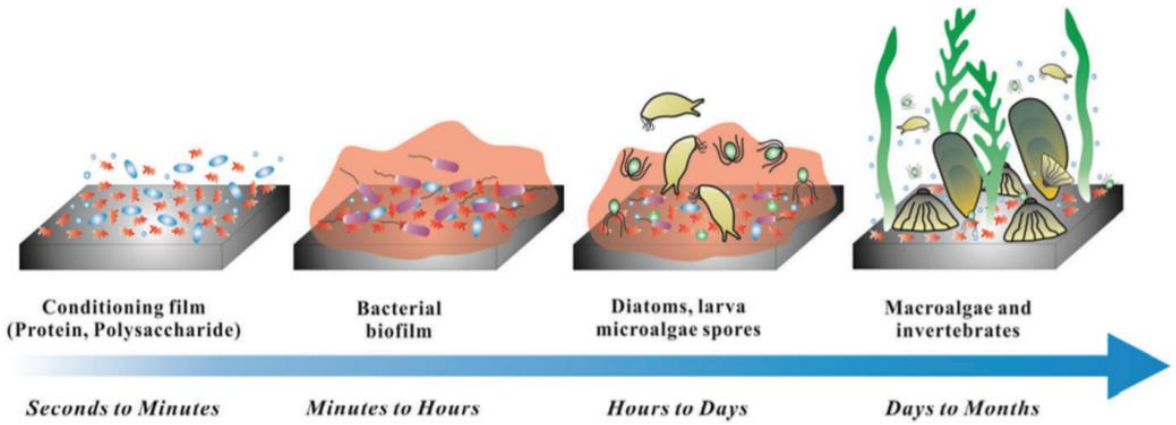

Figure 2-1: Biofouling Mechanism. From (Xie, 2019) with permission.

2.2 Protein Adsorption

Biomacromolecules such as proteins are among the first to adsorb to surfaces. Adsorbed proteins are used by cells to facilitate communication with other cells in cell adhesion and spreading (Khalili, 2015; Rowley, 2019). In biological environments, protein adsorption can trigger subsequent adhesion of particles, bacteria, and other cells that promote inflammation cascades in the body (Khalili, 2015; Rowley, 2019). On sensors, larger cells and organisms can completely cover and block the sensor causing loss of sensitivity/function and the analytical performance of the device (Jiang, 2019; Rabe,

2011). Thus, prevention of non-specific protein adsorption is necessary to avoid propagation of the biofouling process.

2.2.1 Protein Properties Controlling Adsorption

Proteins are polymers consisting of chains of the twenty naturally occurring amino acids. The behavior and functionality of a protein are determined by its folded structure as well as its amino acid composition (Branden, 2012). Specific functional or structural regions of the protein called domains can also be individually folded to expose different chemistries and allow the protein to perform different functions (Alberts, 2002). The domain chemistry that is revealed on the surface of the protein determines its polarity, hydrophobicity, and charge (Andrade, 1992).

Proteins have unique isoelectric points (pI) determined by the content of charged amino acids. The pI is defined as the pH at which the positive and negative charges are in balance. The net charge depends on the solution pH with protons being added or removed, respectively, as the pH decreases or increases. It has been shown repeatedly that protein adsorption typically reaches a maximum as pH nears the protein's pI (Meissner, 2015). This may be due to reduction in charge-charge repulsion at the pI, so that proteins are able to pack more closely together to allow higher surface coverage. Along with pH, the ionic strength and the ion composition change the solubility of the protein and thus its interactions with the surface (Meissner, 2015; Kopac, 2008).

The size of the protein can also affect its adsorption behavior. In a competitive situation, smaller proteins tend to reach the surface earlier, whereas larger proteins arrive later and may attach more firmly to the surface due to the possibility of multi-point attachment (Noh,2007). Larger proteins such as albumin, immunoglobins, vitronectin, fibrinogen, and fibronectin are capable of undergoing conformational change on contact with surfaces (Pasche, 2005).

Proteins of relatively low affinity may be adsorbed early and displaced by later-arriving proteins of relatively high affinity. This is known as the Vroman effect (Vroman, 1969; Wojechiechowski, 1985; Brash, 1988; Horbett, 2018). Once a protein is adsorbed on a surface, it can undergo conformational change and/or denature (Vilaseca, 2013).

Higher molecular weight proteins include lipoproteins and glycoproteins. Lipoproteins contain lipid components and therefore have a high affinity for hydrophobic surfaces (Rabe, 2011). Glycoproteins contain carbohydrate components, rendering them hydrophilic and less prone to adsorption on hydrophobic surfaces.

2.2.2 Surface Properties Controlling Protein Adsorption

Surfaces typically in contact with proteins can be natural or synthetic, metals or polymers, and can have different dimensions and shapes to which proteins respond differently. Protein adsorption is dependent on surface properties including hydrophobicity (Tangpasuthadol, 2003; Malmsten, 1995; Roach, 2005), shape (e.g. curvature) (Gu, 2014), roughness (Rechendorff, 2006), and chemistry (Yuan, 2011). It has been shown that proteins adsorb preferentially to hydrophobic over hydrophilic surfaces, and adsorption in the former case occurs via the hydrophobic effect. Strong hydrophobic interactions between non-polar species in aqueous media result, in the case of proteins, in reconfiguration and adsorption to hydrophobic surfaces via hydrophobic protein domains (Tilton, 1991). Although there is a strong correlation between adsorption and hydrophobicity, other factors such as electrostatic interactions (Pasche, 2005; Malsten,1995) and surface curvature (Roach, 2005) may overshadow hydrophobic interactions. Surface nanostructure was investigated by Scopelliti et al. using a high-throughput analysis method in which surface roughness, protein concentration and protein type were varied (Scopelliti, 2010). They found that porous nanostructured surfaces promote the formation of protein aggregates inside the pores. Increasing surface nano-roughness, increases the number of protein nucleation sites, thereby increasing the amount of protein adsorbed in the pores.

2.3 Non-specific Protein Adsorption on Biomedical Devices

2.3.1 Diagnostic Devices

Early disease detection is a highly relevant and important research topic. The use of biomarkers to identify diseases focuses on achieving maximum sensitivity, specificity, and selectivity for their target biomarker (Jiang, 2019). The sensor surfaces face the challenge that they must respond only to the relevant biomarker and be unreactive to other species.

Surface–based sensing includes immunosensors, microfluidic sensors, and electrochemical sensors (Jiang, 2019). The sensing areas often come into contact with complex mixtures of proteins and other molecules during their operation. The irreversible adsorption of proteins generally onto these surfaces is referred to as non-specific adsorption. Non-specific adsorption to the sensing surface results in strong background signals that are indistinguishable from that of the target molecule, thereby decreasing the sensor's performance.

2.3.2 Blood Contacting Devices

Many medical devices implanted in the human body are in contact with blood (Jaffer, 2019). Blood is composed of water, red cells, white cells, platelets, proteins, and salts. When a biomaterial or device is implanted in the body, an immune response is triggered due to the surgical wound as well as the foreign biomaterial. Within seconds of implantation, proteins in the blood and tissue adsorb to the biomaterial or device surface. The adsorbed protein layer initiates and regulates the coagulation and complement

cascades by activating platelets and triggering phagocytes as illustrated in Figure 2-2 (Jaffer, 2019; Brash, 2019; Franz, 2011). Blood coagulation and thrombosis may lead to device failure (Ukita, 2019) necessitating removal of the device. Pathogens such as viruses and bacteria may also trigger thrombosis (Cunningham, 2019) which emphasizes the need to control bacteria and microbes on device surfaces as well.

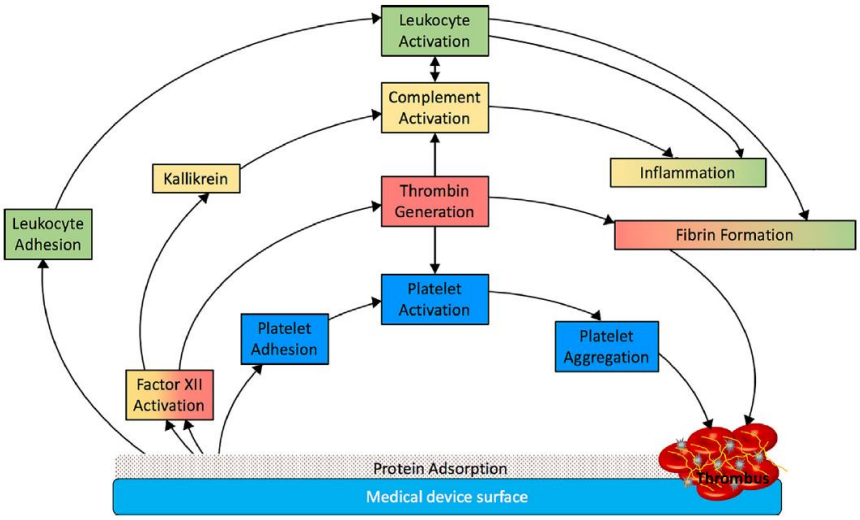

Figure 2-2: Thrombosis on blood-contacting medical devices. Proteins such as fibrinogen, fibronectin, and von Willebrand factor adsorb onto the surface inducing platelet activity. Autoactiviation of adsorbed Factor XII on the surface results in factor XIIa which converts prekallikrein to kallikrein leading to thrombin generation. Thrombin activates platelets and converts fibrinogen to fibrin on the surface. Fibrin strands form a stable thrombus with platelets. Kallikrein, thrombin, and other coagulation enzymes activate the complement cascade, inducing a local inflammatory response. Leukocytes that adhere to the surface are activated and may cause inflammation. From (Jaffer, 2019) with permission.

2.4 Bacterial Biofouling on Medical Implants

Bacteria are single-celled organisms found in diverse environments. Bacteria found in the body can be beneficial in the right concentration or can cause inflammation or disease during chemical and biological disturbances. In addition, pathogenic bacteria in the environment can secrete toxins and cause infections.

When bacteria adhere to surfaces, bacterial colonies can form. Extracellular polymeric substances are secreted by the bacteria to form a biofilm (Limoli, 2015). The biofilm layer is abundant in proteins, DNA, RNA, polysaccharides, and water which provides the colony better access to nutrition and makes it more difficult to remove the film.

In the body, biofilms are a major cause of infection, especially for patients with implanted devices such as catheters, vascular prostheses, heart valves, pacemakers, stents, and orthopedic implants (Wu, 2015). The most common infections are caused by *Staphylococcus epidermidis* and *Staphylococcus aureus*, *Escherichia coli* and *Pseudomonas aeruginosa* (Colilla, 2018). Antibiotics are used to suppress biofilm formation when these devices are first implanted in the hope that eukaryotic host cells can reach the device surface first. This “race to the surface” concept suggests that the

device surface can be “defended” by integrated tissue such that there is little space available for bacterial colonization (Gristina, 1987). However, once a biofilm has developed on the device, immune responses and infection are likely; these are difficult to treat and ultimately result in the implant being removed.

2.5 Some Examples of Fouling on Biomedical Devices

Disease prevention, detection, and diagnosis play a major role in modern day society. A variety of devices are used for diagnosis such as enzyme or DNA assay kits for biomarker detection. In these assays, patients provide a sample of fluid or tissue to be analyzed. Biomarkers in these fluids are often in very low concentration and may need further processing to amplify the biomarkers prior to analysis. Amplification requires increased processing time and introduces the potential for sample contamination due to handling. In addition, the locations where the sample is taken and then analyzed are often separate. There is thus a need to develop non-invasive tests that reduce sample handling and the time required to achieve accurate data.

Point-of-use devices, i.e. devices which provide timely data at the point where the sample is taken are being developed. These devices use optical, electrochemical, and/or biological techniques. For example, Bushan et al. created an electrochemical/enzymatic diagnostic test to monitor uric acid (UA) as an indicator of wound healing (Bushan, 2019). Multi-walled carbon nanotubes (MWCNTs) and gold nanoparticles (AuNPs) were used as electrode materials in conjunction with uricase to oxidize the UA. Horseradish peroxidase (HRP) was used as a biocatalyst to shuttle electrons between the uricase and the electrode. The MWCNT/AuNP material provided excellent conduction and therefore sensitivity due to the high surface area of the nanomaterials. Although this method was successful in measuring differences in UA concentration in peri-lesional fluid, wound exudate contained debris that fouled the electrode and hampered sensor recovery. In addition, the sensitivity was lower than that of other enzymatic methods, possibly also due to fouling.

Recently, Xu et al developed an electrochemical biosensor to monitor the carcinoembryonic antigen (CEA), a broad-spectrum tumor marker and a validated cancer indicator (Xu, 2020). Co-polymerized polydopamine and poly(sulfobetaine methacrylate) (PDA-PSBMA) was used as an antifouling coating to prevent non-specific adsorption on the glassy carbon electrode. The aptamer used to detect CEA was grafted on the antifouling layer and provided excellent specificity for sensing CEA in bovine and human blood. In addition, the accuracy and stability of the sensor were comparable to those of the standard electro-chemiluminescence detection method and showed a very low limit of detection (LOD) of 3.3 fg/mL, thus demonstrating the importance of modifications for antifouling. A review by Jiang et al. compares the antifouling strategies used in various *in-vitro* and *in-vivo* sensing devices in terms of sensing performance (Jiang, 2019).

2.6 Antifouling Strategies

Due to the many factors that determine non-specific protein adsorption and bacterial adhesion, many approaches to antifouling have been taken. Physical methods such as creating nanostructures using photolithography or varying surface wrinkling alters the surface morphology so that proteins have difficulty settling on the surface. These methods are often non-scalable due to their precision; the modified surfaces are easily damaged (Li, 2019), and are often not effective over extended periods of time. To overcome these limitations, physical methods can be combined with chemical ones.

Chemical techniques may also be used on their own; they include self-assembled monolayers of antifouling agents including peptides, and polymers. Antifouling polymers are widely used due to their wide variety and scalability.

2.6.1 Hydrophilic Polymers

As previously mentioned, surface hydrophilicity has a strong influence on protein adsorption, and hydrophilic polymers have been widely used as modifiers to reduce biofouling. Hydrophobic surfaces were shown to attract proteins that trigger inflammation whereas hydrophilic surfaces attracted proteins that provoked anti-inflammatory cytokines. Therefore, hydrophilic surfaces are favored for *in-vivo* applications (Visalakshan, 2019).

Examples of hydrophilic polymers include polyethylene glycol (PEG), poly(vinylpyrrolidone) (PVP), poly(hydroxymethylacrylate) (PHEMA), and poly(N-isopropylacrylamide) (PNIPAM). These polymers are either physically or chemically grafted to the substrate. The polymers bind water at the polymer-solution interface to create a surface hydration layer. This water layer provides a physical and energy barrier to prevent protein adsorption. The extent of hydration depends on the polymer structure, molecular weight, film thickness, chain packing density, and chain conformation. Low grafting densities allow proteins to penetrate the polymer layer to render it ineffective against protein adsorption (Wang, 2020). In addition, for long-chain polymers, chain flexibility also plays a role in protein resistance. As proteins approach the surface, the polymer chains are compressed causing steric repulsion due to a loss of entropy (Chen, 2010). The ionic properties of the solution (Wang, 2013; Kobayashi, 2012) as well as the surface density of the polymer grafts (Brittain, 2007) both have an influence on the brush configuration, i.e whether the more effective extended or less effective collapsed (“mushroom”) configuration is achieved. Therefore, surface hydration and graft density must be balanced in hydrophilic polymer modified surfaces to achieve optimal protein resistance.

2.6.1.1 *Polyethylene Glycol*

The most widely used polymer, and the gold standard for antibiofouling, is polyethylene glycol (PEG). Short ethylene glycol chains are referred to as oligoethylene glycol (OEG),

while longer chains (>20,000 g/mol) are referred to as polyethylene oxide (PEO). PEG can be covalently grafted to the surface as a preformed linear polymer via the “graft-to” approach, or via surface-initiated polymerization of a monomer via “graft-from” methods. In the “graft-to” approach steric hindrance can limit the grafting density such that proteins can penetrate the layer and adsorb to the substrate. Goh et al. corrected for this effect by “backfilling” the “bare” areas with bovine serum albumin (BSA) (Goh, 2018). BSA is used to block non-specific protein adsorption in several applications including solid phase immunoassays and has also been shown to modulate cells and responses that promote anti-inflammatory effects (Vikalakshan, 2019). Goh et al showed that backfilling with BSA was able to reduce fibrinogen adsorption significantly on PEG-modified polycarbonate, PDMS, and glass surfaces (Goh, 2018).

When PEG is anchored to a surface in contact with an aqueous solution, it forms strong hydrogen bonds with the surrounding water molecules. This creates an ideal non-fouling surface for sensors intended to function continuously in aqueous environments. Hsu et al. grafted PEG to a coated PDMS dissolved oxygen (DO) sensor (Hsu, 2014). The modified PDMS surface maintained a sensitivity of 20.7 ($\mu A/cm^2$)/(mg/L) over a DO concentration range of 2-7 mg/L in an accelerated bio-fouling test for 21 days. This was compared to an identical unmodified sensor and a commercial sensor which became fouled within 14 days.

In addition to forming a hydration layer on the surface, PEG is able to change the hydration and conformation of proteins to prevent protein contact with the modified surface (Leng, 2015; Bernhard, 2017). The effect of PEG on protein geometry varies from protein to protein.

Although PEG has been widely used to prevent biofouling, it has been found to be susceptible to oxidation that limits its long-term stability (Ostuni, 2001; Zhang, 2015). In addition, there is evidence that it may be immunogenic (Damodaran, 2016).

2.6.1.2 Zwitterionic Polymers

Zwitterions are structures that possess one negative and one positive charge and are therefore precisely net neutral. The most common anions are phosphate (Ishihara, 1992), sulfonate (Zhang, 2006a), and carboxylate (Zhang, 2006b); cations are usually quaternary ammonium, phosphonium, or imidazolium (Wu, 2019); and common zwitterions include carboxybetaines, sulfobetaines, and phosphatidylcholines. Selection of specific ion types is important for environmental reasons and for the requirements of the application (Blackman, 2019).

Zwitterions have gained popularity as surface modifiers due to their strong antifouling capabilities. Whereas uncharged antifouling polymers like PEG form hydrogen bonds with neighbouring water molecules, the charged groups in zwitterions bind water ionically (solvation) to form stronger bonds (hydration barriers) such that large free energies of the

fouling reaction are required to break them (Zhang, 2019). Hydration barriers that rely on hydrogen bonds are dependent on temperature since bond strength decreases as temperature increases. But ionic solvation provides species that are stable at temperatures above room temperature and are thus useful for *in vivo* applications (Yang, 2009). In addition, zwitterionic groups self-associate to form dipole pairs. Electrostatic repulsion causes zwitterionic polymer chains to extend to different degrees depending on the types and amounts of salts in the medium, thus increasing solubility (Wang, 2013) and hydrophilicity. An in-depth critical review of the antifouling mechanisms of zwitterions is given by Schlenoff (Schlenoff, 2014).

Although hydrophilic polymers perform well in single protein solutions, they tend to fall short when it comes to serum, plasma, whole blood and other real biofluids where high concentrations of species including multiple proteins and cells are present. Yang et al. were able to achieve protein adsorption levels < 5 ng/cm^2 from diluted and undiluted blood serum using poly (carboxybetaine acrylamide (pCBAA) coatings of thickness between 15 and 40 nm and 37°C (Yang, 2009). The stability of zwitterions at body temperature has prompted their use in drug delivery systems as they interact less with blood components and have longer circulation times compared to PEG (Jin, 2014).

Methacryloyloxyethyl Phosphocholine (MPC)

In the late 1970's, Nakabayashi's group patented methacryloyloxyethyl phosphocholine (MPC) (Japanese patent JP 54063025, 1977), and showed that MPC-co-n-butyl methacrylate (BMA) polymers were able to reduce protein and cell interactions and were antithrombogenic in contact with human plasma and whole blood (Ishihara, 1992). However, later research showed that under certain conditions, phosphorylcholine (PC) groups may irreversibly reorient so that their antifouling and antithrombogenic performance is reduced over time as shown in Figure 2-2 (Yang, 2008).

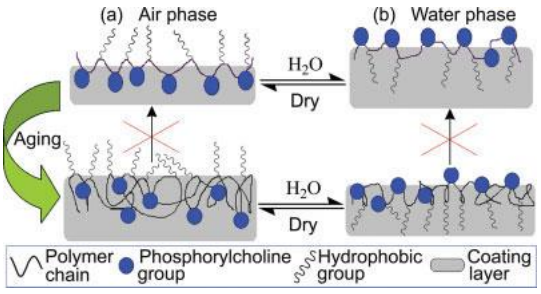

Figure 2-2: Group reorientation and migration taking place in a film of an amphiphilic polymer bearing PC groups. From (Yang, 2008) with permission.

Sulfobetaine and Carboxybetaine

In 2006, Jiang's group introduced poly(sulfobetaine methacrylate) (pSBMA) and poly(carboxybetaine methacrylate) (pCBMA) as super low fouling surface coatings. This

began a trend away from viewing PEG as the gold standard of antifouling coatings (Zhang, 2006a, Zhang 2006b).

Of the three most popular zwitterionic antifouling polymers, poly(carboxybetaines) have proved to be the best performing in complex biological media. Rodriguez used SPR to compare protein adsorption on pCBMA, PEG-COOH, pMPC, pSBMA and block/co-polymers of pCBMA and pSBMA (Rodriguez Emmenegger, 2009). They found that only pCBMA-modified gold prevented adsorption completely from single protein IgG solution and blood plasma. The pSBMA/pCBMA block co-polymer showed very low adsorption from plasma, suggesting that carboxylic groups are important in the antifouling function in plasma.

Jiang's group showed that the distance between the cationic and anionic groups, as determined by the carbon spacer length (CSL), affects the antifouling properties of the zwitterion (Shao, 2013). Using a combination of molecular simulations, experiments, and quantum chemical calculations, they concluded that the charged groups in carboxybetaines (CB) with short carbon spacer lengths (CSLs) are screened to some extent such that their effective charges are dependent on the CSL. Carboxybetaines of shorter CSL have lower pKa indicating stronger acidity of the carboxylic groups. Therefore, the interactions between the carboxylic acid groups and water molecules are weaker. When the CSL ≥ 3, the effective charge did not vary.

Jiang's group also showed that pCBMA with a spacer length of 2, when grafted on glass, resisted biofilm formation for 10 days at 25°C, 8 days at 30°C, and 2.5 days at 37°C. In contrast a pSBMA surface had decreased performance, reducing biofilm formation for 9 days at 25°C (Cheng, 2009).

Although poly(carboxybetaines) (pCBs) are generally better performing than polysulfobetaines (pSBs), pSBs still have very good antifouling properties under certain conditions (Chang, 2008; Yang, 2008), and also have other advantages. For example, SBs are more easily synthesized and some are commercially available. Carboxybetaine polymers have been shown to resist non-specific protein adsorption at pH >5, but not at lower pH. In contrast the antifouling performance of sulfobetaine materials is independent of pH (Leng, 2016).

Applications of Zwitterions

Zwitterionic polymers are relatively stable and have been used in various antibiofouling applications. Jiang's group coated a cellulose paper glucose sensor with pCB and showed that the modified surface detected the analyte more rapidly and with increased sensitivity compared to the unmodified one (Zhu, 2014; Sun, 2017). The sensor could be stored in air for 20 days with retention of its ability to reduce protein adsorption from undiluted serum by 92% (Sun, 2017).

In addition to analytical devices, CB and other zwitterions are being considered for modification of biomedical devices used *ex-vivo* and *in-vivo*. In one example, a poly(carboxybetaine) was chosen as the antifouling modifier to reduce thrombosis on an extracorporeal membrane oxygenation (ECMO) device (Ukita, 2019). In rabbit studies, the pCB modified surfaces showed a reduction in blood clot formation but no significant effect on platelet adsorption. Thus, despite promising results from *in-vitro* studies, these experiments show that challenges remain for clinical applications of these materials.

2.6.2 Superhydrophobic Surfaces

Superhydrophobic surfaces are surfaces having water contact angles >150° and are generally formed by creating nano surface roughness and/or by reducing surface energy (Li, 2019). The ability of these surfaces to repel both water, lipids and oils makes them strong candidates for antifouling applications. An example from nature is the lotus leaf which has a special "self-cleaning" property whereby water forms droplets which easily roll off, carrying dust and dirt with them. The "lotus effect" results in strong water repellency, and thus is a characteristic of superhydrophobic surfaces.

2.6.2.1 Slippery Liquid-Infused Porous Surfaces, SLIPS

Inspired by Nepethenes pitcher plants (Bohn, 2004), so-called Slippery Liquid-Infused Porous Surfaces (SLIPS) are superhydrophobic surfaces that combine nano-roughness with chemical properties that give low surface energy. This approach overcomes problems such as failure under pressure, physical damage and high production costs associated with most types of superhydrophobic surfaces (Wong, 2011). SLIPS requires the surface to be micro or nanotextured. The roughness thereby created provides a large surface area for a "lubricating fluid" to adhere to. The lubricating fluid must be compatible with the surface in that it must wet and adhere stably within the surface texture. Also, it must wet the surface in preference to, and be immiscible with, the fluid that is being repelled (Wong, 2011). The lubricating fluid may be a fluorocarbon (Wang, 2015; Zhao, 2017) or an oil (Manna, 2015). The lubricated surface is able to resist both aqueous and hydrocarbon-based liquids under pressure. The lubricating film protects the textured surface, and its fluidic nature allows it to self-heal if subjected to abrasion or impact by surface-energy-driven capillary action (Ishino, 2007).

The SLIPS concept was applied by Wang et al to hydrophilic aluminum and hydrophobic silicon substrates to prevent microbial adsorption and fouling on marine structures (Wang, 2015). The liquid-like lubricating film creates a surface that is extremely smooth with high contact angle. Wang et al reported a SLIPS surface with contact angle 110° which prevented sulfate-reducing bacteria from adhering over a 14-day period.

In another application, a modified SLIPS technique was applied to catheters which were then assembled into arteriovenous shunts (Leslie, 2014). The shunts were implanted into pigs as a vascular circuit. The modification prevented in-vivo thrombus formation on the

shunts for 8 hours without the use of anti-thrombotic agents such as heparin. The long-term effectiveness of these surfaces in potentially pro-thrombotic environments is yet to be investigated. Other medical applications of liquid-infused surfaces are reviewed by Howell et al (Howell, 2018).

2.7 Grafting Strategies

Polymers can be attached to a surface physically or chemically via three primary mechanisms: i) physisorption, ii) "graft-to" or chemisorption, and iii) "graft-from". Physisorption is the attachment of charged or amphiphilic polymers to the surface via weak intermolecular interactions such as Van der Waals forces. Physisorption techniques change surface properties through a reversible process where the polymers self-assemble onto the surface without chemical reaction (Viefhues, 2011). However, due to the weak interactions, desorption occurs when the polymer is exposed to solvents or is displaced by other adsorbents (Zhao, 2000). In addition, de-wetting of the polymer film occurs at high temperatures. Some of these shortcomings can be remedied by chemisorption "graft-to" and "graft-from" techniques in which polymers are pre-formed with a suitable functional end group for the "graft-to" method. The end group allows the polymer to react with the substrate surface under appropriate conditions via covalent bond formation (Zhao, 2000). Although the tethered chain is robust, the grafting density is limited by the number of reactive sites initially on the surface and by steric hindrance as the surface fills (Zhao, 2000). This method allows the polymer chains to attach on devices that are already assembled. However, the limitations on grafting density may hinder the achievement of optimal antifouling performance.

The "graft-from" approach involves *in-situ* polymerization of a monomer from a surface immobilized initiator. Immobilization of the initiator can be achieved by the creation of functional groups on the substrate surface via plasma, UV, or acid treatments. Common surface polymerization techniques include conventional radical polymerization (Zhao, 2000), iniferter polymerization (Matsuda, 2006; Wang, 2016), atom-transfer radical polymerization (ATRP) (Matyjaszewski, 1997), and reversible addition-fragmentation chain-transfer (RAFT) polymerization (Chiefari, 1998). The grafting density is controlled by the density of initiator sites on the substrate surface while the chain length is controlled by the polymerization conditions such as solvent, temperature, time, and catalysts. The *in-situ* polymerization nature of "graft-from" methods allows high grafting densities and thick polymer brushes to be formed giving surfaces that are optimally antifouling. The drawbacks of "graft-from" methods include complicated polymerization regimes that require optimization of the many variables, the requirement of solvents that may be "harsh", and difficulties in scale-up. Modified polymerization techniques such as Initiators for continuous activator regeneration (ICAR) and Activators regenerated by electron transfer ATRP (ARGET-ATRP) have largely overcome these problems (Matyjaszewski, 2006).

2.7.1 Activators Regenerated by Electron Transfer – ATRP (ARGET-ATRP)

ARGET – ATRP, as used in the present work, is a "controlled" radical polymerization method used to produce polymer chains or brushes with low polydispersities, i.e uniformly distributed chain lengths. Control is achieved via the equilibrium between a dormant alkyl halide (RX) and active propagating radicals (R•) (Wang, 1995) as seen in Figure 2- 3.

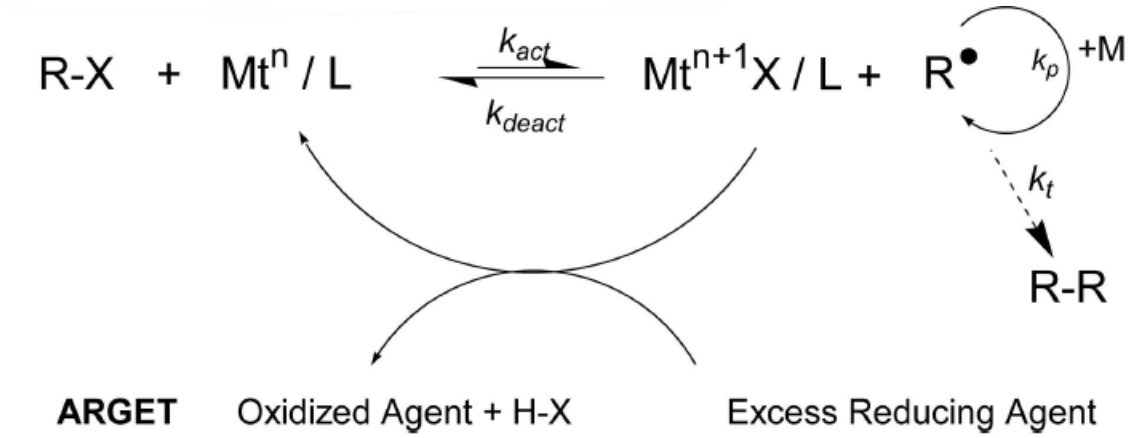

Figure 2- 3: ARGET ATRP process and equilibrium. Equilibrium between propagating radicals and dormant chains controls the livingness of the polymerization reaction. A transition metal-ligand complex cleaves the R-X alkyl halide bond to generate an alkyl radical R• and a higher oxidation state metal halide deactivator, Mt(n+1)X/L. The radical R• can propagate with a vinyl monomer, M, be deactivated by Mt(n+1)X/L or terminate by coupling or disproportionation with another R•. In ARGET ATRP, an excess reducing agent such as ascorbic acid is added to the system to regenerate the oxidized metal halide back to its reduced form to be continuously reused in the reaction; thus, reducing the use of metal catalyst required for the reaction. From (Matyjaszewski, 2006) with permission.

A soluble metal-ligand complex catalyzes the reaction. The equilibrium is shifted to the left thus giving a low concentration of propagating radicals such that termination of the propagating chains is minimized. ARGET – ATRP is a modified ATRP method where the Cu(II) component is "regenerated" to its Cu(I) form using a reducing agent. A relatively low quantity of copper catalyst is required, thus reducing cost and eliminating the need for further purification. Unlike in traditional ATRP procedures, the additional reducing agent also allows air to be present during the polymerization process (Matyjaszewski, 2007; Hong, 2017). The factors that influence the efficiency of ARGET- ATRP polymerization include: i) Cu(I)/Cu(II) ratio in the catalyst (Tang, H., 2006), ii) type of ligand (Tang, W., 2006; 2008; Matyjaszewski, 2006) , iii) type of initiator (Tang, 2008), iv) temperature (Seeliger, 2009), v) solvent (Bergenudd, 2009) , vi) pH (Fantin, 2015), and vii) reducing agent (Dong, 2008; Matyjaszewski, 2007).

2.8 Surface Anchors

Surface modification is dependent on the substrate surface chemistry and tolerance of possibly harsh reaction conditions required for modification. Thus, modification protocols need to be chosen with chemical compatibility of the substrate in mind. A method that works on one type of material may not be suitable for others. For example, thiol chemistry

is used for noble metal surfaces, whereas a variety of chemistries are used with metal oxide surfaces (Pujari, 2014).

Devices and equipment that require surface modification are usually fabricated using several different materials. Therefore, surface anchoring chemistry that is applicable to a variety of different substrates, is easy to handle, is stable for extended periods, and is inert to environmental conditions, is highly desirable (Ye, 2011).

2.8.1 Silanes

Silanes are a common class of surface modifier used to couple oxide substrates with dissimilar materials. Silane coupling agents have the general structure shown in Figure 2-4 and are often used in the form of self-assembled monolayers (SAM) attached to the substrate via their hydrolysable groups. The hydrolysable groups are typically chloride, alkoxy, or hydride, which react with surface -OH groups, hence having the strongest bonds to native oxide surfaces, but varying affinity for other surfaces as seen in Figure 2-5. Generation of -OH groups on non-native oxide surfaces can be achieved using plasma activation or acid/base etching. Table 2-1 presents selected studies using silanes in antifouling applications.

Silane Structure and Surface Modification Mechanism

A typical silane consists of an organofunctional group, a linker, a silicon atom and hydrolysable groups as shown in Figure 2-4. The organofunctional group, for example amino, reacts with the agent to be conjugated to the silane such as an ATRP initiator for polymerization (de los Santos Pereira, 2016), or hydrophilic (Jo, 2000) or superhydrophobic fluorinated polymers (Ohtani, 2014).

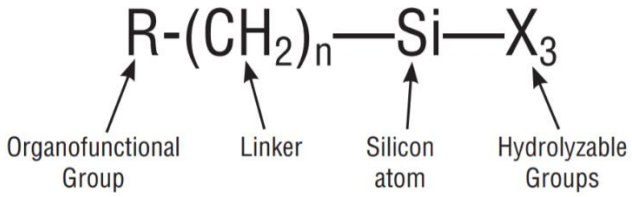

Figure 2-4: Typical silane structure. From (Arkles, 2014) with permission.

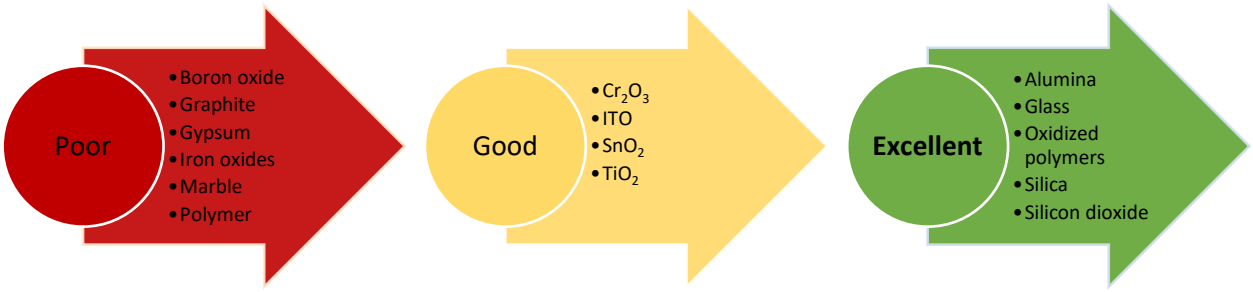

Figure 2- 5: Effectiveness of silane modification of various inorganic substrates adapted from (Pujari, 2014).

Formation of silane SAMs occurs in three steps (Pujari, 2014) as shown in Figure 2-6.

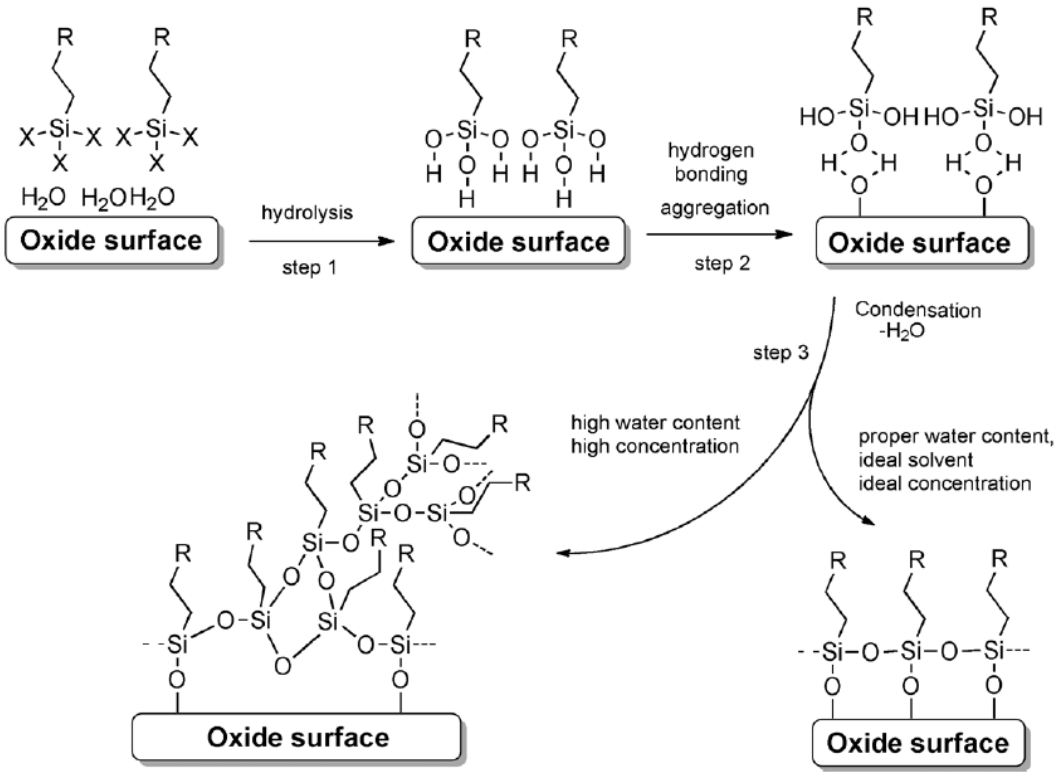

Figure 2-6: a) Hydrolysis of hydrolyzable X groups on a silane in aqueous solution; b) Hydrolyzed silane bonding to oxide surface via intermediate hydrogen bond formation. Condensation creates strong covalent bonds with the oxide surface. From (Pujari, 2014) with permission.

In the first step, the hydrolyzable groups are hydrolyzed by water near the oxide surface to form the corresponding hydroxysilane. Next, the hydroxysilane hydrogen bonds to the surface. Some silanes may aggregate via weak interactions, making them less mobile for

migration over the surface. Finally, reaction of the Si-OH groups with the surface occurs, usually at elevated temperatures, to form covalent Si-O-Si bonds with both the surface and neighboring silane groups to create a cross-linked surface network.

The hydrolysis step controls the quality of the SAM and is dependent on the water content in the environment. Adsorbed water on the surface is necessary for SAM attachment, but too much water results in excessive hydrolysis of the silane in the bulk solution and/or disorganized polysiloxane on the surface. For this reason, anhydrous solvents with trace amounts of water and low silane concentrations are typically used to prepare smooth monolayers of silane (McGovern, 1994; Pujari, 2014; Okhrimenko, 2017). As well as the type of solvent, the amount of water and silane concentration, the reaction time and temperature (Pasternack, 2008), the length of the alkyl linker (Smith, 2008), and the annealing method that drives the reaction of the Si-OH groups with the surface, also influence the SAM quality.

Deposition of Silanes

Surfaces are silanized either in the solution- or vapor-phase. The large number of variables involved makes solution phase deposition of organosilanes difficult to control and reproduce (Zhu, 2012). The alternative chemical vapor deposition method has been shown to produce smooth and highly reproducible monolayers (Yadav, 2014). Yadav et al. showed that although the quality of three different silane layers was high using CVD, solution phase deposition of some silanes was comparable. A drawback of CVD is that it requires specialized high vacuum equipment that is prone to contamination from chemicals used previously (Yadav, 2014). In addition, not all silanes are able to generate a high-density silane layer from the vapor phase, particularly in the case of longer chain aminosilanes (Zhu, 2012).

Table 2-1: Some recent silanization research.

Surface	Silane	Techniques used	Functional Group	Protein studies	Bacteria studies	Notes	References
Glass	-propyltrimethoxysilane - 11-undecyl-trimethoxysilane	-95% EtOH acidic solution deposition -anhydrous toluene solution deposition	PEG	fibrinogen	–	–	Jo, 1999
Glass	(N,N-Dimethylaminopropyl) trimethoxysilane	-Oxygen plasma -99% EtOH solution deposition	-Carboxybetaine -Sulfobetaine	–	–	hydrophilicity studies	Wu, 2016
PDMS	(N,N-Dimethylaminopropyl) trimethoxysilane	- air plasma -99% EtOH solution deposition	Sulfobetaine	-BSA -Lysozyme - Mucin	-S. epidermidis -P. aeruginosa	–	Yeh, 2014
PDMS	Aminopropyltriethoxy silane (APTES)	-oxygen plasma -methanol solution deposition -free radical polymerization - TEA crosslinking	MPC copolymers	-BSA -fibrinogen	-E. coli - S. aureus -P. aeruginosa	Crosslinked MPC co-polymer surfaces stable after 8 days in air or PBS	Zhao, 2019
PDMS	APTES	Aqueous solution deposition	PEG	–	Yeast extract	–	Hsu, 2014

Surface	Silane	Techniques used	Functional Group	Protein studies	Bacteria studies	Notes	References
PDMS	(3-Trimethoxysilyl)propyl 2-bromo-2-methylpropionate	-95% EtOH solution deposition - SI-ARGET ATRP	-polycarboxybetaine	fibrinogen	–	–	Hong, 2017
polyether amide and PTFE coronary catheter	trichloro (1H, 1H, 2H, 2H-perfuorooctyl) silane	-oxygen plasma -solution deposition -CVD	-perfuorodecalin - perfuoroperhydrophenanthrene	whole human blood	–	–	Badv, 2017
Dissolved oxygen - ExStik II DO603 Membrane	Trichloro(1H,1H,2H,2H-perfluorooctyl) silane	solution deposition	perfluorodecalin	–	Yeast extract	–	Osborne, 2019
Titanium sputtered on silicon	APTES	-Ethanol solution deposition -EDC/NHS coupling	-PEG -PEG-Heparin	fibrinogen	–	Platelet and endothelial cell adhesion	Pan, 2014
Titanium -Hydroxyapatite NPs	APTES	-deprotection APTES - Solution deposition in 90% THF - reaction with terminal amine	1-(sec-butylamino)-3-(3,6-dichloro-9H-carbazol-9-yl)propan-2-ol	–	-S.aureus -P. aeruginosa	-in-vivo mice experiments	Gertis, 2016
-calcium phosphate nanocrystalline HA NPs	APTES	-hexane solution deposition - reaction with terminal amine	Arginine-glycine-aspartic acid (RGD-peptides)	–	–	promotion of osteoblast adhesion	Balasundaram, 2006

Silane Limitations

Despite being widely used as coupling agents due to the simple deposition procedures and high reaction rates, silane-modified surfaces face reproducibility and stability issues related to hydration (Smith, 2008; Etienne, 2002). Although vapor deposition is better at controlling the variables associated with obtaining a reproducible and smooth silane layer, its drawbacks as noted above may lead to a preference for solution phase deposition. Likewise, the amount and thickness of solution-deposited silanes varies with the substrate, while their hydrolytic stability is generally poor across all substrates (Okhrimnko, 2017). Silane stability may be improved by keeping the silanated surfaces at low pH (Etienne, 2002) and at temperatures no greater than 40ºC (Smith, 2008), or by covering the silane with superhydrophic materials as in SLIPS technology (Epstein, 2012; Wong, 2011; Zhao, 2017, Sotiri, 2016).

2.8.2 Polydopamine

In 2007, Messersmith's group took inspiration from the adhesion promiscuity of mussels which are able to attach to any organic or inorganic surface (Lee, 2007). They found that the adhesive property of mussel foot proteins is likely due to high concentrations of 3,4-dihydroxy-L-phenylalanine (DOPA) forming covalent and non-covalent bonds with the substrate. Since then, variations of DOPA and other catechols (Figure 2-7) have been studied.

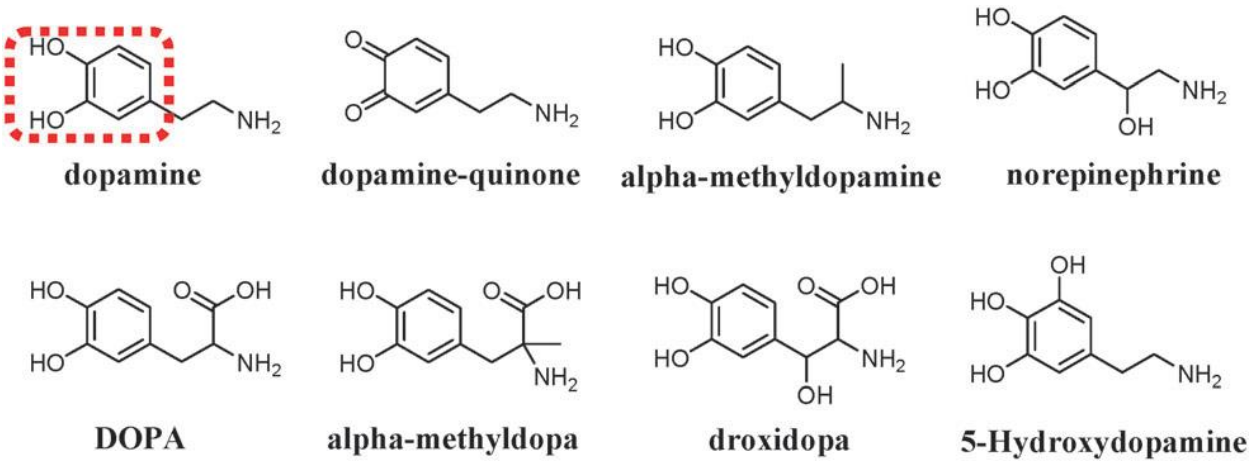

Figure 2-7: DOPA analogues. From (Ye, 2011) with permission.

Dopamine is a water-soluble catechol with an amino functional group. It is able to self-polymerize to form polydopamine (pDA) in oxygenated and slightly alkaline aqueous environments. The pDA precipitates out of the solution and deposits on a substrate to form a thin film layer. Most importantly, a wide range of substrates including polymers, metals, and composites are amenable to this procedure (Pop-Georgievski, 2011). pDA coatings are stable in aqueous conditions including strong acid and mild oxidizing or reducing conditions (Dreyer, 2013). The thickness of the pDA layer is controlled by adjusting the dopamine concentration, deposition time, oxygenation, and temperature (Ball, 2012).

pDA Formation Mechanism

The adhesion mechanism of polydopamine is not well understood. It depends on the substrate and reaction conditions such as buffer and pH. When dopamine is deposited in solution and air oxygenated, it undergoes the first steps of melanin biosynthesis as illustrated in Figure 2-8 (Ding, 2016). Following this, covalently bonded polymers (Figure 2-8 I and II) or supramolecular aggregates formed via weak interactions such as hydrophobic interactions, hydrogen bonding, and pi- stacking can be formed (Figure 2-8 III and IV), as reviewed by Ding et al (Ding, 2016).

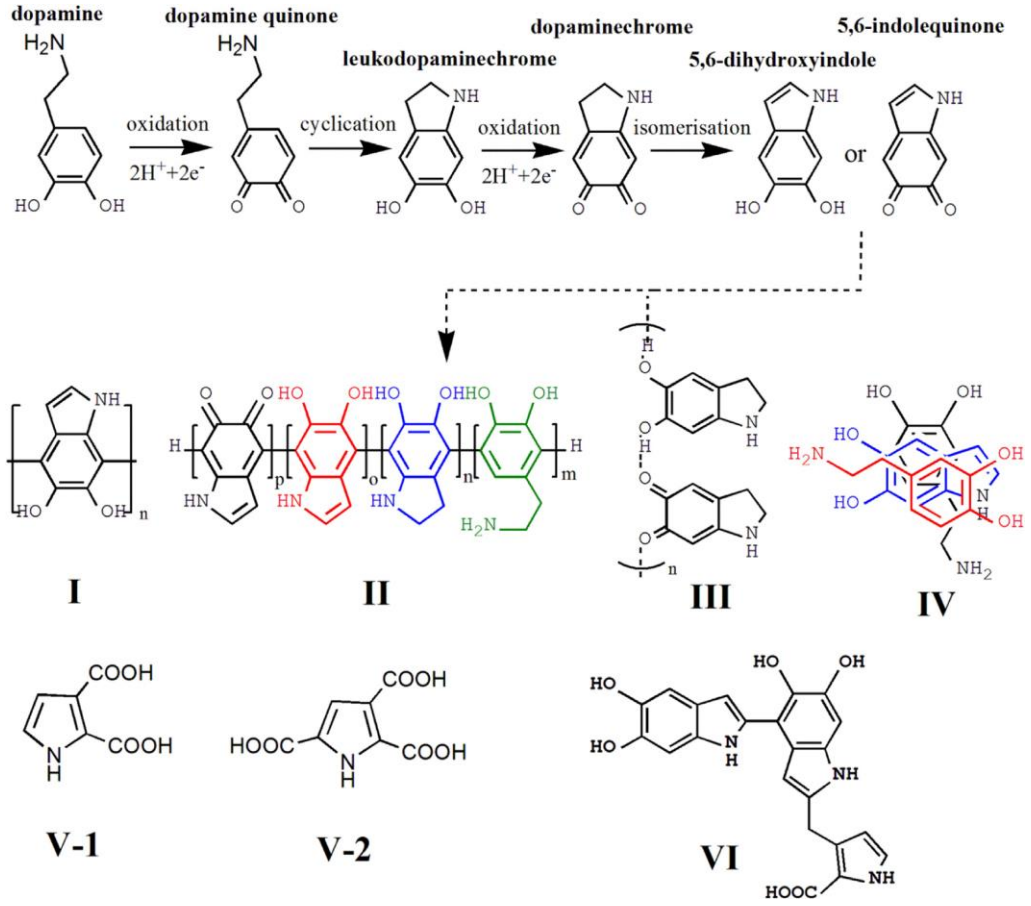

Figure 2-8: Melanin formation by dopamine oxidation and theoretical models of pDA structure: I) 5,6-dihydroxyindole (DHI) trimer undergoes branching reactions to form covalent pDA structure, II) Various indole units with different degrees of saturation forming a covalently bonded pDA structure, III) DHI interacting via charge transfer , pi-stacking, and hydrogen bonding to form supramolecular pDA structure, IV) physical assembly of dopamine and DHI trimer, V-1 and V-2) A collection of pyrrolecarboxylic acid degradation moieties from uncyclized catecholamine/quinone oligomers and cyclized DHI oligomers form a macromolecular pDA structure, VI) Initial stages of pDA formation includes covalent interactions with (DHI)2 – pyrrolecarboxylic acid trimer complexes, followed by non-covalent interactions. From (Ding 2016) with permission.

Catechols such as pDA can also covalently bond to organic substrates through Michael-type addition. It is believed that covalent bonds are formed between the hydroxyl groups of the catechol and the amino group on the substrate (Lee, 2006).

Hong et al. found evidence that pDA layers form via two pathways after the formation of 5,6-dihydroxyindole (DHI) — (a) a covalent oxidative route that leads to crosslinking, and (b) physical assembly of (dopamine)$_2$/DHI trimer (Figure 2-8 IV) (Hong, 2012). Physical assembly originates from hydrogen bonding, which promotes adhesion to many biological surfaces such as mucosal tissues and hydroxyapatite. $\pi - \pi$ stacking, which allows attachment to surfaces rich in aromatic compounds and to gold-based substrates; and cation-π electron interactions, which allow the catechol group to adhere to charged surfaces, contribute to cohesion on surfaces with aromatic and cationic functional groups,

and enhance the under water adhesiveness of catechol (Forooshani, 2017). The tight binding of the (dopamine)$_2$/DHI trimer in covalent crosslinks of polydopamine prevents the unpolymerized trimer from being released into the bulk medium, thereby explaining the low-level toxicity of polydopamine (Hong, 2012).

Messersmith's group designed an AFM experiment to study the interactions between DOPA and TiO_2 and between DOPA and Si-amino surfaces (Lee, 2006). Using Si_3N_4 AFM tips with a single DOPA residue linked by an excess of PEG they found that the mechanisms of attachment were different in the two systems. In the Si-amino case, the quinone group was able to react with amino and thiol groups via Schiff-base and Michael addition reactions whereas the TiO_2 formed a metal – oxygen coordination bond as shown in Figure 2-9. The chelation of the catechol groups to the metal atoms gives a strong, but reversible complex that is significantly more stable than products formed by bonding between catechol and polymeric acids or amino acid-based ligands (Forooshani, 2017). Depending on the valency of the metal ion, the concentration of the catechol, and the pH, the catechol can form mono, bis, or tridentate bridges or chelates with the metal (Ye, 2011).

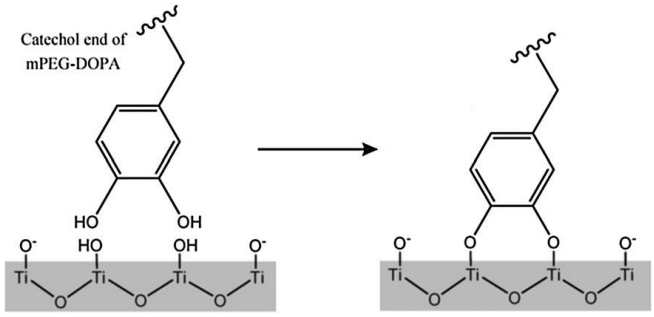

Figure 2-9: Proposed mechanism of mPEG-DOPA binding to TiO2 surfaces. From (Ye, 2011) with permission.

Surface Deposition of Polydopamine

Dopamine is traditionally deposited onto the surface in an air-oxygenated TRIS or PBS buffered solution. The process takes from hours to days depending on the size, type of material, and layer thickness required. Post-modification with a functional group such as PEG or a zwitterion is required for antifouling purposes. In addition, for larger devices, solution deposition may not be viable based on size and device components. Recent developments such as co-deposition (Huang, 2015; Kang, 2012; Zhang, 2012; Zhao, 2017), use of oxidant (Wei, 2010; Wu, 2016; Hong, 2016) and pH variation (Huang, 2014), controlled deposition, UV polymerization (Sheng, 2015), and sprayable pDA (Hong, 2016), methods have been proposed to reduce the time and other requirements for pDA deposition. Dopamine can also be conjugated to the functional group prior to surface deposition, but synthesis of the conjugate is often tedious. Also, to achieve the desired substrate binding affinity, protection and deprotection of both the catechol and amino ends of dopamine, which are potentially active, is required. For example, Sun et al. found

that four dopamine groups were required to achieve effective protein resistance via the graft-to method (Sun, 2017). This was also chosen as a better method for surface modification in *in-vivo* artificial lung studies when compared with other "graft-to" and "graft-from" methods (Ukita, 2019). These new dopamine deposition methods will hopefully pave the way for the use of pDA in other applications.

Advantages and Disadvantages of Polydopamine

The facile surface modification procedure using polydopamine is applicable to a wide range of substrates and the surfaces are stable under diverse conditions. In addition, the mild deposition conditions and the ability to functionalize the layer through the amino or hydroxyl groups also make polydopamine a versatile linker platform. However, a number of drawbacks limits its use in the modification of multiple materials:

1) pH sensitive materials are not suitable for pDA modification since deposition requires pH 8 – 8.5.
2) Strong bases such as bleach (Dreyer, 2013) and abrasion (Goh, 2018) will remove pDA films.
3) The polymerization of dopamine produces a dark brown coloration, thus reducing its usefulness in the treatment of optical sensors.
4) The long-term stability of pDA is poor (Miller, 2012). Miller et al. found that pDA-PEG coated polysulfone membranes showed signs of bacterial fouling after only 3 days in continuous biofouling tests.

Therefore, pDA may be better suited for short-term applications.

2.8.3 Plant-Derived Polyphenols

Polyphenols are phytochemicals that are naturally found in plants and in many of the foods that we consume such as fruits, vegetables, grains, teas, coffee, legumes, wines, and chocolate (Sileika, 2013). In plants, the function of polyphenols is to provide chemical "defence" against diseases, pigmentation, structural support, and to prevent radiation damage (Xu, 2018). Interest in polyphenols is attributable to their many attractive biological functions including antioxidant, antiallergenic, antibacterial, antidiabetic, and antiviral (Xu, 2018) functions. In addition, polyphenols absorb UV radiation, scavenge radicals, and form complexes with metal ions (Sileika, 2013). These properties may lead to further application of polyphenols.

Polyphenols contain multiple hydroxyl groups connected to aromatic rings. The hydroxyl groups facilitate hydrogen bonding, electrostatic interactions, and coordination bonding whereas the aromatic rings allow for hydrophobic interactions (Xu, 2018). These features provide various adhesion mechanisms for bonding to surfaces. Similar to pDA, polyphenol layers on surfaces are formed in oxygenated, mildly alkaline solutions through phenolate ion intermediaries (Sileika, 2013). Precipitation of the polyphenol caused by

oxidation of oligomers leads to deposition on the surface. Subsequent functionalization of polyphenols is possible via esterification of the hydroxyl groups with carboxylic acids, via etherification with alkyl halides and epoxides, and via Michael addition/Schiff base formation with nucleophilic compounds (Xu, 2018).

Polyphenols share many of the same attributes as pDA including adhesiveness to a wide range of substrates and mild deposition conditions. Plant phenol coatings have several advantages over pDA including that they are cheaper and therefore more scalable (Sileika, 2013), and are optically clear (Xu, 2018). Some polyphenols such as gallol also have greater adhesion strength compared to pDA. Zhan et al. showed that polygallol was 7-fold stronger than pDA as an underwater adhesive, attributable to its being tridentate vs the bidentate DOPA (Zhan, 2017), thereby providing a greater density of reactive groups. Selected examples of surface modifications using polyphenols are shown in Table 2-2.

Table 2-2: Some Recent Polyphenol Research. Abbreviations: Indium tin oxide (ITO), Iron (Fe), Polyethylenimine (PEI), Polyethersulfone (PES), Polyethylene terephthalate (PET), Poly(lactic-co-glycolic acid) (PLGA), Polypropylene (PP), Polystyrene (PS), Polytetrafluoroethylene (PTFE), Stainless Steel (SS), Titanium(Ti).

Surface	Polyphenol Type	Techniques used	Functional Group	Protein studies	Bacteria studies	Notes	Author
SS	Tannic Acid	layer-by-layer deposition	Parasin I	–	- Pseudomonas -E.coli - S. aureus -S. epidermidis	15 day stability in seawater	Xu,2015
-SS -Nylon	Tannic Acid and PDA	Fe(III) coordination	PEG	Fibrinogen		antifouling stability of diatoms of 6 days in seawater	Kim,2014
-Strawberries - Mandarin oranges -Shoe insoles -Gold -Silicon -Ti -Aluminum -SS -Silver -Copper -Nickel -Tin -Zinc -PS -PTFE	Tannic Acid	Fe(III) coordination	–	–	Trichophyton rubrum (fungus)	–	Park, 2017
-PES membranes	Tannic Acid	-Fe(III) coordination -crosslinking via alkaline solution deposition	-quaternized PEI	-BSA -Lysozyme	-E.coli -S. aureus	–	Chen, 2018
SS	Tannic Acid	-High salt alkaline solution deposition -SI-ATRP	-P(META) -P(MPC) -P(SBMA)	–	-Pseudomonas	–	Pranantyo, 2014

Surface	Polyphenol Type	Techniques used	Functional Group	Protein studies	Bacteria studies	Notes	Author
Glass Slides	Tannic Acid	-Alkaline solution deposition -SI-ATRP	-PNIPAAm	–	–	–	Dong, 2018
PLGA NPs	Tannic Acid	-alkaline solution deposition	-fluoresceinamine -PEG -Albumin -chitosan -drug compounds	–	–	–	Abouelmad, 2016
-Aluminum - Glass - PVC - PTFE - Pig skin	poly(vinylgallol)	- High salt, alkaline solution deposition	-Butyl acrylate	–	–	Bond strength comparison with PDA	Zhan,2017
-Gold -Titanium Dioxide - SS - PTFE	- Tannic Acid - Pyrogallol	-High salt, alkaline solution deposition	PEG	–	-P. aeruginosa -S. aureus	–	Sileika, 2013
SS	Tannic Acid	-Alkaline solution deposition - catalyst free-RAFT - copper-free Click Chemistry	MPC	BSA	- E. coli -S. epidermidis	Direct functionalization of TA is rare as it is sensitive to metal ions.	Xu, 2019
-SS -Aluminum -PET -cast PP -Nylon -Glass -Cellulose acetate filter -Plant leaf -fine granite	-Dopamine -Catechin/catechol -Ferulic acid/catechol -Catechin/syringic acid -Tannic Acid/catechol	-acid, alkaline, or high salt solution deposition	BSA	–	–	–	Jeon, 2013
-ITO -Carbon	Tannic Acid	-HRP catalyzed alkaline solution deposition	-goat anti-rabbit IgG -goat anti-mouse IgG -Folic acid -thiolated DNA	–	–	electroactive small molecule capture sensor	Kumar, 2018

Tannic acid

Tannic acid is a large, commercially available polyphenol (Figure 2-10). It contains a central glucose unit surrounded by galloyl groups. It has been used as a bonding agent (Sileika, 2013), in leather manufacturing (Sileika, 2013; Kurzbaum, 2018) and in antimicrobial applications (Park, 2017). There is currently interest in tannic acid as a bioadhesive because like dopamine, it is able to form various bonds with different material types (Yan, 2020). Tannic acid undergoes oxidation-induced oligomerization at pH 7 (Abouelmagd, 2016). The adhesive mechanism of tannic acid is similar to that of pDA and is due to the outward-facing hydroxyl groups that allow for hydrogen bonding, electrostatic interactions, and covalent bonding (Guo, 2018; Xu, 2018). The proton of phenol hydroxyls can be displaced (Xu, 2018), making the TA layer negatively charged at neutral pH, and thereby permitting strong coordination bonding with multivalent metals (Xu, 2018 Abouelmagd, 2016). The aromatic rings in tannic acid allow for pi-pi stacking

(Guo, 2018). Tannic acid forms strong coordination bonds with metal ions such as Fe(III) to form thin film coatings that can be solution deposited (Ejima, 2013), or sprayed onto surfaces (Park, 2017). Tannic acid has also been deposited on various substrates in aqueous solutions of high ionic strength without the need for Fe(III) (Sileika, 2013, Dong, 2018, Pranantyo, 2015).

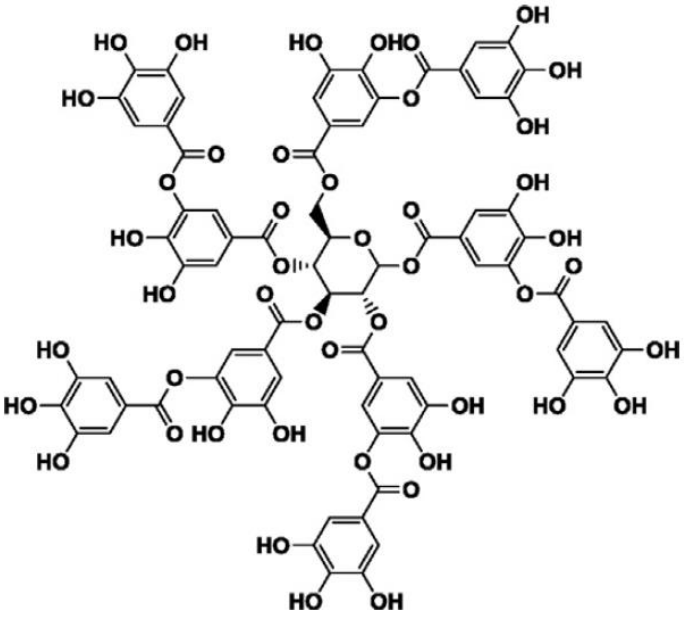

Figure 2-10: Tannic Acid, a high molecular weight polyphenol.

Advantages and Disadvantages of Tannic Acid

As with most coupling agents or primers, the long-term stability of tannic acid is limited when it is attached to a surface. Dong's group showed that tannic acid was stable only in near-neutral aqueous environments and in isopropyl alcohol (IPA) when there was no further post-functionalization (Dong, 2018). In more extreme acidic or basic solutions and in other alcohols, much of the exposed tannic acid dissociates from the surface within 24 to 48 h. However, Chen et al. showed that upon further modification with a quaternized polyethyleneimine zwitterion, the stability of the tannic acid linker improved significantly in acidic and basic conditions (Chen, 2018). Kang's group has shown that when tannic acid was post-functionalized by polymerization of zwitterionic brushes or layer-by-layer deposition of parasin I peptide, the surfaces were stable in seawater for at least 14 days (Pranantyo 2014; Xu, 2016).

Due to the lack of long-term antifouling behavior of surfaces grafted with tannic acid, it is not clear where it will be useful as an antifouling coupling agent in the biomedical field. But, several inherent characteristics make tannic acid (and other polyphenols) a potentially excellent candidate for the modification of multiple materials: i) its low toxicity and occurrence in foods indicates that tannic acid can be used in prolonging food storage (Dong, 2018; Park, 2017); ii) its good stability in water indicates that it can be used to

protect marine surfaces (Pranantyo, 2014; Xu, 2016); and iii) its optical clarity on glass substrates indicates that it can be used as a coupling agent in optical sensors or lenses (Dong, 2018; Park, 2017).

3.0 Modification of multiple substrates with pCBMA and pSBMA: physicochemical properties and resistance to protein fouling

After PEG, zwitterions have proven to be the next “gold standard” among antifouling materials. Modification with zwitterions has been applied to a range of materials including gold and PDMS (Hong, 2017), glass (Zhang, 2009), PET (Kang, 2018), PVDF (Tang, 2016), and cellulose paper (Sun, 2017). Depending on the surface chemistry of the substrate to be modified, different techniques and surface anchors have been used to attach the zwitterion to the substrate to create stable antifouling surfaces.

Due to differences in surface chemistry, it is difficult to modify multiple surfaces to achieve a given biologic functionality using the same method. This problem can be overcome using a multi-stage approach; in the first stage the surface is modified by a universally applicable method to achieve surface chemistry that is amenable, in subsequent stages, to the attachment of bio-functional agents. In this work oxygen plasma was used to activate the surfaces via introduction of hydroxyl groups (first stage); a molecule containing both a silanol function (for reaction with the surface hydroxyls) and a polymerization initiator function was then attached (second stage); in the third stage polymerization of monomers containing zwitterionic groups, initiated from the surface localized initiator, was carried out.

This chapter describes methods of this kind that were used to modify four different materials commonly used in biomedical devices and environmental sensing devices. The modified surfaces were characterized physically and chemically, and their anti-fouling properties assessed via their effects on inhibition of protein adsorption.

3.1 Materials

Grade 2 titanium and PEEK were purchased from McMaster Carr (Aurora, Ohio). Sylgard 184 silicon elastomer kits were purchased from Dow Corning (Midland, MI). Acrylic acid, acetic acid, aluminum oxide, bipyridyl, copper (II) bromide, 2-(dimethylamino) ethyl methacrylate (DMAEMA), L-ascorbic acid, N-(3-sulfopropyl)-N-methacryloyloxyethyl- N, N-dimethylammonium betaine, bovine serum albumin (BSA) (lyophilized powder, >98% purity) were purchased from Sigma Aldrich (Oakville, ON). 3–(Trimethoxysilylpropyl)-2-bromo-2-methylpropionate (TMSP-BMPP) was purchased from Gelest. 10x phosphate buffered saline (PBS) pH 7.4, from BioShop Canada Inc. (Burlington, ON), was diluted to 1x strength using Milli-Q water (18.2 MΩ.cm). Radio-iodinated sodium iodide ($Na^{125}I$) was obtained from the McMaster Nuclear Reactor (McMaster University, Hamilton, ON). AG 1-X4 Resin was purchased from Bio-Rad (Mississauga, ON).

3.2 Methods

3.2.1 Chemical Synthesis of Carboxybetaine Methacrylate (CBMA)

A 250 mL round bottom flask was cooled in an ice bath and DMAEMA (0.12 mol, 20.4 mL) was added. Acetic acid (0.12 mol, 6.75 mL) was added dropwise. Acrylic acid (0.24 mol, 16.25 mL) with radical inhibitor removed was then added dropwise over 30 min. The reaction was carried out in an ice bath (4°C) for 30 min, then at room temperature for 4 h. As the solution became more viscous, acetone (12.5 mL) was added and the reaction mixture stirred overnight. To precipitate the monomer, a mixed acetone/triethylamine (1:1, v/v) solution was added over 60 min with stirring. The obtained white solid was filtered through Whatman ashless, grade 42 filter paper, washed with acetone and dried under vacuum. Product yield is 54%.

3.2.2 PDMS preparation

Polydimethyl siloxane (PDMS) was prepared using a Sylgard 184 silicone elastomer kit with a 10:1 weight ratio of base-to-curing-agent, as per the manufacturer's instructions. After overnight curing at 60ºC, 1 mm thick PDMS films were obtained and punched into 6 mm diameter discs.

3.2.3 Titanium polishing

Titanium sheets were cut into 6.5 mm squares or 6.5 x 20 mm rectangular coupons using a metal shear. The coupons where then polished using a Struers Tegramin – 25 polishing machine with the following polishing agents in sequence: silicon carbide paper 320 grit, MD Largo 9-micron diamond, MD MOL 3 micron diamond, and MD CHEM colloidal silica 0.05 micron + 10% H_2O_2. Ethanol washing was used to remove residual polishing agents.

3.2.4 Substrate preparation

Silicon wafers and titanium were rinsed with acetone, ethanol, and DI water, then sonicated for 10 min. The surfaces were rinsed twice with DI water before use. PDMS and PEEK were rinsed with ethanol and DI water under sonication for 10 min. The surfaces were rinsed twice with DI water before use.

3.2.5 Oxygen plasma activation

Cleaned substrates were dried in N_2 before use. The substrates were then transferred to a Bio-Rad RF Plasma Barrel Etcher PT1750 and treated at 50W power and 0.3 mbar pressure for 3 min. Once activated, the substrates were rinsed and stored in DI water.

3.2.6 Formation of ATRP Initiator Monolayer

The plasma activated substrates were dried with N_2. They were immersed in the initiator solution (3%) containing (3-trimethoxysilyl) propyl-2-bromo-2-methylpropionate (TMSP-BMPP) in 95% ethanol for 6 h under agitation. The initiator-functionalized substrates were then rinsed with ethanol and water and dried over N_2 before modification using SI-ARGET ATRP.

3.2.7 SI – ARGET ATRP of CBMA and SBMA

A stock solution of $CuBr_2$ (0.064 mM) and bipyridine (0.39 mM) was prepared in mixed distilled water/MeOH (4:1, v/v). 500 mg of CBMA and 3.2 mL of the stock solution were placed in 4 mL glass vials and the activated substrates added. 133 µL of an aqueous solution of ascorbic acid (77.5 mM) was quickly dispensed into the vials and the lids were sealed tightly to limit access of oxygen. The vials were incubated on an orbital shaker at room temperature for 3-5h. The modified surfaces were then rinsed and stored in Milli-Q water. The complete surface modification is illustrated in Figure 3-1.

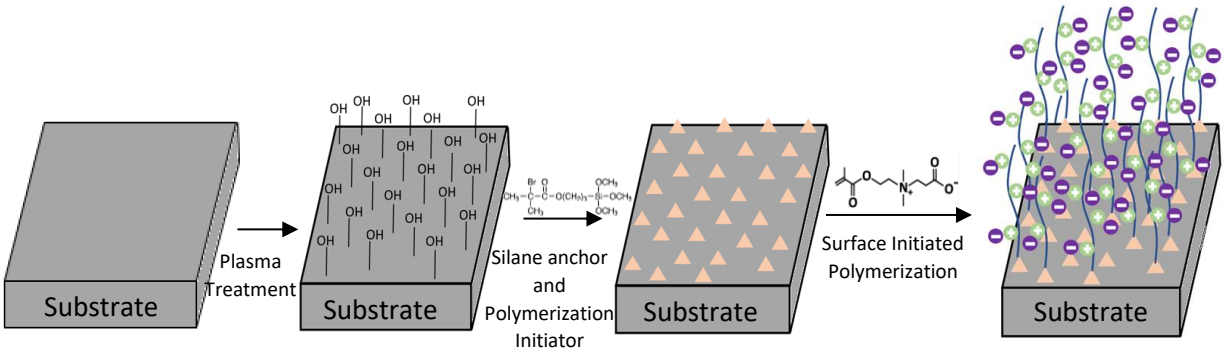

Figure 3-1: Antifouling modification protocol. Substrates are cleaned and subjected to oxygen plasma surface activation to form reactive OH sites on the surface. The surface is quenched in water and immediately immersed in the TMSP-BMPP solution and incubated for 6 hours. TMSP-BMPP functionalized surfaces are dried under a stream of nitrogen prior to the formation of anti-fouling polymer brushes. Zwitterionic polymer brushes are formed by polymerization from the surface using SI-ARGET ATRP with limited access to oxygen for 3-5 hrs.

3.2.8 Nuclear Magnetic Resonance Spectroscopy (NMR)

NMR was performed on the synthesized CBMA. Samples were prepared in NMR tubes by dissolving ~ 5 mg of CBMA in 1 mL deuterium oxide. ^{1}H NMR spectra were taken on a Bruker Advance 200 MHz spectrometer with 16 scans, pulse width 7.4 µs, and relaxation delay 1 s. The spectra were Fourier transformed and analyzed using Bruker's TopSpin v2.1 software. Duplicate samples were analyzed.

3.2.9 ARGET-ATRP Solution Synthesis of pCBMA

The pCBMA polymer was prepared in solution for gel permeation chromatography (GPC). The stock solution and polymerization solution were prepared the same way as described in the section on SI-ARGET ATRP of CBMA and SBMA. Before addition of the ascorbic acid, 30 µL of the ATRP initiator, TMSP-BMPP, was pipetted into the polymerization solution. Finally, the ascorbic acid was dispensed into the vial and the lids were sealed quickly to limit the access of oxygen. Polymerization was halted at the desired polymerization time by opening the vial. The polymer was precipitated from the polymerization solution using 20 mL of acetone. The acetone was decanted, leaving the pCBMA polymer.

3.2.10 Gel Permeation Chromatography

The molecular weight of pCBMA was measured using an Agilent 1260 Infinity gel permeation chromatography (GPC) instrument with refractive index detector. The mobile phase was a solution of 0.2 M Na_2HPO_4 in PBS buffer. Samples were prepared as 1 mg/mL solutions in 0.2 M Na_2HPO_4 in PBS. The flow rate was set to 1 mL/min and the analysis time was 40 min. The detector wavelength was set to 650 nm and the temperature to 30°C. Linear polyethylene glycol standards were used for calibration. Agilent GPC Software V 2.1.9.34851 was used for data analysis.

3.2.11 Water Contact Angle Analysis

Static contact angles were measured using a Dataphysics OCA 35 contact angle instrument (Filderstadt, Germany). Milli-Q water droplets of 4 µL volume were placed on the surface at room temperature and analyzed using the SCA 20 software provided with the instrument. 3-to-5 replicate measurements were performed for each surface.

3.2.12 Ellipsometry

The initiator layer and pCBMA layer thicknesses were determined using a variable angle spectroscopic ellipsometer (J.A. Woollam Co., Lincoln, NE). The measurements were performed over the wavelength range 246 – 1688 nm at incidence angles from 50 - 75° at 5° intervals. The data were modelled using the CompleteEASE software v. 5.26 provided. Silicon wafer was modelled using the software's built-in optical constant model, SI_JAW with the oxide layer modelled with the software's built-in native silicon oxide layer, NATIVE_JAW set to a 2 nm thickness. Titanium was modelled with the B-Spline model with n = 2.226 and k = 3.105. Both the initiator and the pCBMA film were modelled using a Cauchy film model. The average thicknesses are reported with modelling confidence MSE < 5 nm for silicon wafer.

3.2.13 Atomic Force Microscopy

Surface roughness was measured using either a Veeco Dimension Icon AFM (Plainview, NY) or a Bruker BioScope Catalyst AFM. Measurements were taken in tapping mode under dry conditions, at room temperature, using ScanAsyst mode with PeakForce tapping. A silicon nitride cantilever with spring constant k = 0.4 N/m was adjusted to a scan rate of 1 Hz while acquiring 512 samples/line. Nanoscope Analysis v. 1.5 was used for surface roughness analysis and data are reported as the root mean square average (R_{rms}) of the height deviations taken from the mean data plane as described by Equation 3-1,

$$R_{rms} = \sqrt{\frac{1}{n}\sum_{i=1}^{n}(h_i - \bar{h})^2} \quad (3\text{-}1)$$

Where $\bar{h}$ is the mean data plane height, h_i is the measured height value, and n is the number of points within the selected image region.

3.2.14 X-ray Photoelectron Spectroscopy (XPS)

XPS was used to investigate the chemical composition of the surfaces. Survey and high-resolution scans were performed on PDMS using a JEOL JPS – 9200 XPS equipped with a monochromatic Al Kα x-ray source at 1486.7 eV. Survey spectra were obtained at a 90° take off angle with the x-ray power at 180 W and 12 kV. PDMS samples were analyzed for Si, C, O, Br, and N, and the data were analyzed using the Casa XPS software. Titanium, silicon wafer, and PEEK samples were analyzed on a PHI Quantera II scanning XPS equipped with Al Kα x-ray source at 1486.7 eV. The x-ray power was set to 50 W at 15 kV. Spectra were obtained at a 45 degree take off angle with a spot size of 50 µm. The survey spectra were obtained with a pass energy of 224 eV and a step size of 0.8 eV. The high-resolution spectra were obtained with a pass energy of 55 eV and a step size of 0.2 eV.

3.2.15 Protein Radiolabelling

Bovine serum albumin (BSA) was used as a model protein in this work. BSA was radiolabelled with $Na^{125}I$ using the iodine monochloride method. The unbound iodide ions were removed from the radiolabelled BSA solution using an AG 1X4 anion exchange resin column. A free iodide test was conducted to ensure minimal levels of unbound iodide. The free iodide test involved mixing 10 µL of radiolabelled BSA with 990 µL of 10 mg/mL BSA solution. These are referred to as the “stock” samples. In half of the prepared stock samples, 500 µL of 20% trichloroacetic acid was added to the solution to precipitate the radioactive protein-bound iodide. After 5 min, the protein solution was centrifuged at 2,795 relative centrifugal force (RCF) for 5 min. The radioactivity of the supernatant was compared with that of the stock samples. Free iodide was calculated using Equation 3-2. Levels <1% were considered acceptable.

$$Free\ Iodide = \frac{Average\ of\ supernatant}{Average\ of\ Stock} \tag{3-2}$$

3.2.16 Protein Adsorption

Surface samples were soaked overnight in PBS to equilibrate with the experimental environment. The surfaces were then incubated in BSA solution containing 10% ^{125}I BSA with a total concentration of 1 mg/mL. Samples were incubated for 2 h at room temperature, rinsed with PBS, and the surface radioactivity determined using a Perkin Elmer Wallac Wizard 3” 1480 Gamma Counter. The quantity of protein adsorbed to the surface was determined by comparing the surface radioactivity to that of a solution of labelled BSA of a known concentration. Five replicate measurements were performed for each surface modification.

3.3 Results and Discussion

3.3.1 Synthesis of Carboxybetaine Methacrylate

Carboxybetaine methacrylate is a zwitterionic molecule containing a cationic quaternary ammonium group and an anionic carboxylic acid group. The conventional method of

synthesizing carboxybetaine methacrylate (CBMA) involves reacting the tertiary amino group in dimethylaminoethyl methacrylate (DMAEMA) with beta-propiolactone as shown in Figure 3-11 (Zhang, 2006). Beta-propiolactone is an expensive and toxic reagent with cost and safety issues in production and scale-up. Alternatively, as shown in Figure 3-2, CBMA can be prepared by reacting DMAEMA with acrylic acid (Li, US Patent 2014/0275614 A1). Acrylic acid is less toxic than beta-propiolactone and because it is a commodity reagent, it is much cheaper. The CBMA monomer is purified after the reaction by precipitation from solution using an organic base. It is then vacuum dried.

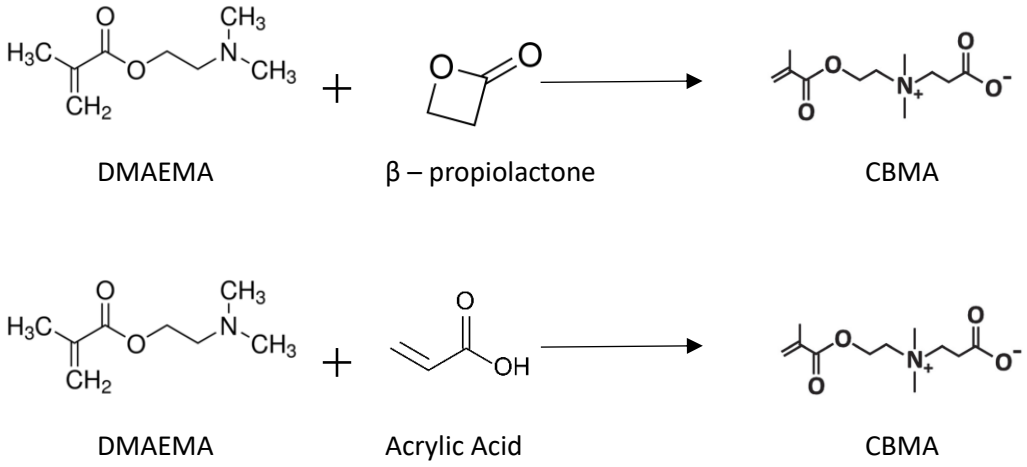

Figure 3-11: Synthesis routes of carboxybetaine methacrylate

Figure 3-3 shows NMR spectra of the purified CBMA monomer prepared by these two methods. The CBMA monomer prepared in this work using acrylic acid and DMAEMA showed an “extra” peak at 2.05 ppm. This extra peak indicates the presence of an additional hydrogen atom in the molecule. Laschewsky notes that an anionic acrylate intermediate can undergo side reactions during the alkylation coupling reaction which may be the reason for the impurity peak in this spectrum (Laschewsky, 2014). The anionic group can be protected by esterification to avoid these side reactions, but this approach introduces an extra step to remove the protecting groups.

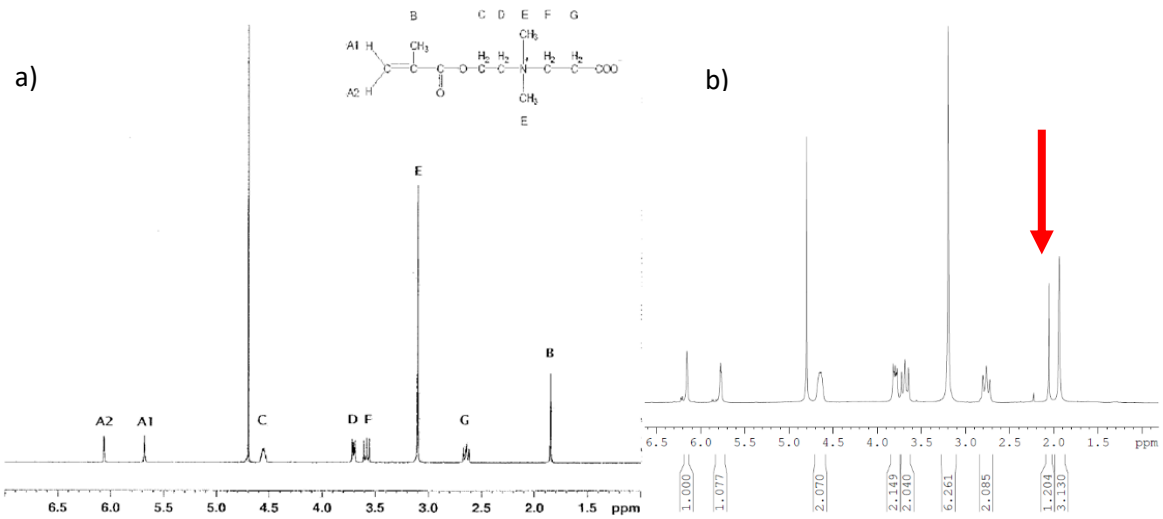

Figure 3-3: NMR spectra of: (a) CBMA monomer synthesized using beta-propiolactone (Jiang, US 2011/ 7879444B2), (b) monomer synthesized using acrylic acid. An "extra" peak at 2.08 ppm indicates that this monomer is different from the monomer synthesized using beta-propiolactone.

3.3.2 Polymer Chain Length

Of the many different ATRP methods, ARGET-ATRP was chosen in this work due to the minimal amounts of copper catalyst required and the ability to polymerize in the presence of air/oxygen. The equilibrium reaction for ARGET ATRP is shown in Figure 3-12. Polymer chains of pCMBA were prepared by ARGET-ATRP in solution for either 3h or 5h.

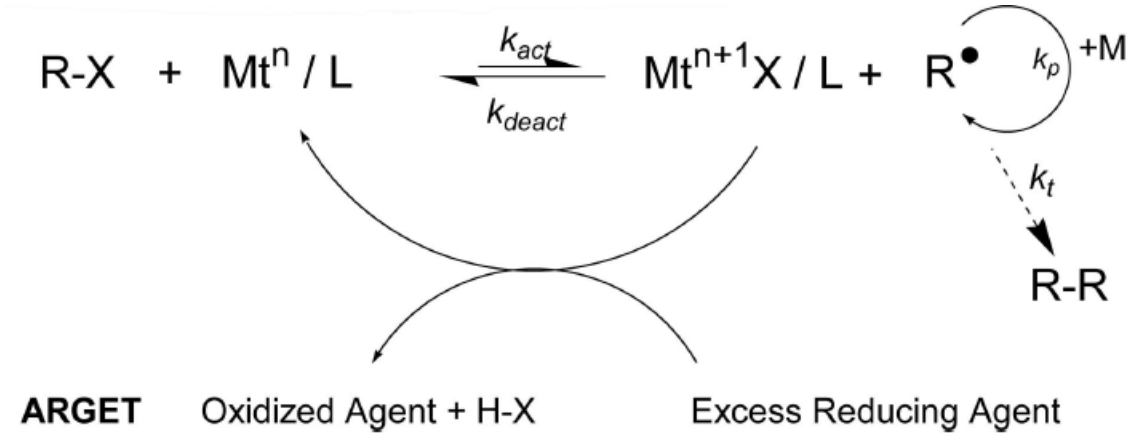

Figure 3-12: ARGET ATRP process and equilibrium. Adapted from (Matyjaszewski, 2006).

In graft-from methods, the thickness of film generated by SI-polymerization is typically used to characterize the amount of polymer on the surface. However, one of the antifouling mechanisms of hydrophilic polymers is the creation of the hydration barrier that depends on chain length. Thus, chain length is investigated using GPC. In many previous investigations, the antifouling polymer is formed on the surface and then cleaved from the surface for GPC analysis (Zoppe, 2017). Therefore, we investigated chain length

using GPC in a separate solution-based ARGET-ATRP experiment. The polymerization was performed in the same conditions as the SI-ARGET-ATRP conditions without the surface substrates. This method avoids cleavage of grafted polymers from the surface, which involves the use of solvent conditions that are incompatible with some materials. However, the procedure introducing a sacrificial initiator during surface-initiated polymerization and using the loose chains in the bulk solution may be more representative than this separate solution-based experiment, although it has been reported by others (Yang, 2018). Table 3- shows the number average and weight average degree of polymerization (DP), as well as the polydispersity index (PDI) of the pCBMA. DP is the average number of CBMA monomers per polymer chain. It is often referred to as the chain length and has been shown to influence protein adsorption. Feng et al. showed that longer chains (100 – 200 monomer units) of poly (methacryloyloxyethyl phosphorylcholine) (pMPC) were able to resist fibrinogen adsorption more at lower grafting densities, but at high grafting densities, the chain length was less of a factor (Feng, 2006). This may be due to the ability of the longer chains to compensate and “fill in” the space between chains in the less densely grafted surfaces (Kingshott, 2002).

The PDI, calculated as the ratio Mw/Mn, gives a measure of the polymer size distribution associated with ARGET ATRP for each set of conditions. It appears that the molecular weight was not significantly different for polymerization times of 3h and 5h. PDI values around 1.5 indicate a broader distribution than expected for ARGET ATRP, which is a living polymerization method that usually gives PDI around 1.3 indicating a narrower distribution (Fantin, 2015). Sun et al. (Sun, 2017) grafted pre-formed pCBAA on a cellulose paper surface. The polymer MW and PDI were, respectively, 29,600 g/mol and PDI 1.08. These values are indicative of a controlled polymerization. Factors that may contribute to the lack of control in our experiments include the use of water solution as a polymerization medium (Tsarevsky, 2009), and the ligand type and concentration (Simakova, 2012). Matyjaszewski’s group has shown that while controlled aqueous ARGET-ATRP is possible (Simakova, 2012), the halide ligand can dissociate in aqueous solution, and water can coordinate with the copper ligand complex through hydrogen bond formation, causing a decrease in deactivator concentration (Tsarevsky, 2009). The decrease in deactivator results in an inability to deactivate propagating radicals, leading to uncontrolled polymerization and therefore increased PDI (Tsarevsky, 2009).

Table 3-1: GPC data for pCBMA formed in solution by ARGET-ATRP. Mn is the number average, Mw is the weight average, and Mz is the Z-average molecular mass. PDI is the polydispersity = Mw/Mn.

	Mn (g/mol)	Mw (g/mol)	Mz (g/mol)	DP	PDI
5h ARGET ATRP	60,300	92,400	130,000	260	1.53
3h ARGET ATRP	63,800	97,400	135,000	280	1.53

3.3.3 SI-ARGET-ATRP on PDMS substrate.

Surface initiated ARGET ATRP was performed using air plasma activated PDMS as the substrate and CBMA as the monomer. Based on the findings and procedures from the work of Hong et al (Hong, 2017), the effect of ARGET-ATRP polymerization time was investigated to determine conditions for optimal antifouling properties of the obtained surface.

Water contact angles decreased significantly after pCBMA modification. As shown in Figure 3-5, unmodified PDMS is extremely hydrophobhic, with an average water contact angle of 113.8°. After pCBMA modifcation, contact angles were found to be less than 30° for all polymerization times. Using ANOVA and a post hoc Tukey Kramer test at $\alpha = 0.05$, the water contact angle of the surface formed at 5h polymerization time was found to be different from those at the 3h and 7h polymerization times. This result may be due to different handling of the substrates during analysis; a duplicate experiment should be conducted to verify it.

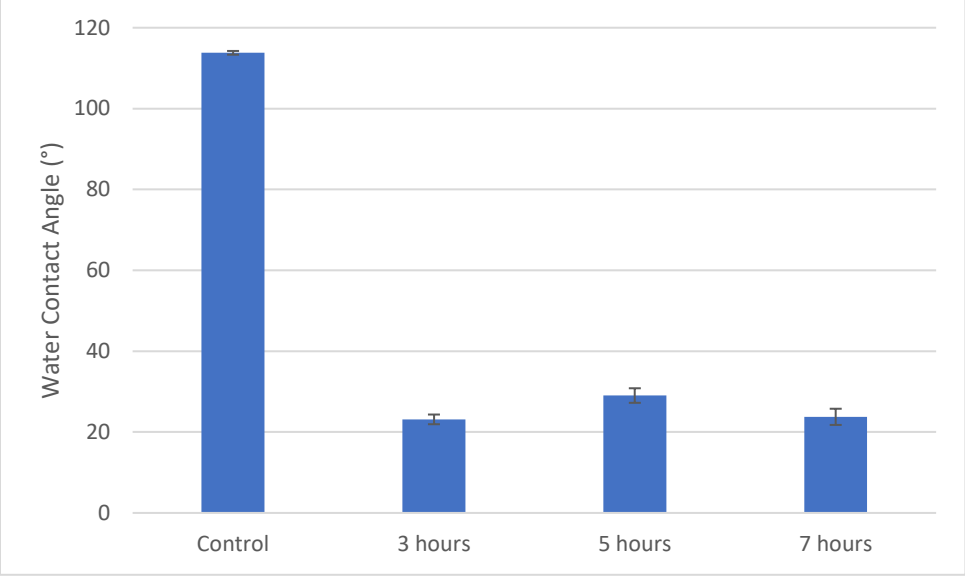

Figure 3- 5: Water contact angles of control and pCBMA-modified PDMS substrate. The PDMS substrates were first oxygen plasma treated and a silane-ATRP initiator was attached before ARGET-ATRP polymerization. A large reduction in water contact angle after modification with pCBMA indicates increased hydrophilicity. A significant difference between the 5h versus the 3h or 7h surfaces was determined based on a single factor ANOVA with post hoc Tukey Krama test at $\alpha = 0.05$. Error bars are standard deviations for $n > 3$.

The elemental composition of the pCBMA-modified surfaces was determined by XPS (Table 3-2). Detection of bromine indicates the presence of the initiator, whereas nitrogen indicates the presence of pCBMA on the modified surfaces. The reduction in silicon content and the increased nitrogen content following modification indicates masking of the substrate by the pCBMA layer. Additional discussion of these and other XPS data is given below.

Table 3- 2: Elemental composition (atom %) of unmodified and modified PDMS surfaces from XPS analysis. Typical precision for each component is ± 5%.

Sample	Oxygen	Carbon	Silicon	Bromine	Nitrogen
PDMS Control	15.4	25.5	56.7	-	-
PDMS Initiator	18.6	24.1	56.8	0.5	-
3h PDMS-pCBMA	17.9	40.9	38.9	-	2.3
5h PDMS-pCBMA	18.4	46.7	32.3	-	2.6
7h PDMS-pCBMA	15.7	30.0	54.0	-	0.3

BSA adsorption was used to assess the antifouling potential of the pCBMA-modified surfaces (Figure 3-6). Adsorption was lowest for a polymerization time of 5h. The high adsorption and large standard deviation for the polymerization time of 3h may be caused by insufficient polymer coverage. The increase in protein adsorption, as well as the decrease in surface nitrogen content from 5h to 7h polymerization time, were unexpected and are discussed further below. Taken together, the XPS and BSA adsorption data show that a polymerization time of 5h gave modified PDMS with the highest pCBMA coverage and the lowest albumin adsorption. This polymerization time was used in all subsequent experiments with the other substrates.

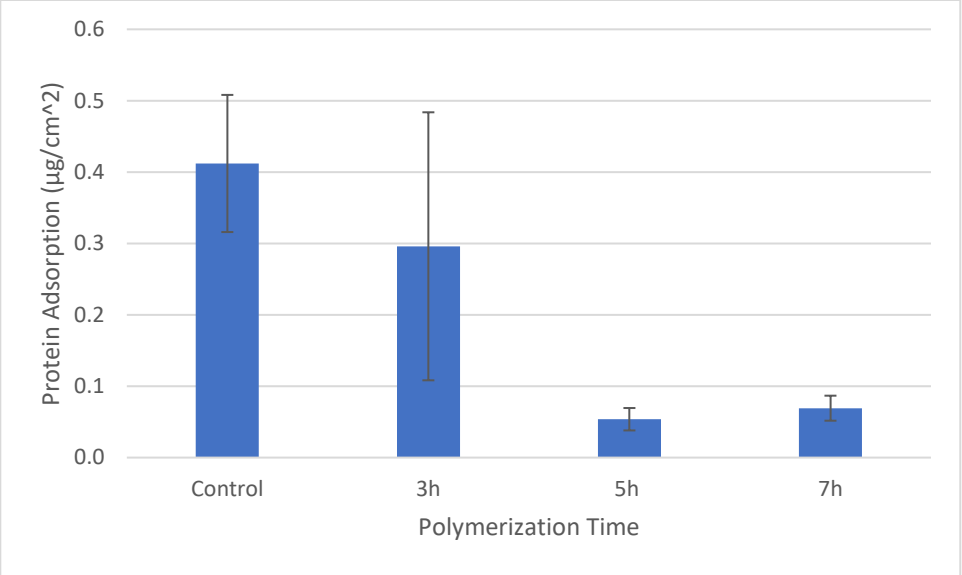

Figure 3- 6: BSA adsorption as a function of pCBMA polymerization time on PDMS substrate. Error bars are standard deviation for n =5.

The 7h polymerization gave a surface with slightly higher protein adsorption; this was unexpected, and the reason is unclear. It may be related to relatively low thickness of the polymer layer and low surface density of the pCBMA. Thickness of the polymer layer for this material could not be determined by ellipsometry since the layer had low optical contrast with the PDMS substrate. Hydrophilic polymer brushes can take on different conformations depending on surface density, brush thickness, and environmental conditions. In a study using the sulfobetaine, poly[2-(methacryloyloxy) ethyl dimethyl-(3-sulfopropyl) ammonium hydroxide] (pMEDSAH), it was found that thin brushes (<50 nm) gave consistently hydrophilic surfaces of contact angle ~ 12°, while thicker brushes (>100 nm) showed a linear increase in hydrophobicity as thickness increased (Cheng, 2008). This behaviour was attributed to the existence of two different polymer conformation "regimes". The "non-associated regime" occurs when the zwitterionic groups do not interact with each other due to water interactions, resulting in swollen polymer brushes that form a hydration/energy barrier to resist protein adsorption. In contrast, the "self-associated regime" occurs when inter- and intra-chain associations cause the polymer chains to collapse on themselves resulting in a hydrophobic surface.

The large standard deviation of the 3h surfaces may also be attributed to low pCBMA density. The low density of pCBMA on the 3h and 7h surfaces raises questions regarding the robustness of the polymerization step but does show that even small amounts of pCBMA can make a surface hydrophilic and that hydrophilicity does not necessarily confer antifouling properties.

It may also be that on the 5h surface the polymer chains were in the collapsed state giving a more hydrophobic surface, which, when rehydrated during protein adsorption, the

polymer molecules are able to extend away from the surface into the water. Since there was a higher density of pCBMA on this surface compared to those formed at the other polymerization times, it may have been able to form a more effective hydration/energy barrier, resulting in low protein adsorption. Based on these results for PDMS substrate a 5h polymerization time was used to prepare pCBMA-modified surfaces in all subsequent experiments including on the other substrates.

3.3.4 Modification of Multiple Substrates

The substrates chosen for this study are commonly found in environmental sensing devices and medical devices, all of which are used in aqueous environments. Two polymeric materials, shown in Figure 3-7, were investigated: PDMS, commonly used in constructing microfluidic devices, and PEEK, used in orthopaedic and specialized plastics applications. Titanium, commonly used in medical implants, and silicon, the most commonly used material in the semi-conductor industry and also in brain implant technologies were also studied.

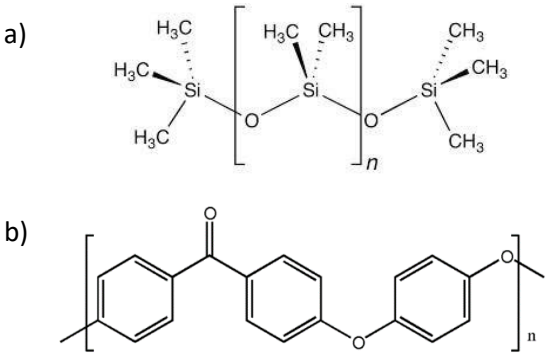

Figure 3-7: Chemical Structure of a) polydimethylsiloxane (PDMS) and b) poly ether ether ketone (PEEK)

3.3.5 Surface Chemical Composition

The surface elemental compositions of the four substrates in both unmodified and modified forms were determined using XPS as shown in Table 3-3. Successful modification by initiator, pCBMA, and pSBMA is indicated by increased bromine, nitrogen, and sulphur content, respectively. Bromine is difficult to detect using XPS as bromine-containing polymers tend to degrade with prolonged exposure to the x-ray beam.

It has been shown that silane attachment works well on oxide or oxidizable surfaces. Silicon and titanium form natural oxide surface layers, whereas PDMS can be activated with oxygen plasma to expose OH groups. PEEK is an oxidation-resistant material and therefore oxygen plasma may not be as effective in bonding silanols as for the other oxidizable surfaces, as shown by the low Br content. Occhiello et al. showed that inert gases such as argon and nitrogen are better at activating PEEK than air and oxygen plasma (Occheillo, 1992). Inert gas plasma induces cross-linking activated by chain

scission with some oxidation promoted by long-lived radicals. Thus, our experiment has shown that oxygen plasma may not be the most effective surface activation method, resulting in fewer active sites available for binding of TMSP-BMPP.

PEEK is an organic polymer containing only carbon and oxygen. In addition to these elements, nitrogen was also detected on the unmodified PEEK surface in this work. It is unclear why or how nitrogen appears on these surfaces. However, the decrease in nitrogen and appearance of silicon and bromine after modification with TMSP-BMPP indicates that modification with the silane coupling agent was successful. For pCBMA modified PEEK, it is difficult to determine if pCBMA is present as the elements detected are the same as those on the precursor. Modification with pSBMA is judged successful due to the high percentage of sulfur found in the spectrum.

Successful modification of PDMS should result in an increase in bromine after TMSP-BMPP modification and a reduction of silicon after zwitterion is polymerized on the surface. A decrease in silicon was seen after pCBMA modification, but no significant change between the pSBMA modified and TMSP-BMPP modified PDMS was seen. This indicates the pSBMA may not have polymerized effectively on the PDMS surface resulting in higher water contact angles and higher protein adsorption.

Trace amounts of phosphorus were found on the unmodified silicon surface although this element was not quantified. The Si wafers may have been doped with phosphorus, a common n-type dopant used with this material. Phosphorus may also give silicon a more hydrophilic character (and possibly inherently better antifouling capabilities). Although bromine was found in the survey scan shown in Figure 3-8, a high-resolution scan was not taken and therefore bromine was not quantified in the silicon samples. Further evidence that TMSP-BMPP attached to the silicon substrate is that pSBMA successfully polymerized on the silicon surface and gave good coverage as indicated by the low silicon content and high nitrogen and sulfur contents from the sulfobetaine molecules. PCBMA modification did not seem to be effective on silicon as indicated by the low content of nitrogen and high content of silicon, indicating very low coverage.

Changes after modification of titanium are easy to see because its elemental composition, as a pure element, is different from those of all the modifiers. The carbon and some of the oxygen found on the virgin titanium is adventitious carbon deposited when the surface is exposed to the air and environment. Titanium also forms an oxide layer when exposed to air, hence the high oxygen content of the unmodified titanium. Modification with TMSP-BMPP was successful, but it is unclear why nitrogen, calcium, and fluorine peaks appeared. This sample may have been positioned near the PEEK samples that had high nitrogen and some calcium. Cross contamination of materials due to the high energy x-ray could have occurred but would require further investigation to verify. High coverage

of titanium with pCBMA and pSBMA are indicated by the high nitrogen and sulfur contents and low titanium content in these samples.

Table 3-3: Elemental composition (atom %) of PEEK, PDMS, silicon wafer, and titanium modified with initiator (Si-Br), pCBMA, and pSBMA. XPS instrument error is ± 5%.

	C	O	Br	N	S	Si	Ti	Ca	F
PEEK Control	80.4	16.9	-	2.7	-	-	-	-	-
PEEK- TMSP-BMPP	75.7	20.4	0.07	0.6	-	2.6	-	0.6	-
PEEK-pCBMA	79.5	19.0	-	1.5	-	-	-	-	-
PEEK-pSBMA	72.9	21.2	-	3.1	2.9	-	-	-	-
PDMS Control	41.3	23.9	-	-	-	34.8	-	-	-
PDMS-TMSP-BMPP	41.5	28.6	0.6	-	-	29.3	-	-	-
PDMS-pCBMA	53.7	26.8	-	2.9	-	16.5	-	-	-
PDMS-pSBMA	48.4	23.9	Trace	0.52	Trace	27.2		-	-
Silicon Control	5.7	35.0	Trace	-	Trace	59.3	-	-	-
Silicon- TMSP-BMPP	11.4	41.1	N/A	-	-	47.5	-	-	-
Silicon pCMBA	16.4	35.3	-	0.9	-	47.5	-	-	-
Silicon pSBMA	64.1	26.0	-	5.1	4.1	0.8	-	-	-
Titanium Control	28.3	51.0	-	-	-	-	20.7	-	-
Titanium-TMSP-BMPP	18.6	56.8	0.3	2.9	-	4.2	13.6	1.5	2.1
Titanium-pCBMA	49.2	42.8	-	2.3	-	-	5.8	-	-
Titanium-pSBMA	41.9	46.7	-	2.6	0.9	-	7.9	-	-

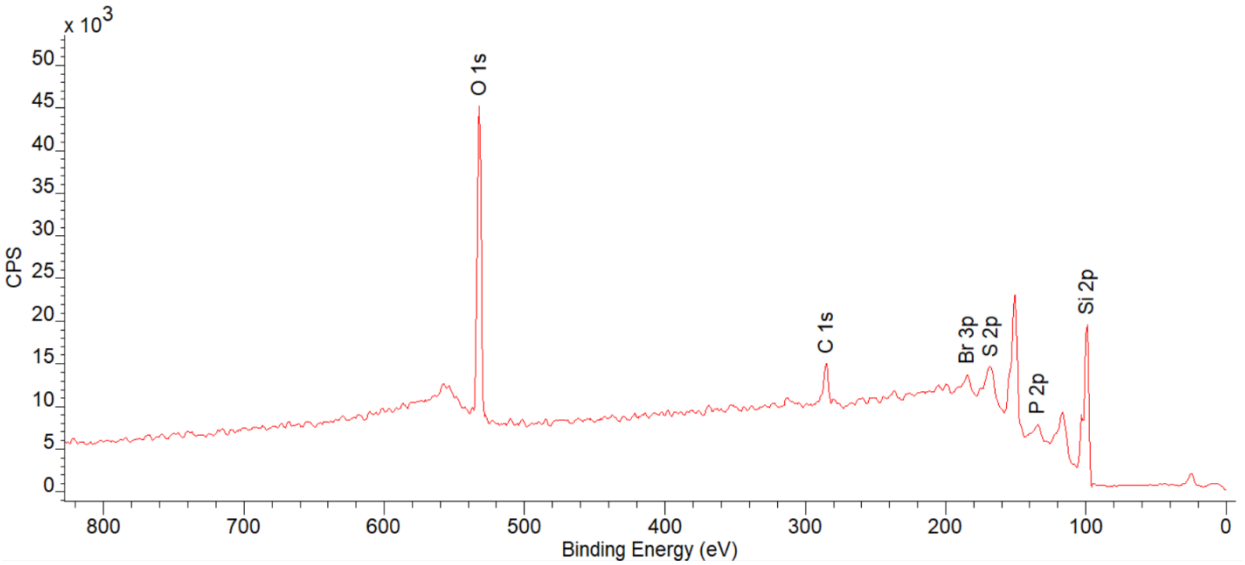

Figure 3-8: Survey scan of silicon-TMSP-BMPP. Bromine, sulfur, and phosphorus were found in this sample although high-resolution scans were not taken.

3.3.6 Water Contact Angles

Water contact angle measures the wettability of a surface and can verify rapidly if changes in surface chemistry have occurred after modification. The average water contact angles for multiple sample sets of each of the surfaces studied are shown in Figure 3-9. Data for oxygen plasma and pSBMA modified polished titanium were not performed due the limited supply of polished titanium substrates.

Oxygen plasma was used to remove surface contaminants and ensure sufficient hydroxyl groups on each surface. These hydroxyl groups significantly decreased the contact angle of the surfaces. Subsequent TMSP-BMPP modification following surface activation increases the water contact angle as expected (Ghaleh, 2018). Further reduction in the contact angle (≤ 36°) was seen after modification with the hydrophilic antifouling polymers, pCBMA and pSBMA.

Of the surfaces studied, only unmodified PDMS was strongly hydrophobic, showing an average contact angle of 112.8 ± 3.6°. A large standard deviation is seen for plasma-activated PDMS which is attributed to two outliers. This experiment was done separately from the other experiments and due to the sample size (n=5), it is unclear whether these outliers are meaningful. Polished titanium exhibited the same trend after TMSP-BMPP modification and is the second most hydrophobic of the materials studied.

PEEK is generally considered a moderately hydrophobic material. Water contact angles ~ 70° have been reported (Barkarmo, 2019), but a value of 40° was found for the material used in this study. The PEEK surfaces were stored in contact with water before use in a lab area with an abundance of sunlight which may have caused photochemical reactions at the surface resulting in increased hydrophilicity.

Silicon and titanium both form natural thin oxide layers when exposed to air/oxygen and moisture (Yang, 2014; Holysz, 2008). Surface wettability is then determined by the extent/thickness of the oxide layer, the relative humidity of the measurement environment, and the surface roughness (Holysz, 2008). Therefore, water contact angles on titanium and silicon can vary widely depending on conditions (Holysz, 2008). Holysz et al. reported angles ranging from 29.8 to 54.5° as humidity increased (Holysz, 2008). In the present work, despite careful drying after cleaning, residual water may have remained giving angles generally lower than reported by others with an average of 26.1°± 5.6°. In addition, the oxide layer can react with solvents used to clean the surface. Becker et al showed that for titanium cleaned with acetone, the water contact angle increased to 86° whereas cleaning with isopropanol and other solvents led to angles of ~63° (Becker, 2016). Water rinsing was not done after solvent cleaning in these experiments. Peng et. al. also reported high contact angles of ~73° for polished titanium after cleaning with acetone and subsequently rinsing with distilled water (Peng, 2013). Water rinsing generally gives lower water contact angles. Therefore, since most of the unmodified materials used in this work were stored in distilled water after cleaning to protect from contaminants, the water contact angles observed are generally lower than reported in the literature.

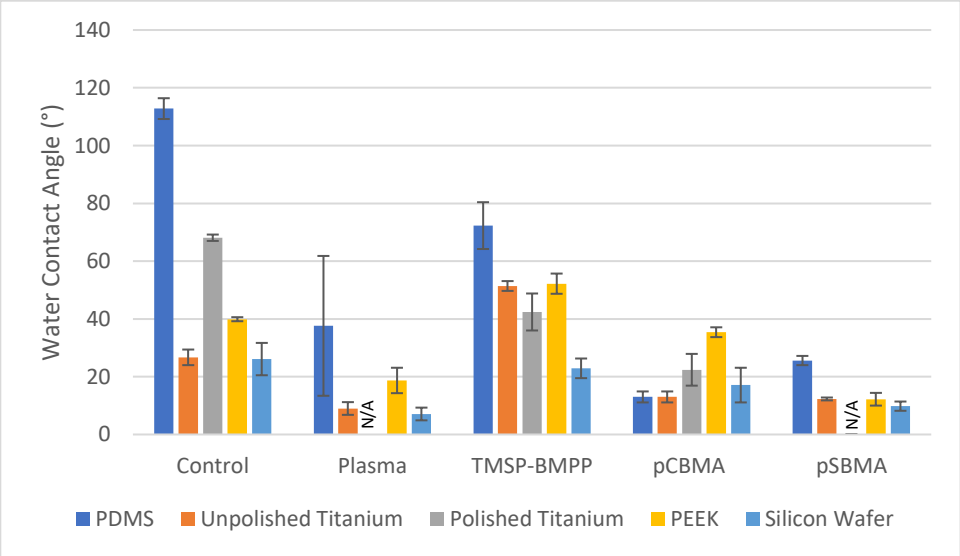

Figure 3-9: Water contact angles of PDMS (blue), unpolished-Ti (orange), polished-Ti (grey), PEEK (yellow), and silicon wafer (green). Figure includes all data over multiple sets of experiments. Error bars are standard deviation for n ≥ 4.

Water droplet images on surfaces prepared using standard modification procedures are presented in Figure 3-. Polished titanium photos were not obtained as unpolished titanium was used in subsequent experiments. This sample set is a subset of the materials shown in Figure 3-9 and was used for the XPS, ellipsometry, and BSA adsorption measurements.

As seen in Figure 3-10, the TMSP-BMPP modified silicon wafer showed a slight decrease in contact angle whereas an increase was expected, indicating that TMSP-BMPP modification did not occur to any significant extent on this silicon surface in this particular experiment. This conclusion is supported by XPS data in which the expected bromine signal from the initiator was not detected.

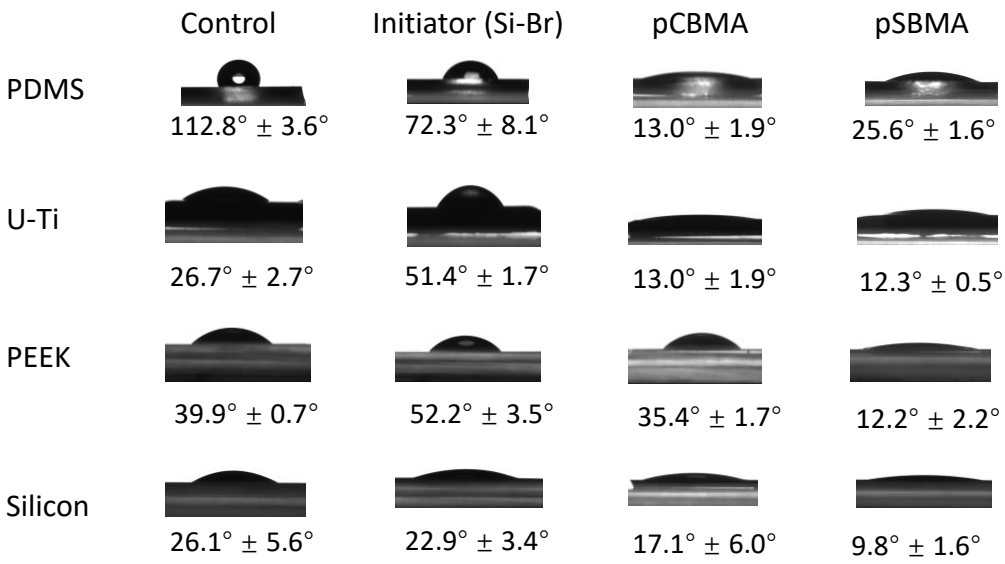

Figure 3-10: Water droplet images on four substrates with various modifications. Images were taken of samples modified under conditions outlined in the materials section. Samples were used for XPS, ellipsometry, and BSA adsorption experiments after water contact angle measurement. Data are mean ± standard deviation (n=5).

3.3.7 Surface Topography and Roughness

The roughness of the modified surfaces was investigated using AFM. Roughness data taken from 2 x 2 µm images are shown in Figure 3-11 and the quantitative data in Figure 3-12. Increased roughness after a modification can be attributed to a number of scenarios: substrate damage or incomplete thin-film formation (insufficient coverage exposing the substrate surface). In contrast, a smoother surface may indicate controlled formation of a dense polymer brush.

The first step in the surface modification process is surface activation using oxygen plasma followed by modification with TMSP-BMPP. Cracks can be seen in the PDMS-TMSP-BMPP surface. Oxygen plasma treatment involves generation of high energy oxygen ions using radio frequency power. The oxygen ions bombard the surface at a high rate resulting in activated hydroxyl sites on the surface. The energy of the oxygen plasma, if too high, can etch or damage the surface; this seems to have happened in the image shown for the PDMS TMSP-BMPP sample. The plasma power is difficult to control, which sometimes results in such damaged surfaces. Cracks and damage on PDMS were not seen when the power was set to 50 W for 3 min.

The cracks in the PDMS sample shown were still present after pCBMA modification but not after pSBMA modification. This could indicate that the pCBMA film was very thin and/or that the pSBMA surface was not damaged at the initiator stage. The PDMS-pSBMA surface does show some unique defects that caused the surface to be rougher and thus to give the high standard deviation shown in Figure 3-12.

The as-received titanium samples were physically heterogenous and the large standard deviations in Figure 3-12 show that the roughness led to difficulties in quantifying changes. The more “chaotic” roughness of unpolished titanium led to data that were not meaningful at the 2 x 2 µm scan size; therefore, 20 µm scans (Figure 3-13 and Figure 3-14) were used for this surface. Modifications with pCBMA and pSBMA on U-Ti produced smoother surfaces when compared to unmodified U-Ti.

The surface of PEEK is typically quite smooth with roughness <5 nm for machined and injection molded materials (Torstrick, 2018). The AFM image in Figure 3- shows that the PEEK used in this work was moderately rough at 10.6 ± 0.47 nm. Images of unmodified PEEK showed vein-like patterns which were not seen after surface modification. These patterns could be caused by mechanical damage due to handling and abrasion during cleaning. Culhaoglu showed that different chemical and physical treatments cause changes in surface roughness to different degrees (Culhaoglu, 2020). Physical treatment such as particle abrasion and laser irradiation roughen the surface more than chemical treatment (Culhaoglu, 2020). All of the materials in this work, except for PDMS, were washed first with acetone which is known to cause slight crazing (Ebnesajjad, 2013). Effects of this kind may have led to the observed low contact angle and rougher surface topography on the unmodified PEEK surface, but further investigation is required to validate this hypothesis.

Silicon is a very smooth, flat surface. TMSP-BMPP- and pCBMA-modified silicon showed similar decreases in surface roughness, while pSBMA and unmodified silicon showed similar roughness. This may suggest that the pSBMA modification was not as effective as the pCBMA modification on silicon.

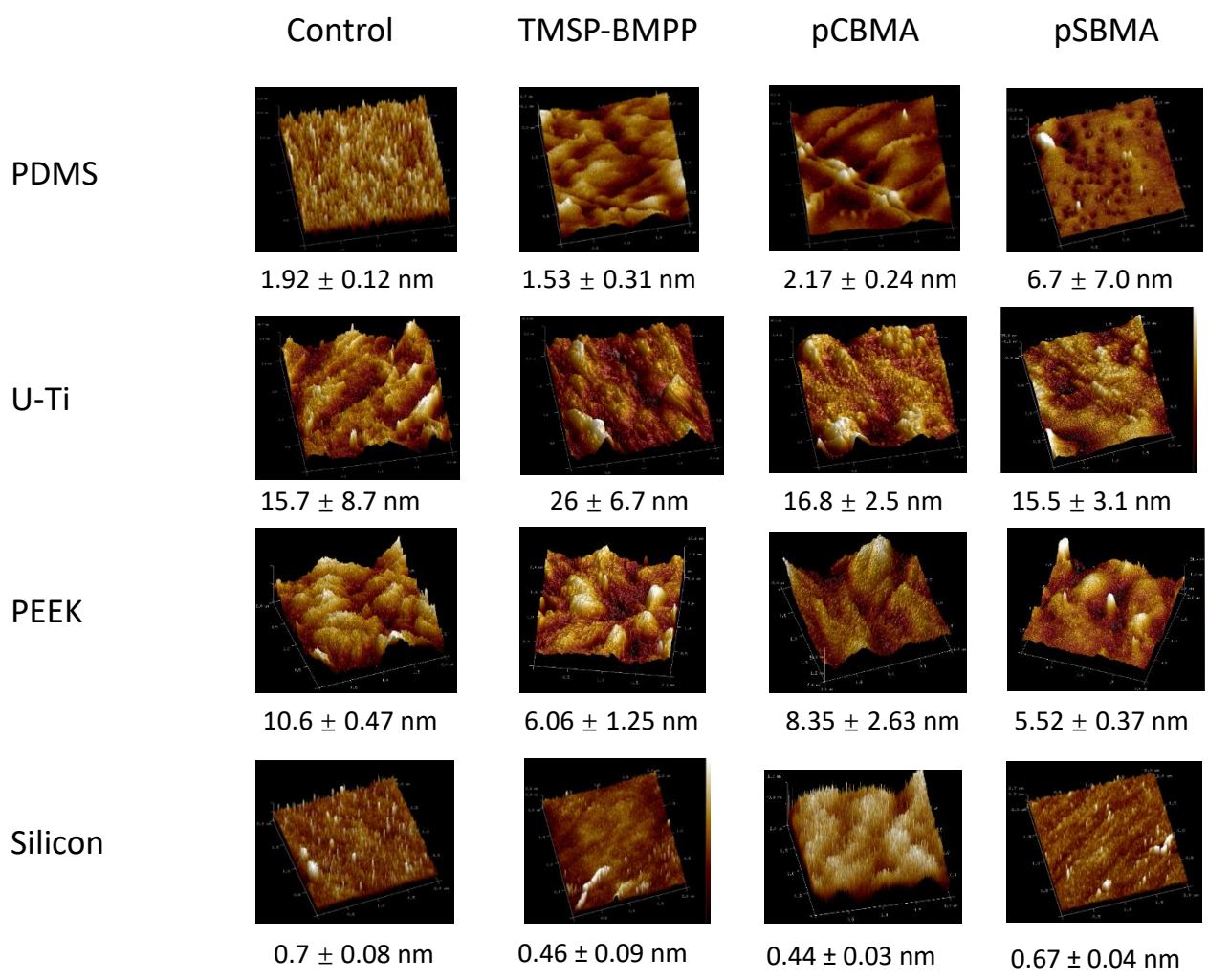

Figure 3-11: AFM images with root mean square (RMS) surface roughness data, scan size 2 µm. Roughness values are based on profiles at randomly selected positions (n ≥ 2).

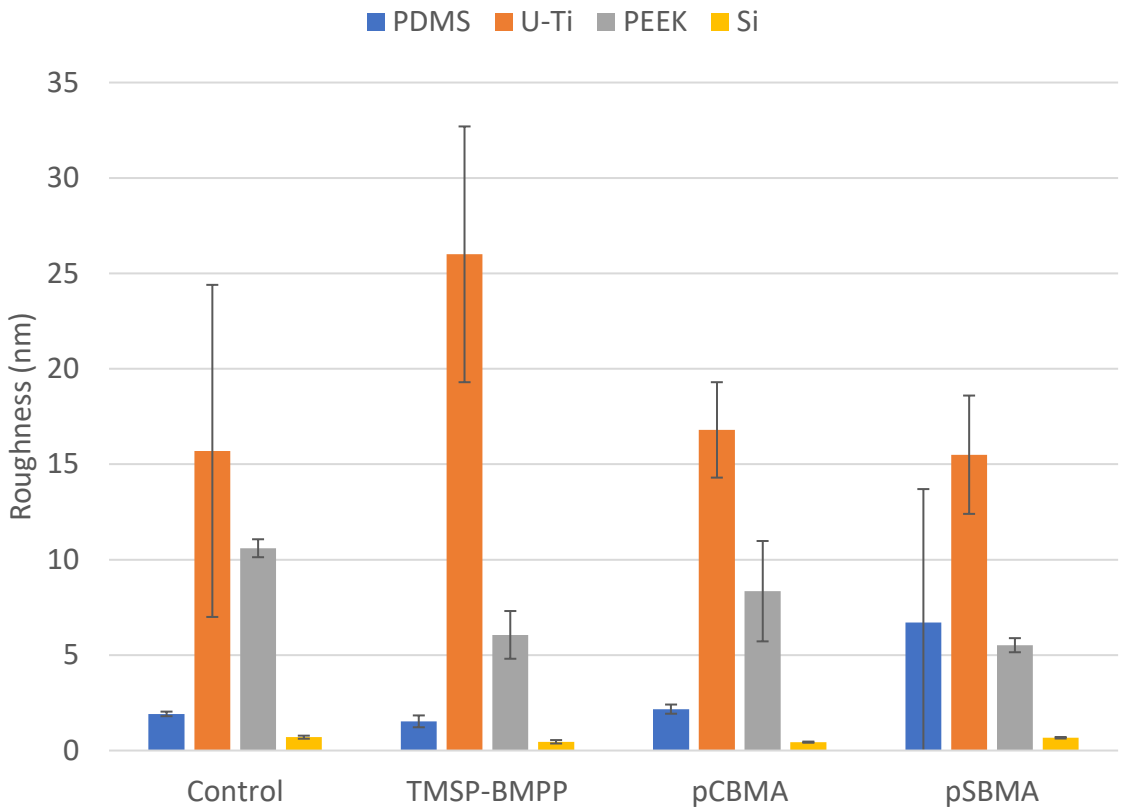

Figure 3-12:AFM root mean square (RMS) surface roughness data associated with the images in Figure 3-11, scan size 2 µm. Roughness values are based on profiles at randomly selected positions (n ≥ 2).

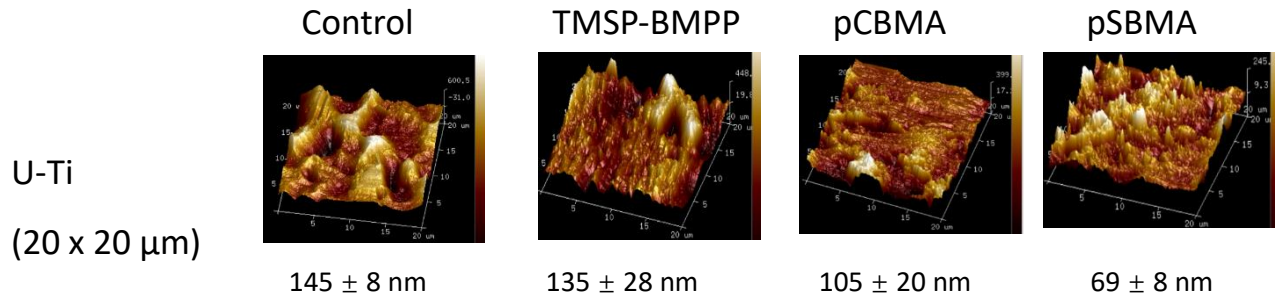

Figure 3-13: AFM images of unpolished Ti surface at various stages of modification, with root mean square (RMS) surface roughness data, scan size 20 µm. Roughness values are based on profiles at randomly selected positions (n ≥ 2).

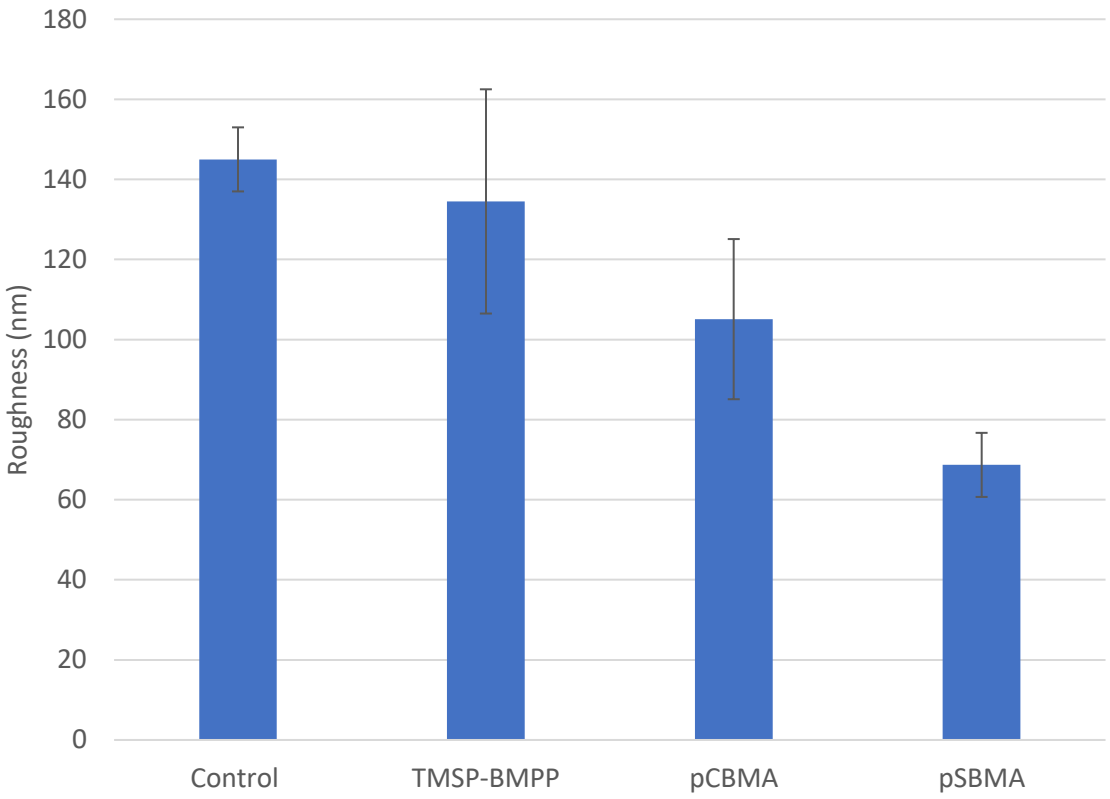

Figure 3-14: AFM root mean square (RMS) surface roughness data for U-Ti associated with the images in Figure 3-13, scan size 20 µm. Roughness values are based on profiles at randomly selected positions (n ≥ 2).

3.3.8 Effect of Polishing on Titanium

When used as received from the manufacturer, the high roughness of the titanium material made characterization by ellipsometry difficult. Surface roughness causes incoherent reflection and can contribute to depolarization and other artifacts (Jun, 2003). Mechanical polishing to give a smooth, mirror-like finish was carried out to minimize these effects. Figure 3-15 shows 2 µm x 2 µm AFM images of the titanium coupons before and after mechanical polishing. Surface topographical features of greater magnitude are seen on U-Ti, with a maximum peak of 136 ± 56.1 nm. After polishing, the features were much smaller with a maximum peak of 36.1 ± 10.3 nm.

Although the unmodified polished titanium surface was amenable to ellipsometric analysis, a good surface model was difficult to achieve after modification. This may have been due to etching caused by the plasma treatment. Despite reducing the treatment time from 5 to 3 min and even to 1.5 min, and decreasing the power from 60 to 40 W, etching of polished titanium (p-Ti) was still observed. Even after modification with pCBMA, etching was still noticeable as shown in Figure 3-16. Therefore, after this experiment, modification on polished titanium was abandoned.

a)

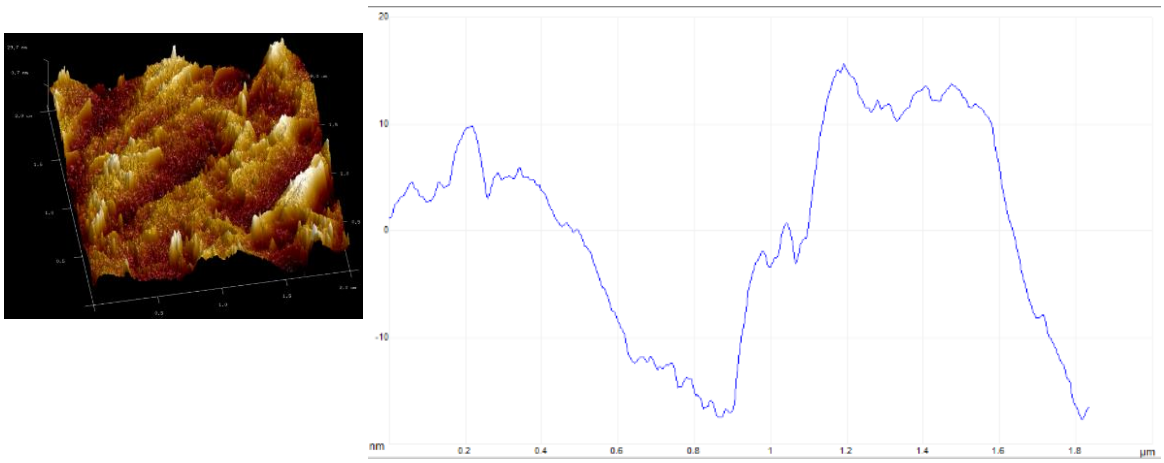

b)

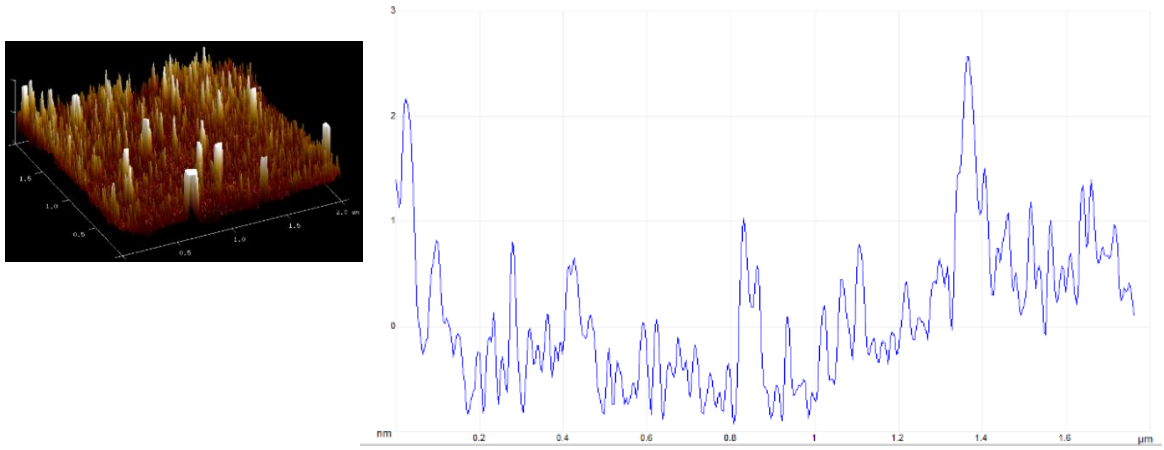

Figure 3-15: Representative AFM images of unpolished Ti (a) and polished Ti (b) at scan size 2 µm. The traces show the height profiles (nm) of cross-sections at selected locations on the AFM images.

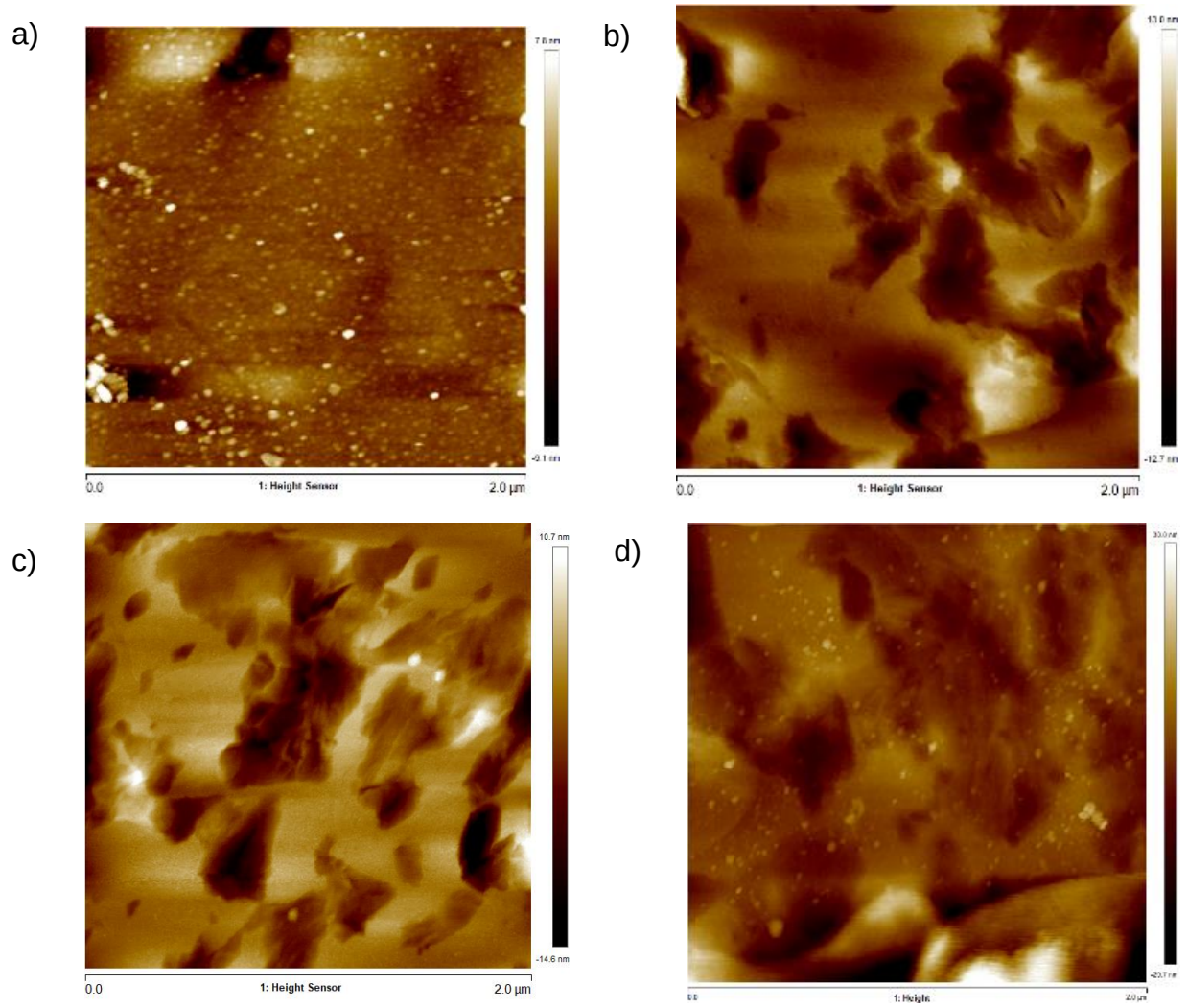

Figure 3-16: Representative AFM images of unmodified polished Ti (a), oxygen plasma treated polished Ti (b), oxygen plasma treated polished Ti modified with Si-Br (c), and polished Ti plasma treated and modified with Si-Br and then with pCBMA (d). Scan size, 2 µm.

3.3.9 "Film" Thickness and Grafting Density of Zwitterionic Polymers on Modified Surfaces

Thickness measurements were carried out using ellipsometry. Film thickness measurements were not performed on PDMS, titanium, and PEEK because of low signal intensity due to depolarization of the reflected light. PDMS is smooth and transparent on both sides. The PDMS samples were about 0.5 – 1 mm in thickness and thick enough for light beams to overlap so that data are collected from two different path lengths: the front and the back of the sample (Kostruba, 2015). For PEEK, anisotropic light scattering due to the high refractive index of PEEK (n = 1.8) causes the depolarization. Surface roughness can also cause depolarization. As shown with AFM, U-Ti is very rough, necessitating polishing. Unfortunately, as seen in the previous section, polished titanium was easily damaged by plasma treatment, again causing scattering due to surface

roughness. The damage effectively re-introduced surface roughness leading ultimately back to light depolarization.

Silicon wafer, which is extremely flat and smooth as observed by AFM, has high refractive index contrast with the polymer films without backside reflection. In addition, this material was able to withstand the high energy plasma treatment; it was therefore suitable for ellipsometry measurements.

The thickness of a thin film is directly related to the surface density of the molecules comprising the film. The graft densities of the thin films were estimated using Equation 3-3:

$$\sigma = \frac{h\rho N_A}{M_n} \tag{3-3}$$

where σ is the graft density, h is the film thickness from ellipsometry measurements, ρ is the density of the grafted molecule (values of 1.24 g/cm^3 (Gelest, SDS) for TMSP-BMPP and 1.34 g/cm^3 for pSBMA (Sakamaki, 2019) and pCBMA (as an estimate) were used), N_A is Avogadro's number, and $M_n$is the number average molecular weight determined using GPC for pCBMA and as an estimate for pSBMA (Mn = Mw = 329.26 g/mol for TMSP-BMPP).

Table 3-4 shows the thickness and surface density of TMSP-BMPP on silicon wafer as obtained by ellipsometry. Samples 1-3 were modified using the same conditions and thickness measurements on a given surface were performed twice. Despite the conditions being the same, the estimated thickness and grafting density of the three samples were very different. Achieving reproducibility in liquid phase deposition of silanes is known to be difficult (Zhu, 2012; Pujari, 2014; Badv, 2017), and this is reflected in the present ellipsometry data. The number of samples for a given measurement was small, which may also have contributed to the poor reproducibility.

Table 3-4: Surface density of 3-(trimethoxysilylpropyl)-2-bromo-2-methylpropionate (Si-TMSP-BMPP) ad-layer on silicon substrate estimated by Equation 3-3 and ellipsometry.

Experiment	Thickness (nm)	Graft density (molecules/nm^2)
1	0.2	0.45
2	0.705	1.6
3	3.46	7.85

Data from ellipsometry for the pCBMA and SBMA films on silicon are shown in Table 3-5. It is seen that pCBMA formed much thicker films than pSBMA. Jiang et al. prepared pCBMA and pSBMA films on gold with thicknesses of 30 nm (Cheng, 2009) and 90 nm (Yang, 2008), respectively. The layer of pSBMA on silicon in this work appears to be very thin, possibly due to a low extent of grafting.

Table 3-5: Zwitterionic polymer film thicknesses on silicon wafer from spectroscopic ellipsometry. pCBMA and pSBMA were polymerized on silicon surfaces using identical SI-ARGET ATRP conditions. Data are mean ± SD, n =4.

	Thickness (nm)	Graft density (molecules/nm^2)
Si-pCBMA	34.60 ± 9.24	0.43
Si-pSBMA	2.75 ± 0.46	0.03

3.3.10 Bovine Serum Albumin (BSA) Adsorption

BSA was used as a model protein for assessment of protein resistance of the surfaces due to its good solubility in water and its potential to foul materials in aqueous conditions. The BSA was labelled with I-125 radioisotope which emits strong gamma radiation at 35 keV (Hlady, 1999). I-125 is incorporated into the protein by replacing a hydrogen in the protein's tyrosine aromatic rings (Hlady, 1999). Surface samples were immersed in a 1 mg/mL, 10% radiolabelled, 90% unlabelled, BSA solution for 2.5 h. After rinsing with DI water, the radioactivity on the surfaces was measured using a gamma counter. The surface radioactivity provides a measure of the quantity of BSA adsorbed. The data from these experiments are shown in Figure 3-17 and Figure 3-18.

Of the four surfaces studied, PDMS in the unmodified form showed the highest adsorption of BSA, i.e., 0.54 ± 0.03 μg/cm^2. After modification with pCBMA, PDMS showed the lowest relative adsorption, i.e., 0.041 ± 0.006 μg/cm^2, a reduction of 92%. For PEEK, the other polymeric material examined, pCBMA modification reduced adsorption by only 43% compared to the control, i.e., a much lower effect than for PDMS. Unmodified silicon had the lowest BSA adsorption, i.e., 0.28 ± 0.12 μg/cm^2 and also had the lowest absolute adsorption, i.e. 0.03 ± 0.02 μg/cm^2. Unmodified titanium showed BSA adsorption of 0.43 ± 0.04 μg/cm^2. After pCBMA modification, adsorption decreased to 0.08 ± 0.02 μg/cm^2, a reduction of 82%.

Surfaces modified with pSBMA showed less resistance to BSA adsorption than when modified with pCBMA (Figure 3-18). PDMS surfaces modified with pSBMA reduced BSA adsorption by only 36%, significantly less than when modified with pCBMA. In contrast, PEEK modified with pSBMA showed better resistance to BSA (80% reduction) than when modified with pCBMA. Silicon and titanium surfaces modified with pSBMA reduced adsorption by 77%.

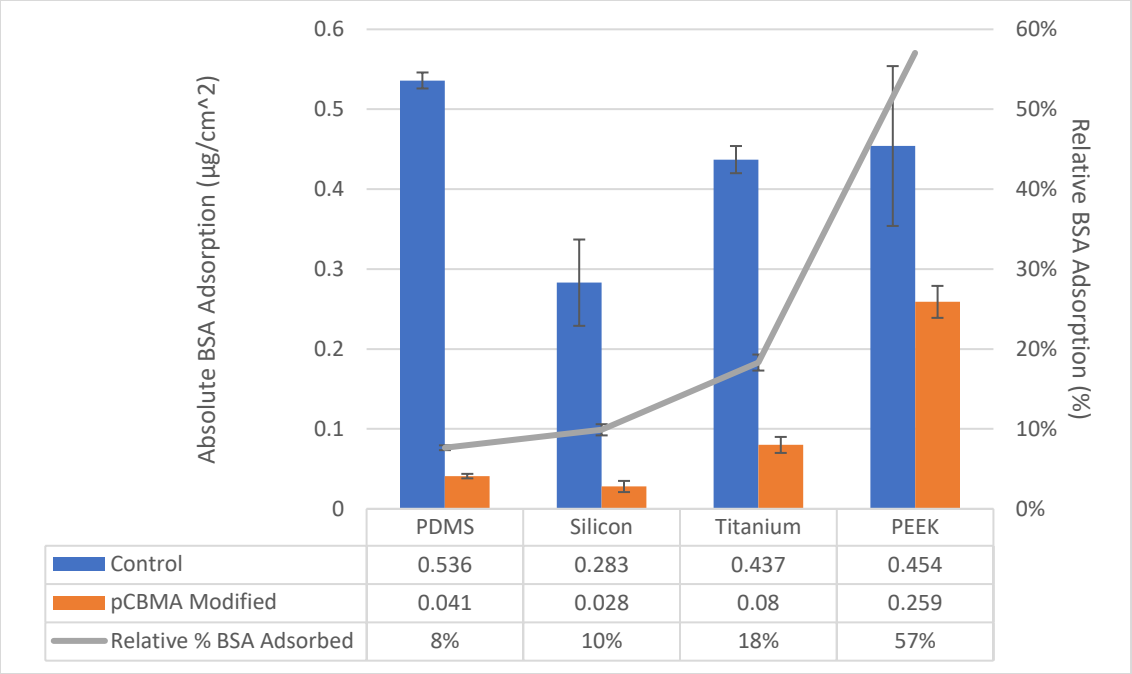

	PDMS	Silicon	Titanium	PEEK
Control	0.536	0.283	0.437	0.454
pCBMA Modified	0.041	0.028	0.08	0.259
Relative % BSA Adsorbed	8%	10%	18%	57%

Figure 3-17: BSA adsorption on various surfaces modified with pCBMA. The control surfaces are unmodified substrate. The pCBMA modified surfaces were prepared by attaching the silane initiator ad-layer followed by ARGET ATRP polymerization of CBMA. The grey line shows the relative percentage of BSA adsorbed to each surface compared to its control. Data are mean ± standard deviation (n=5).

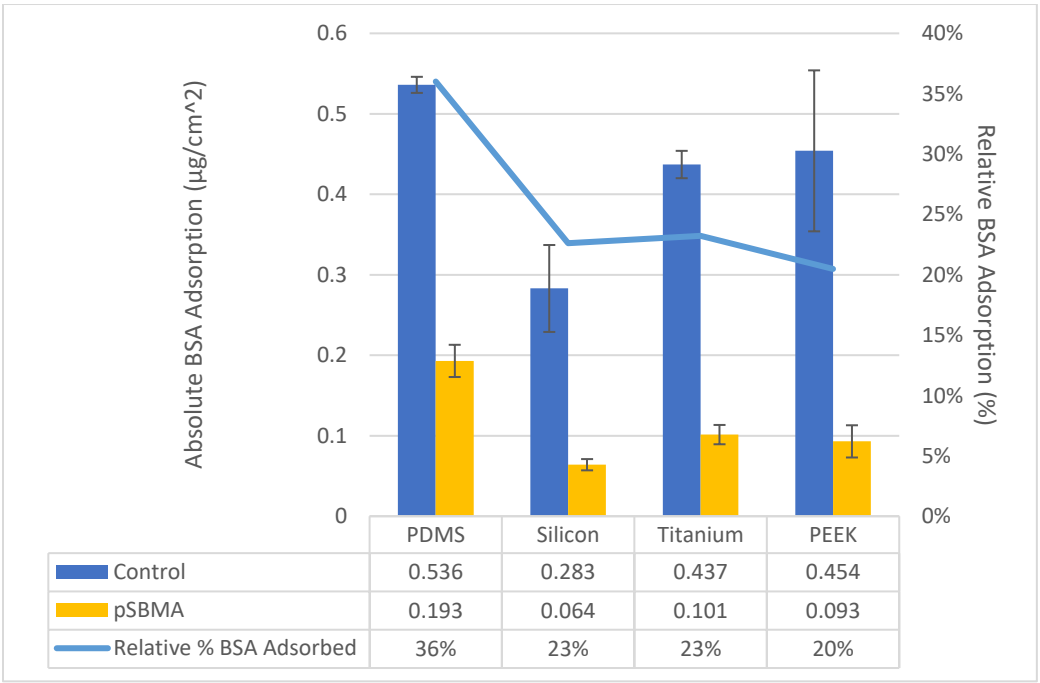

	PDMS	Silicon	Titanium	PEEK
Control	0.536	0.283	0.437	0.454
pSBMA	0.193	0.064	0.101	0.093
Relative % BSA Adsorbed	36%	23%	23%	20%

Figure 3-18: BSA adsorption on various surfaces modified with pSBMA. The control surfaces are unmodified substrate. The pSBMA modified surfaces were prepared by attaching the silane initiator ad-layer followed by ARGET ATRP polymerization of SBMA. The grey line shows the relative percentage of BSA adsorbed to each surface compared to its control. Data are mean ± standard deviation (n=5).

3.3.10.1 Effects of Surface Cleaning

Since the goal of the project was to develop an anti-fouling modification method that would be applicable to multiple materials, the cleaned substrates were used without further mechanical or chemical modification prior to modification with the zwitterionic polymers. However, it was found difficult to characterize the as-received titanium surface using ellipsometry and AFM. Mechanical polishing was therefore employed with this surface with a view to improving the quality of AFM and ellipsometry observations. Becker et al. showed that the type of solvent used to clean titanium and steel surfaces affects the surface chemistry and contact angles (Becker, 2016). However, in the present work, unpolished titanium and polished titanium showed no significant differences in XPS and BSA adsorption. These observations indicate that the surface chemical properties of polished and unpolished titanium are similar and appear to play a larger role in protein adsorption than topography. Polished titanium had a much smoother surface than its unpolished counterpart, giving it thereby a higher contact angle.

Of the unmodified polymer surfaces, PDMS and PEEK showed the highest BSA adsorption (Fig 3-17), presumably due to their specific surface chemistries and relative hydrophobicities. Unmodified silicon showed the lowest adsorption, attributable to its intrinsically smooth surface and relative hydrophilicity. Of the four substrates modified with pCBMA, PDMS performed the best in terms of resistance to BSA adsorption.

3.3.10.2 Effects of TMSP-BMPP

Successful polymerization of the zwitterionic monomers on the various substrates is dependent on the surface density of the TMSP-BMPP ad-layer. The greater the number of initiator sites on the substrate accessible to the monomer, the greater the probability that the substrate will be fully covered by the polymer and protected from fouling. TMSP-BMPP contains a silanol linker to anchor it to the surface, and the ATRP initiator for polymerization to form the anti-fouling zwitterionic brushes. Silanes can be deposited either by solution deposition or chemical vapor deposition (CVD). Although CVD can provide a higher packing density, solution-based deposition is a simpler process that does not require sophisticated equipment.

Equation 3-3 above, was used to estimate the surface density of the grafted TMSP-BMPP on silicon wafer. A monolayer of TMSP-BMPP should have surface coverage similar to that of other silanes i.e., about 1 molecule/nm^2, as obtained using spectrophotometry by Saini et al. (Saini, 2018). It is assumed that a higher density of TMSP-BMPP would provide more sites for the zwitterionic monomers to polymerize from and therefore give a surface with greater resistance to protein adsorption. However, from Figure 3-19 and Table 3-6 it is seen that there is no correlation between the thickness (and therefore grafting density) of the TMSP-BMPP layer and BSA adsorption, although the thickest TMSP-BMPP layer (3.46 nm) did show the lowest adsorption. It may be that an optimal thickness exists where the TMSP-BMPP ad-layer provides optimal access to the initiator

sites for polymerization. More data and further work is required to draw a definitive conclusion on the stability and thickness/grafting density of the TMSP-BMPP layer and its effect on protein resistance of the grafted zwitterionic polymers.

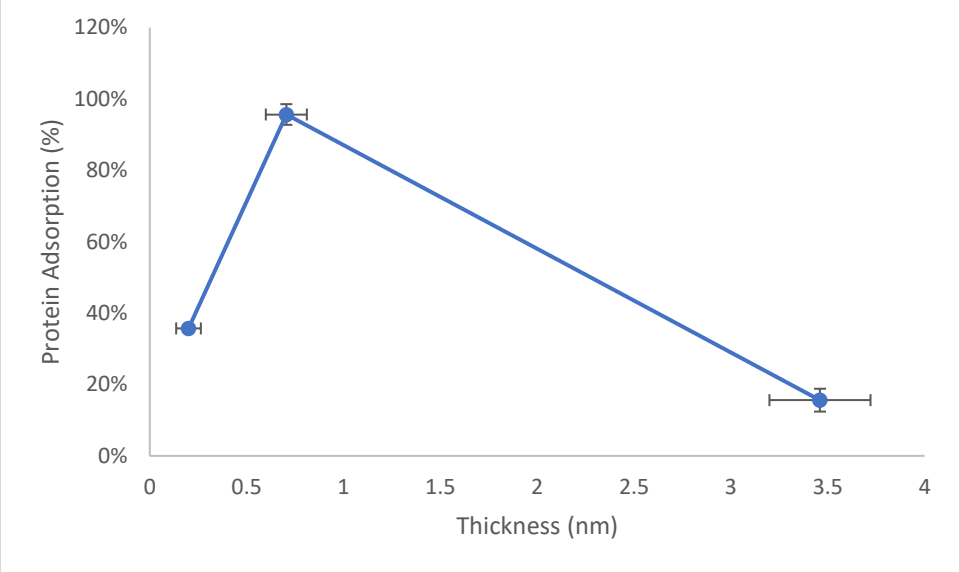

Figure 3-19: Protein adsorption as a function of TMSP-BPP layer thickness on silicon wafer. Protein adsorption data points are reported as mean ± standard deviation (n ≤ 4). Thicknesses are reported as mean ± standard deviation (n = 2 measurements per sample).

Table 3-6: Si-TMSP-BMPP layer characteristics on silicon substrate. Thicknesses acquired using ellipsometry. Graft density calculated using Equation 3-3. BSA adsorption shown as % versus unmodified material.

Thickness (nm)	Graft density (molecules/cm^2)	% BSA Adsorption
0.200	1.20E+14	36
0.705	4.24E+14	96
3.460	20.80E+14	16

3.3.10.3 Effects of Zwitterionic Polymer

It has been hypothesized that the antifouling mechanism of zwitterionic polymers involves strong electrostatic interactions with water, forming a hydration/energy barrier to prevent adsorption. The effectiveness of this barrier is attributed to the precisely balanced charge structure and characteristic chain conformation. Polyzwitterionic brushes are unique such that they have some of the properties of neutral hydrophilic brush polymers as well as of polyelectrolytes. Neutral brush conformation depends on both grafting density and the quality of the solvent (Brittain, 2007). At high grafting densities steric repulsion forces the polymer chains into an extended brush regime as shown in Figure 3-20 (Zoppe, 2017). In a good solvent, the brushes stretch into the solvent, away from the surface due to steric and osmotic repulsion (Li, 2014). At low grafting densities and poor solvent conditions, the polymer chains collapse on themselves due to the lack of excluded volume effects (Li, 2014). An intermediate regime called the “mushroom regime” also exists (Zoppe, 2017).

Similar to polyelectrolytes, poly(sulfobetaine) (pSB) brushes are sensitive to ionic concentration. At high salt concentrations, pSB brushes swell to give a brush configuration since the excluded volume effects produced by the hydrated ions are greater than the intramolecular dipole-dipole interactions (Petroff, 2019; Kobayashi, 2012). However, these ionic effects are dependent on the zwitterionic moiety as pMPC remains in the brush configuration at low and high salt concentrations (Petroff, 2019).

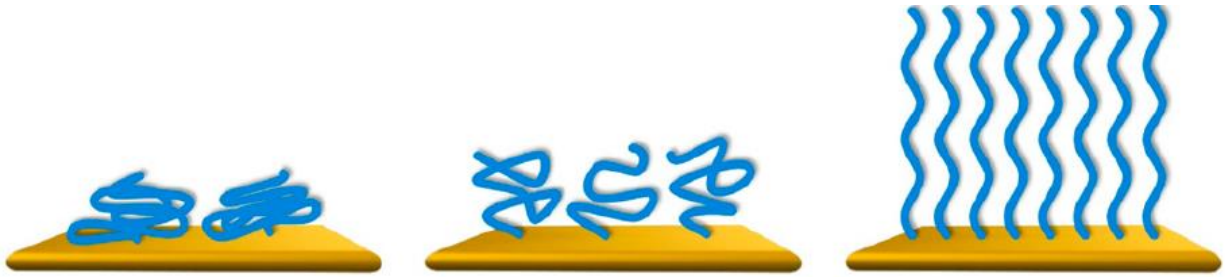

Figure 3-20: Surface grafted polymer brush in a) pancake, b) mushroom, and c) brush regimes. From (Zoppe, 2017) with permission.

Given the conditions for formation of good polymer brushes, it should be noted that most characterizations (WCA, AFM, XPS, and ellipsometry) were all performed in air or vacuum (XPS). Thus, the polymers may all be in the pancake or mushroom regime meaning that the thickness layer may be smaller than if the polymer layer were in a hydrated state.

The variation in performance of the different modified substrates depends on both their physical and chemical properties. The unmodified silicon surface was very smooth which may account for the fact that the absolute adsorption (mass/area) on this substrate was the lowest of the four. After pCBMA modification, PDMS and silicon surfaces both remained relatively smooth (roughness < 3 nm). In principle the greater the surface roughness, the greater the “true” surface area (i.e., relative to the “nominal” or geometric area) available for proteins to adsorb (Rechendorff, 2006). This effect will of course depend on the size of the roughness elements relative to the size of the protein. However, there seems to be little correlation between the roughness of the surfaces with protein adsorption in this study, which means that surface chemistry is the main driver in BSA adsorption.

3.3.10.4 Effect of Surface Chemistry of Substrate

Sulfur and nitrogen content from XPS were used to quantify sulfobetaine on the surfaces. For the different substrates the XPS data (Table 3-) showed pSBMA content decreasing in the order silicon > PEEK > titanium > PDMS. This trend aligns with that of the adsorbed quantity of BSA, indicating that pSBMA surface density dictates protein absorption behavior.

Pure, unmodified PEEK should contain only carbon and oxygen, but the control PEEK sample contained nitrogen making it difficult to determine if the zwitterionic polymer modifications were successful since nitrogen is the marker atom for pCBMA. Only a small quantity of bromine was present after TMSP-BMPP modification of PEEK, indicating that only a very low density of ATRP initiator sites was available for polymerization. On pCBMA modified PEEK surface, there was a very slight decrease in carbon and nitrogen, and a slight increase in oxygen, and therefore it is not clear whether pCBMA was present on the surface to any significant extent or if the initial nitrogen was removed through the modification process. Whitesides et al showed that even a monolayer of sulfobetaine or phosphocholine can resist non-specific adsorption of protein (Holmlin, 2001). Since the hydrophilicity and surface roughness of PEEK changed upon pCBMA modification, and since some reduction in protein adsorption was seen, there may be small patches of pCBMA on the surface. In addition, the small content of bromine in the PEEK-TMSP-BMPP surface may suggest that the density of oxidized activated sites on PEEK was low resulting in incomplete/patchy coverage of the surface. Since activation sites produced by oxygen plasma are short lived, subsequent modification treatments must be carried out rapidly after plasma treatment. The thickness and grafting density of the TMSP-BMPP on the PEEK surfaces would be important information to understand the coverage (or lack thereof) of the silane ad-layer on PEEK. The PEEK surfaces modified with pSBMA showed an increase of nitrogen and the presence of sulfur, indicating the presence of pSBMA and thus better capacity to prevent BSA adsorption (80% reduction) than the pCBMA modified PEEK.

The PDMS-pCBMA surface showed the lowest BSA adsorption among the surfaces investigated, which may be a result of, i) optimal surface modification; and ii) a high density silane-initiator layer resulting in dense polymer brush formation. The surface modification procedure was previously optimized for pCBMA with PDMS as substrate. It may be that such optimization is required for each substrate individually to achieve maximal resistance to protein adsorption. XPS did show significant nitrogen content and reduced silicon content compared to the control, indicating a significant layer of pCBMA to resist protein adsorption on PDMS. Conversely, the PDMS modified with pSBMA adsorbed the most protein of the four surfaces. XPS data in Table 3-3 indicate that there was very small content of nitrogen and sulfur on the PDMS-pSBMA surface and trace amounts of bromine from the initiator. These data suggest that pSBMA did not polymerize well on the PDMS surface leading to the increase in protein adsorption seen in Figure 3-18.

XPS showed that titanium modified with pCBMA contained 2.3% nitrogen (Table 3-3). In addition, the titanium content decreased from 20.7 to 5.8% and the carbon and oxygen contents increased significantly after pCBMA modification, indicating significant pCBMA coverage of the titanium surface, and thus leading to reduced BSA adsorption (Figure 3-

17). Although only a small content of sulfur was found on the pSBMA modified titanium surface, nitrogen was high and titanium was low, indicating satisfactory coverage to reduce BSA adsorption by 77% (Figure 3-18).

Silicon modified with pCBMA showed relatively small content of pCBMA as shown by the low nitrogen content (Table 3-3). However, the pCBMA modification caused a reduction of 90% in BSA adsorption. It could be that the XPS was done on a sample that was not optimally modified; alternatively, it may be that only a low density of pCBMA is required to provide antifouling on silicon wafer. For pSBMA modified silicon, XPS data indicate relatively large content of pSBMA when compared with other surfaces. This and the low content of silicon on silicon-pSBMA surface indicates significant coverage of the silicon wafer with pSBMA, which should thus resist protein adsorption more effectively than its pCBMA modified counterpart. However, this was not the case as pSBMA modified silicon reduced adsorption by only 77% vs. 90% for pCBMA modified silicon. This result may indicate that pCBMA, even without full surface coverage, may be more effective in preventing BSA adsorption on silicon wafer.

3.3.10.5 Comparison of Effects of pSBMA and pCBMA Modifications on Protein Adsorption

BSA adsorption on the pSBMA-modified surfaces investigated in this work was shown to be reduced compared to controls, but the effect was not as great as on pCBMA-modified surfaces. Jiang's group also observed a similar difference and showed that it depends on the type of protein and on the complexity of the protein medium (Jiang, 2010). Differences in protein resistance may be due to differences in hydration of the polymers (Lin, 2016). By measuring the number of non-freezable water molecules per polymer repeating unit Lin et al. showed that pCBMA was able to bind more water than pSBMA and that the binding was tighter (Lin, 2016), thus providing a more effective hydration layer to prevent unwanted protein adsorption.

As discussed above for pCBMA, the thickness of the antifouling polymer layer also plays an important role in protein resistance. Table 3- shows that pCBMA formed much thicker films on silicon than did pSBMA. Optimization relative to reaction time was performed for CBMA polymerization but not for SBMA and it may be that the time of 5 h used was not optimal for SBMA. Other ARGET-ATRP parameters may also require tailoring to tune the thickness of the pSBMA brush. It may also be that pCBMA is a better antifouling polymer than pSBMA on some surfaces.

3.4 Conclusion

All unmodified surfaces showed different extents of protein adsorption but all of them were highly adsorbing. After modification with pCBMA or pSBMA, a reduction in protein adsorption related to the amount polymer on the surface was observed. High zwitterionic

polymer content along with low exposure of bare substrate (as seen in XPS) produced the most effective antifouling surfaces.

Unmodified surfaces of lower water contact angle and greater hydrophilicity showed lower protein adsorption. The modified surfaces having lower contact angles showed better antifouling performance than more hydrophobic ones (i.e., PDMS- pSBMA- and PEEK-pCBMA).

Despite the low thickness of the pSBMA film on silicon, it nonetheless reduced adsorption by 77% relative to the control, meaning that a thin a layer of pSBMA is sufficient to provide a degree of antifouling character. Films of greater thickness may provide for still lower protein adsorption; however, additional experiments would be required to verify this possibility.

Although increased roughness often leads to increased protein adsorption (Sopelliti, 2010), no clear correlation between surface topography/roughness and protein adsorption was found in this research.

4.0 Additively Manufactured Stainless Steel Modified with pCBMA and pSBMA

Additive manufacturing or 3D printing of materials is now an increasingly popular choice to prototype and manufacture custom parts rapidly while producing less waste. Plastics such as polylactic acid (PLA) and PEEK have commonly been used (Singh, 2020). In the past decade, many other 3D printing processes and materials have been used for additive manufacturing. Metals have become popular materials to be manufactured using 3D printing as this produces less waste than traditional metal fabrication techniques when used for rapid prototyping and complex customized parts (Motaman, 2020).

Limitations that come with additive manufacturing include high upfront cost of the equipment and significantly slower production speeds compared to traditional manufacturing techniques (Bai, 2019). The size of the parts being printed is also limited by the size of the build plate which varies between machines. The 3D printing process is not a straightforward one, with process parameters varying between materials and machines used for 3D printing. It is difficult to predict optimal production results based on process parameters (Oter, 2019). Designing the parts for manufacturing can also be challenging as most parts need to be completely redesigned with proper wall thicknesses, parts orientations, and “print supports” that would not be found in traditional manufacturing techniques. Print parameters are also specific to the printer (Huang, 2020). Perhaps one of the biggest drawbacks of additive manufactured parts is that they have very poor surface finishes for the intended application due to the nature of the layer-by-layer build process (Hollander, 2019). Therefore, 3D printed parts require surface modification to achieve the desired surface finish which can be rougher or smoother, or to add functionality such as antifouling properties.

The typical additive manufacturing process for metal 3D printing is powder bed fusion (PBF) (Bai, 2019). In this method, metal powder is spread over the top of previous layers and selectively melted in a layer-by-layer fashion to bond the particles together (See Figure 4-1). PBF processes are most common because nearly any geometry or complex shape can be manufactured with tight tolerances and good mechanical properties (Bai, 2019). A variety of metals and alloys can be used to fabricate parts and can be machined or put through further processing. However, parts produced by PBF are attached to the build plate which may require specialized equipment to remove and produces waste by the supports.

Direct metal laser sintering (DMLS) is a powder bed fusion technique used for metal alloys (Oter, 2019). A laser selectively melts the metal particles so that they can fuse together. Zhang et al. reviewed other common metal 3D printing methods including metal binder jetting – used for large scale products, and direct energy deposition which can be used

to repair broken metal parts (Zhang, 2018). Both techniques have a quicker build time than PBF techniques but cannot produce the same level of mechanical property strength and detailing that PBF can achieve.

In the present work, austenitic stainless steel (SS) 316L was chosen as a model substrate as it is not only found in medical implant applications (Bai, 2019), but is also commonly used for equipment and sensors in biotechnology, pharmaceuticals (Thompson, 2017), and food processing industries (Flint, 2019) due to its low corrosion rates and resistance to cleaners and disinfectants. For use in these fields, the materials are often polished to a surface finish of < 20 µm to reduce biofouling (as noted previously, the surface finish of 3D printed parts is generally quite poor). The aim of the present study was to investigate protein adsorption on 3D printed steel and test whether the pCBMA and pSBMA modifications described in the previous chapter, can offer a better surface finish from an antibiofouling perspective.

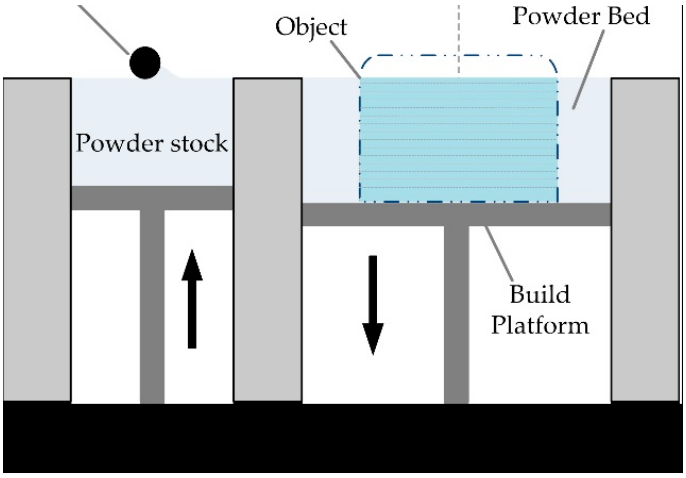

Figure 4-1: Schematic of Powder Bed Fusion Process. From (Bai, 2019) with permission.

4.1 Materials and Methods

Stainless steel 7 x 7 x 3 mm coupons were designed using Materialise Magics Software and printed on an EOS M200 Direct Metal Laser Sintering system. The SS 316L powder was purchased from LPW Technologies and has a particle size distribution of 15 – 45 µm. Figure 4-2(a) shows the coupons printed on the build plate. Figure 4-2 (b) shows that the sample print height was 1.5 mm with island support heights of 3 mm. The island supports were built using a laser power of 100 W and a scanning speed of 850 mm/sec. The island supports are hatched such that there is space between material lines as shown in Figure 4-3. The sample prints were designed to be solid using a laser power of 285 W, scanning speed of 960 mm/sec, hatch spacing of 0.11 mm and stripes overlap of 0.08 mm.

Thin samples (< 4mm) are vulnerable to warping during removal from the build plate and require supports to reduce or eliminate this effect. The printed sample surface was shiny and had raised edges possibly due to the nature of the melt pool boundaries (Oter, 2019).

The coupons were taken off the build plate by wire electrical discharge machining (EDM) (Yu, 2019) in which sparks between a thin metallic wire and the 3D prints are applied to cut the pieces from the electrically conductive plate (Qudeiri, 2019). The EDM process allows small, delicate, but difficult to machine materials to be machined or removed from a build plate without damage. There are no mechanically induced contact forces because EDM cuts through the material using electrical sparks between the wire and workpiece. This left the bottom surface with a matte and homogenously flat machined surface and a support height of 1.5 mm after the sample was removed from the build plate.

The 3D printed stainless steel coupons were cleaned and modified using the same procedure as in section 3.2 for the pCBMA- and pSBMA-modified surfaces.

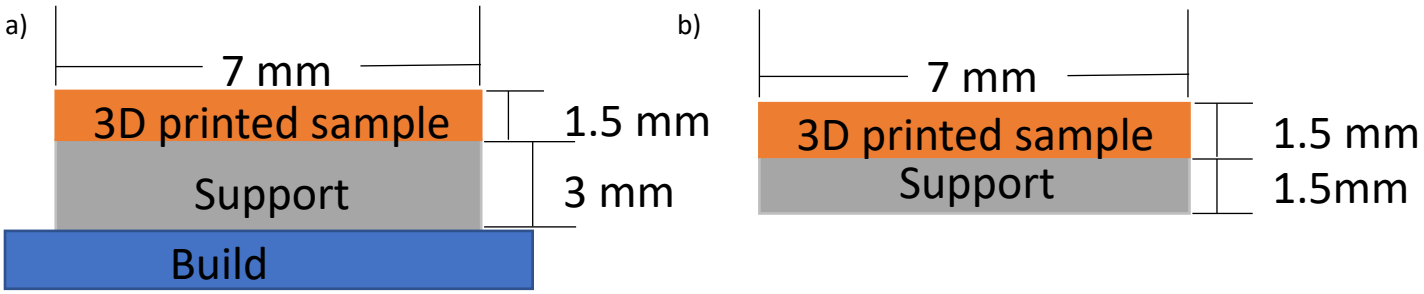

Figure 4-2: 3D Print Dimensions a) on vs b) off the build plate

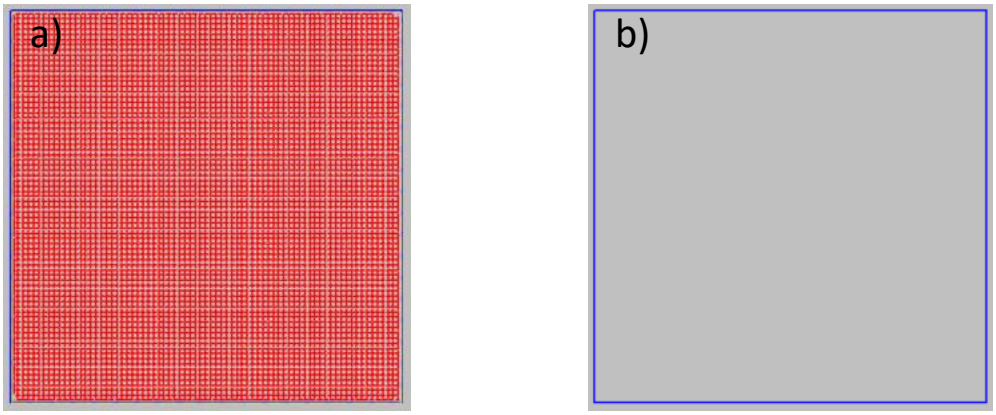

Figure 4-3: Visual representation of a) Island supports, b) Solid sample prints

4.2 Results and Discussion

4.2.1 Water Contact Angles

As shown in Figure 4-5, 316 stainless steel was found to have a contact angle of θ = 84.3°. Due to the nature of 3D printing, the printed 316L stainless steel substrates had three different surface finishes as shown in Figure 4-4: a shiny top side, a matte bottom side where the part was removed from the build plate, and the sides of the part which were too thin for contact angle measurement. The shiny side of the 3D printed surface showed a water contact angle, θ = 53.6°, whereas the matte side was more hydrophilic, with θ = 20.6°. When modified with polymerization initiator, the contact angle was reduced to 6.7° for the matte side and 10.5° for the shiny side. After further modification with pCBMA or pSBMA, the surface was completely wetted by the water drop on the matte side and showed contact angles of 14.6° and 8.3°, respectively, on the shiny side.

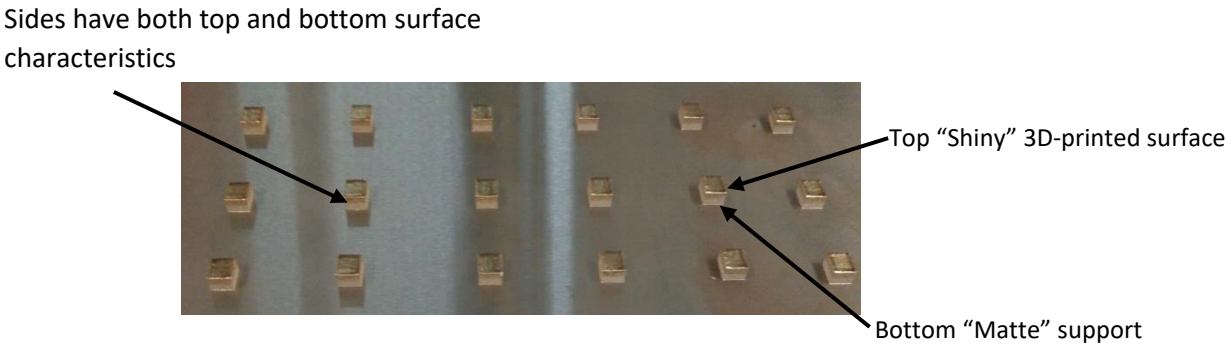

Figure 4-4: 3D printed samples on build plate

Although surface roughness measurements were not investigated, 3D printed materials typically have a higher roughness than conventionally manufactured surfaces (Obeidi, 2019). This is because the surface is formed by melting the particles layer by layer. Based on this assumption, the water contact angle on stainless steel can be modelled by the Wenzel Model which states that surface wettability increases with increasing surface roughness:

$$\cos(\theta^*) = r\cos(\theta) \tag{4-1}$$

Where $\theta^*$is the angle between the tangent to liquid-fluid interface and the macroscopic-geometrical solid surface or the apparent contact angle (Fadeeva, 2016)

r is the roughness ratio = actual surface area of rough surface/ effective geometric surface area

θ is the actual contact angle where the liquid-air, solid-air, and solid-liquid interfaces meet.

The machined (matte) surface showed an even smaller contact angle than the sample (shiny) surface suggesting that the machined surface is rougher than the printed sample

surface. The supports were produced with a hatched design to save print time and material, as they were intended to be removed from the printed sample. Hatching creates spaces within the material that allow water to penetrate below the apparent surface. Therefore, the contact angle measurements for the matte support side may not be meaningful since the water penetrates into the pores on the surface. Although water contact angle hysteresis was not measured, it is predicted that due to the pores on the surface, hysteresis would be large.

After surface modification with the antifouling zwitterionic polymers, the surfaces on both sides were completely water wettable. Reports of contact angles on modified additively manufactured stainless steel are limited. Sin et al. reported a contact angle of 24.8° on conventional 316L stainless steel; no contact angle data for carboxybetaine on stainless steel have been reported (Sin, 2014). Jiang et al. reported a contact angle of 10° for pCBMA on PDMS substrate prepared using the same polymerization method as in this work (Hong, 2017). Since the 3D printed surfaces were significantly more hydrophilic than conventional stainless steel, smaller contact angles on the zwitterionic polymer-modified 3D surfaces should not be surprising. Despite the difference of appearance of the matte and shiny sides, the decreasing contact angle trend after subsequent modification stages is consistent with the trends found in Chapter 3. Thus, the same technique of plasma activation, silanization, and zwitterion modification can be applied to make more hydrophilic 3D printed stainless steel surfaces.

The theory behind the antifouling mechanism for hydrophilic polymers is that the amount of tightly bonded water to the polymer brushes creates a hydration and energy barrier that disfavors the adsorption of cells, proteins and other biomacromolecules. This suggests that contact angles should always be taken using water, the fluid in which they are intended to be used. Measurements both with pure water and aqueous solutions of diiodomethane etc. having different surface tensions can facilitate surface energy calculations. Knowledge of surface energy may allow improved prediction of protein adsorption due to hydration and brush conformation (Kobayashi, 2012).

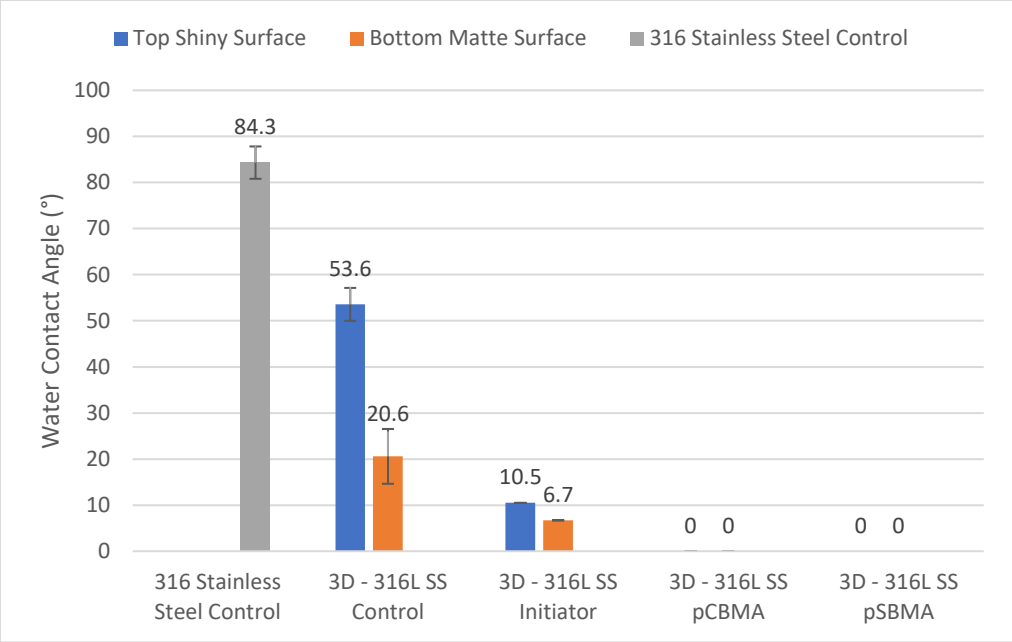

Figure 4-5: Water Contact Angles of Stainless Steel and modified Stainless Steel.

4.2.2 Protein Adsorption

Bovine serum albumin (BSA) was used as a model protein to allow comparison with the adsorption data in the previous chapter. Data on protein adsorption to 3D printed stainless steel (3D-SS) are shown in Figure 4-6. Adsorption on unmodified 3D printed stainless steel was 0.334 ± 0.002 μg/cm². After modification with the ATRP initiator (TMSP-BMPP), a slight increase in adsorption was observed; this is expected and consistent with other surfaces modified with TMSP-BMPP as seen in the previous chapter. The bromine of the initiator is likely to interact with certain amino acids in the protein (Kortagere, 2008) which may be the cause of the observed increase in adsorption on the TMSP-BMPP modified surfaces.

After further modification with zwitterionic polymer antifouling agents, the surfaces showed profoundly different effects. All parameters were kept the same as much as possible for the modifications with pCBMA and pSBMA. On the pCBMA-3D-SS surface, BSA adsorption increased by 184%, but decreased by 76% on the corresponding pSBMA modified surface. NMR spectra of the monomer (not shown) showed the same peaks as the original synthesized product, although the “mystery peak” was greater. If the mystery peak is indeed an impurity, this may have inhibited polymerization leading to an insufficient amount of CBMA polymer to form a layer dense enough to prevent protein adsorption. However, this does not explain why there was more protein adsorption on pCBMA modified 3D-SS than on unmodified 3D-SS and on TMSP-BMPP modified 3D-SS. Further investigation of the topography of these materials relating to surface roughness is required.

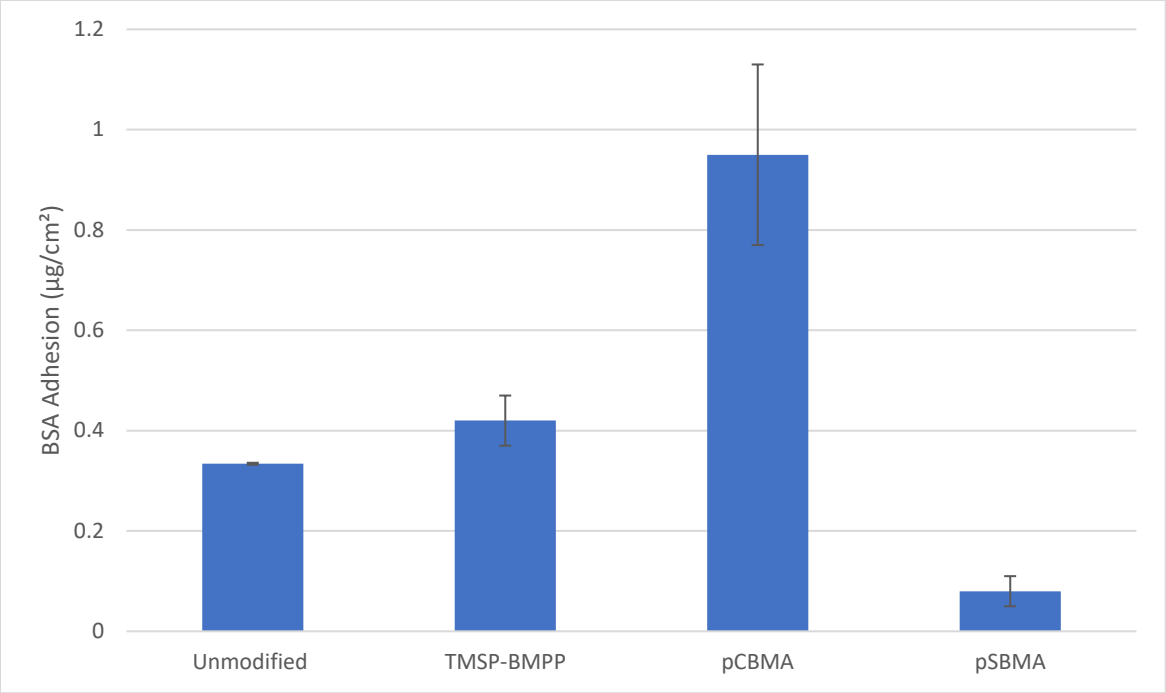

Figure 4-6: BSA Adsoprtion on 3D-printed unmodified and modified 316L stainless steel surfaces. Error bars are standard deviations for n = 4.

Since both the pCBMA- and pSBMA-modified surfaces showed promising water contact angle data, it was hypothesized that they should also have antifouling properties that would result in low protein adhesion. However, the pCBMA-modified surface showed almost 3-fold more adsorption than the 3D-SS control surface, despite showing complete water wetting (contact angle 0°).

Water contact angles were measured immediately after modification and 3xDI water rinse cycles prior to measurement. After WCA measurement, the substrates were incubated in phosphate buffered saline overnight in preparation for protein adsorption measurements. Residual pCBMA polymers physically adsorbed on the surface during WCA measurement may have been present, but after a longer soaking period, the pCBMA polymers were desorbed. The modified surfaces were handled more extensively than the control surfaces; therefore, it is likely that other contaminants that attract proteins may have remained on the pCBMA-modified surfaces. After the phosphate buffer soak overnight, water contact angles possibly should have been repeated to check if any change in contact angle had occurred indicating the presence of residual polymer and/or contaminant.

The procedure for the BSA adsorption tests on the 3D stainless steel surfaces did not allow for protein adsorption measurements on the 3 different surfaces (top, sides, and bottom) of the samples. The difference in water contact angle between the shiny top and matte bottom surfaces for the control and initiator modified surfaces show that surface

topography does play a role in wettability. Topography could therefore affect BSA adsorption since we hypothesized that, generally, the more hydrophilic the surface, the more it is protein resistant (Rabe, 2011). Both sides of the 3D printed sample showed complete wetting after pCBMA and pSBMA modifications. There is no clear correlation between water contact angle and BSA adsorption because although the initiator modified samples showed a lower contact angle than the pre-modified ones, they also showed greater fouling. Even more surprising is that the pCBMA modified surface adsorbed significantly more protein than the control. Jiang et al. have shown that using, the same ad-layer and polymerization method, pCBMA modified gold surface adsorbed less than 0.3 ng/cm^2 of fibrinogen (using SPR, Hong, 2017). However, SPR is a dynamic label-free method so that a direct comparison cannot be made with the static radiolabelling technique used in the present experiments. Wang et al. found, using a solution depletion method (bicinchoninic acid, BCA) under static conditions that poly(carboxybetaine) grafted on PET adsorbed about 5 µg/cm^2 BSA from buffer solution, representing only a 15% reduction (Wang, 2016). This technique and the adsorption levels are comparable to those in the experiments reported herein. For pSBMA modified stainless steel, Sin et al. achieved a reduction in fibrinogen adsorption of about 85% using an enzyme-linked immunosorbent assay (ELISA) method (Sin, 2014) to measure adsorption.

4.3 Conclusion

A novel approach to surface modification using the ARGET-ATRP method of polymerization with SBMA as monomer and a silane linker, was applied successfully for the modification of 3D-printed stainless steel. Water contact angle data showed that a change in surface properties occurred after modification with the zwitterionic polymers. Protein adsorption measurements showed that pSBMA modification reduced BSA adsorption significantly.

However, more work needs to be performed to understand why the pCBMA modified surface showed, contrary to expectation, increased protein adsorption despite being completely water wettable. In this regard it should be noted that although the contact angle technique is a rapid and simple method to detect changes in overall surface properties, it does not give insight into the detailed nature of the changes, e.g chemical vs physical, details on surface chemical composition. Additional experiments such as AFM to relate surface topography, and XPS to relate thickness of the polymer coating and surface chemistry to antifouling behavior would be required to explain why pCBMA modified surfaces showed higher protein adsorption than pSBMA, despite being completely water wettable.

5.0 Conclusion and Recommendations

5.1 Summary of Conclusions

A multi-material anti-fouling surface modification platform for aqueous based sensors and devices is highly sought after. Preventing non-specific protein adsorption must first be inhibited such that biofouling cannot progress. To accomplish this, a wide variety of potential antifouling agents have been developed and are commercially available. Among them, PEG is the gold standard but has oxidative stability and immunogenicity challenges. In addition, it loses its antifouling activity in complex media. Zwitterion-containing polymers are a new class of antifouling agent that are gradually taking the place of PEG as they have been shown to have superior antifouling functionality in “real world” biofluids. Since they are a new class of antifoulants, zwitterionic materials may be difficult to obtain commercially, so that in-house synthesis is required.

5.1.1 CBMA Synthesis and Polymerization

We first attempted to synthesize carboxybetaine methacrylate monomer using a less toxic and less expensive method with acrylic acid rather than β-propiolactone as reagent. Although the product obtained showed NMR spectra similar to literature data for the CBMA monomer, an “extra” peak appeared in our spectra. This peak remains unidentified but may simply be an impurity introduced during the synthesis process. Despite the presence of this unidentified impurity, the monomer polymerized readily via ARGET-ATRP to yield a product of high molecular weight as shown by GPC.

5.1.2 Surface Activation and Silanization

Silanes are commonly used as universal agents for coupling modifiers to surfaces. In this work oxygen plasma was used to create OH groups on surfaces to provide silane attachment sites. These OH sites were used to attach an ATRP-initiator-conjugated silanol to the surfaces. The density of initiator controls the density of subsequently grafted polymer chains which is crucial in forming an effective antifouling film. After plasma activation, all surfaces were found to be more hydrophilic but to different degrees, presumably due to the unique surface properties and chemistries of each surface, as shown by AFM and XPS.

Silanes are known to have hydrolytic stability challenges. Even with a given surface, solution phase deposition of the silanol initiator was not reproducible. Therefore, firm conclusions regarding the performance of the final modified surfaces are difficult to draw due to differences at the silanization stage of the surface preparation process in different experiments.

5.1.3 Modification with Zwitterions on Planar Surfaces

Subsequent modification of the silanized surfaces with pCBMA or pSBMA using SI-ARGET-ATRP allowed the surfaces to resist protein adsorption. Higher zwitterion content present on the surface was able to decrease protein adsorption. The overall protein

adsorption trends suggest that pCBMA may be the better antifouling polymer as it was able to resist protein adsorption to a higher degree than pSBMA on three of the four surfaces.

5.1.4 Modification with pSBMA on Additively Manufactured Stainless Steel

The same silanization and ARGET-ATRP procedure was performed on 3D printed stainless steel. The 3D structure of this material effectively gives rise to 3 different types of surface on the same substrate, thus creating challenges in the interpretation of surface characterization and protein adsorption experiments. The pCBMA-modified 3D-SS showed increased BSA adsorption compared to the control; this was unexpected based on the super wetting behavior seen in the WCA data.

5.2 Recommendations for Future Work

5.2.1 Repeatability of Experiments

Some of the data was inconsistent including the XPS which was only performed on one sample, ellipsometry which requires more thickness measurements to verify the grafting density and film thickness trends, and protein adsorption on the pCBMA modified 3D printed surfaces. Repeat experiments will verify the robustness of the TMSP-BMPP and SI-ARGET ATRP modifications.

5.2.2 Further Optimization of ARGET-ATRP

The PDI of the pCBMA chains were 1.53 which indicates opportunity to improve the control of polymerization. There are many parameters affecting SI-ARGET ATRP such as different types and concentrations of ligands, concentration of oxygen present during polymerization, and ascorbic acid concentration that could affect the chain length and film thicknesses. Optimized chain lengths are expected to decrease protein adsorption.

5.2.3 Long Term Hydrolytic Stability

As mentioned above, the long-term stability of both the silanol- and zwitterionic polymer-modified surfaces should be investigated thoroughly. All surface analyses of materials should ideally be completed in sequence without long time lags between. Given the long surface modification process and time-consuming nature of the analyses, this may not be possible and therefore, at a minimum, water contact angles should be taken prior to each analysis to determine if the surfaces have changed over time.

5.2.4 Grafting density and Film Thickness Effect on Protein Adsorption

The grafting of thick polymer layers that are in the “brush regime” is required for effective protein resistance. Further investigations with AFM, ellipsometry and XPS should be carried out to determine the grafting density of TMSP-BMPP required as this determines the density of the subsequent polymer grafts. Polymer brush thickness was difficult to obtain using ellipsometry on the different surfaces as some of the materials caused depolarization. An alternative method to determine polymer brush thickness would be angle resolved XPS (ARXPS) which provides data at different surface depths (Masotti,

2020). Also, as much as is possible, all characterizations should be completed in the environment in which the surfaces will be used, i.e., the aqueous environment. In-situ AFM and ellipsometry experiments, although they require specialized experimental setups are strongly recommended.

5.2.5 Protein Adsorption Studies with Other Relevant Proteins and in Complex Media.

The experiments described in this thesis to assess surface fouling involve only single component solutions of albumin. The typical *in situ* environment faced by a device would be much more complex, and would include multiple proteins, bacteria and other cells, cell fragments etc. Some of our surfaces have shown resistance to adsorption in a single protein environment, but antifouling performance may be diminished in complex media such as whole blood, plasma or serum. Systems of two proteins can be investigated using the radiolabelling technique. Each protein is radiolabelled with a different isotope. Fibrinogen and albumin together could be studied as a simplified plasma simulant with relevance to thrombosis. Other multiprotein methods are SDS-PAGE electrophoresis with immunoblotting and proteomics/mass spectrometry. In addition, real-time in situ techniques such as surface plasma resonance (SPR) (Köβlinger, 1995). and quartz crystal microbalance (QCM-D) can provide supplementary information (Köβlinger, 1995; Tonda-Turo, 2018). Bacteria are also important components of biofouling phenomena (Gristina, 1987; Karimi, 2015) and should be investigated in future work.

5.2.6 Use of Other Coupling Agents

Other platforms for coupling antifouling polymers to surfaces are available such as polydopamine (PDA) (Lee, 2007; Wang, 2016; Goh, 2018) and polyphenols (Pranantyo, 2015; Xu, 2018; Dong, 2018) as reviewed in Chapter 2. Both these compounds use both covalent and weaker interactions to bond to the surface and are ubiquitous/universal adhesives that attach without requiring surface pre-activation. The surface modification method used in this study was rather long and tedious: e.g., silanol attachment requires 6 h incubation time. The use of PDA or polyphenols would reduce the processing time significantly by eliminating the surface activation step and shortening the incubation time, typically to 2-4 h with PDA. However, for polymer brushes to be formed from these agents, a polymerization initiator would have to be incorporated. Such complexes of PDA/dopamine or polyphenol with initiator would have to be synthesized in house.

6.0 References

Abouelmagd, S. A., Meng, F., Kim, B. K., Hyun, H. & Yeo, Y. Tannic Acid-Mediated Surface Functionalization of Polymeric Nanoparticles. *ACS Biomater. Sci. Eng.* **2,** 2294–2303 (2016).

Abu Qudeiri, J. E. *et al.* Advanced electric discharge machining of stainless steels: Assessment of the state of the art, gaps and future prospect. *Materials* **16,** (2019).

Adly, N. Y. *et al.* Observation of chemically protected polydimethylsiloxane: Towards crack-free PDMS. *Soft Matter* **13,** 6297–6303 (2017).

Alberts, Bruce, et al. "The shape and structure of proteins." *Molecular Biology of the Cell. 4th edition*. Garland Science, 2002

Andrade, J. D., Hlady, V. & Wei, A. P. *Adsorption of complex proteins at interfaces*. *Pure & Appl. Chem* **64,** (1992).

Andrade, J. D. *et al. Proteins at Interfaces : Principles, Multivari Aspects, Protein Resistant Surfaces, and and Manipulation of Adsorbed Prote*. *Clinical Materiais I I* (1992).

Arkles, B. *Tailoring Surfaces with Silanes*.

Arkles, B. *Silane Coupling Agents: Connecting Across Boundaries*. (Gelest, Inc, 2014).

Asenath Smith, E. & Chen, W. How to prevent the loss of surface functionality derived from aminosilanes. *Langmuir* **24,** 12405–12409 (2008).

Badv, M., Jaffer, I. H., Weitz, J. I. & Didar, T. F. An omniphobic lubricant-infused coating produced by chemical vapor deposition of hydrophobic organosilanes attenuates clotting on catheter surfaces. *Sci. Rep.* **7,** (2017).

Bai, L., Gong, C., Chen, X., Sun, Y., Zhang, J., Cai, L., Zhu, S., Xie, S. Additive manufacturing of customized metallic orthopedic implants: Materials, structures, and surface modifications. *Metals* **9,** (2019).

Balasundaram, G., Sato, M. & Webster, T. J. Using hydroxyapatite nanoparticles and decreased crystallinity to promote osteoblast adhesion similar to functionalizing with RGD. *Biomaterials* **27,** 2798–2805 (2006).

Ball, V., Frari, D. Del, Toniazzo, V. & Ruch, D. Kinetics of polydopamine film deposition as a function of pH and dopamine concentration: Insights in the polydopamine deposition mechanism. *J. Colloid Interface Sci.* **386,** 366–372 (2012).

Barkarmo, S. *et al.* Biofilm formation on polyetheretherketone and titanium surfaces. *Clin. Exp. Dent. Res.* **5,** 427–437 (2019).

Becker, S., Merz, R., Hasse, H. & Kopnarski, M. Solvent cleaning and wettability of technical steel and titanium surfaces. *Adsorpt. Sci. Technol.* **34,** 261–274 (2016).

Bengani-Lutz, P., Converse, E., Cebe, P. & Asatekin, A. Self-Assembling Zwitterionic Copolymers as Membrane Selective Layers with Excellent Fouling Resistance: Effect of Zwitterion Chemistry. *ACS Appl. Mater. Interfaces* **9,** 20859–20872 (2017).

Bergenudd, H., Coullerez, G., Jonsson, M. & Malmström, E. Solvent effects on ATRP of oligo(ethylene glycol) methacrylate. exploring the limits of control. *Macromolecules* **42,** 3302–3308 (2009).

Beristain-Covarrubias, N. *et al.* Understanding Infection-Induced Thrombosis: Lessons Learned From Animal Models. *Frontiers in Immunology* **10,** (2019).

Bernhard, C. *et al.* Repelling and ordering: The influence of poly(ethylene glycol) on protein adsorption. *Phys. Chem. Chem. Phys.* **19,** 28182–28188 (2017).

Bhushan, P. *et al.* Biosensor for Monitoring Uric Acid in Wound and Its Proximity: A Potential Wound Diagnostic Tool. *J. Electrochem. Soc.* **166,** B830–B836 (2019).

Blackman, L. D., Gunatillake, P. A., Cass, P. & Locock, K. E. S. An introduction to zwitterionic polymer behavior and applications in solution and at surfaces. *Chemical Society Reviews* **48,** 757–770 (2019).

Bogaerts, A., Neyts, E., Gijbels, R. & Van Der Mullen, J. *Gas discharge plasmas and their applications*. *Spectrochimica Acta Part B* **57,** (2002).

Bohn, H. F. & Federle, W. Insect aquaplaning: Nepenthes pitcher plants capture prey with the peristome, a fully wettable water-lubricated anisotropic surface. in *Proceedings of the National Academy of Sciences* **101,** 14138–14143 (2004).

Branden, C. I. & Tooze, J., 2012, *Introduction to protein structure*. Garland Science, New York.

Brash, J. L., Horbett, T. A., Latour, R. A. & Tengvall, P. The blood compatibility challenge. Part 2: Protein adsorption phenomena governing blood reactivity. *Acta Biomaterialia* **94,** 11–24 (2019).

Brittain, W. J. & Minko, S. A structural definition of polymer brushes. *J. Polym. Sci. Part A Polym. Chem.* **45,** 3505–3512 (2007).

Chang, Y. *et al.* A highly stable nonbiofouling surface with well-packed grafted zwitterionic polysulfobetaine for plasma protein repulsion. *Langmuir* **24,** 5453–5458 (2008).

Chapman, J. & Regan, F. Nanofunctionalized superhydrophobic antifouling coatings for environmental sensor applications-advancing deployment with answers from nature. *Adv. Eng. Mater.* **14,** (2012).

Chen, S., Li, L., Zhao, C. & Zheng, J. Surface hydration: Principles and applications toward low-fouling/nonfouling biomaterials. *Polymer* **51,** 5283–5293 (2010).

Chen, S. *et al.* Tannic acid-inspiration and post-crosslinking of zwitterionic polymer as a universal approach towards antifouling surface. *Chem. Eng. J.* **337,** 122–132 (2018).

Cheng, G. *et al.* Zwitterionic carboxybetaine polymer surfaces and their resistance to long-term biofilm formation. *Biomaterials* **30,** 5234–5240 (2009).

Cheng, N., Brown, A. A., Azzaroni, O. & Huck, W. T. S. Thickness-dependent properties of polyzwitterionic brushes. *Macromolecules* **41,** 6317–6321 (2008).

Chiefari, J. *et al. Living Free-Radical Polymerization by Reversible Addition-Fragmentation Chain Transfer: The RAFT Process*. **18,** (UTC, 2021).

Choi, S. & Chae, J. Methods of reducing non-specific adsorption in microfluidic biosensors. *J. Micromechanics Microengineering* **20,** (2010).

Coclite, A. M. *et al.* 25th Anniversary Article: CVD polymers: A new paradigm for surface modification and device fabrication. *Advanced Materials* **25,** 5392–5423 (2013).

Colilla, M., Izquierdo-Barba, I. & Vallet-Regí, M. The Role of Zwitterionic Materials in the Fight against Proteins and Bacteria. *Medicines* **5,** 125 (2018).

Çulhaoğlu, A. K., Özkır, S. E., Şahin, V., Yılmaz, B. & Kılıçarslan, M. A. Effect of Various Treatment Modalities on Surface Characteristics and Shear Bond Strengths of Polyetheretherketone-Based Core Materials. *J. Prosthodont.* **29,** 136–141 (2020).

Damodaran, V. B. & Murthy, S. N. Bio-inspired strategies for designing antifouling biomaterials. *Biomater. Res.* **20,** (2016).

De Los Santos Pereira, A. *et al.* Antifouling Polymer Brushes Displaying Antithrombogenic Surface Properties. *Biomacromolecules* **17,** 1179–1185 (2016).

Dearmitt, C. & Rothon, R.N., 2011. Applied Plastics Engineering Handbook: Processing and Materials. *Chapter 25 Dispersants and Coupling Agents*. Myer Kutz, PDL.

Ding, Y. H., Floren, M. & Tan, W. Mussel-inspired polydopamine for bio-surface functionalization. *Biosurface and Biotribology* **2,** 121–136 (2016).

Dong, F. *et al.* Highly transparent thermoresponsive surfaces based on tea-stain-inspired chemistry. *J. Appl. Polym. Sci.* **135,** (2018).

Dong, H. & Matyjaszewski, K. ARGET ATRP of 2-(Dimethylamino)ethyl methacrylate as an intrinsic reducing agent. *Macromolecules* **41,** 6868–6870 (2008).

Dreyer, D. R., Miller, D. J., Freeman, B. D., Paul, D. R. & Bielawski, C. W. Perspectives on poly(dopamine). *Chem. Sci.* **4,** 3796–3802 (2013).

Ebnesajjad, S. and Ebnesajjad, C., 2013. *Surface treatment of materials for adhesive bonding*. William Andrew.

Ejima, H. *et al. One-Step Assembly of Coordination Complexes for Versatile Film and Particle Engineering*. *Source: Science* **341,** (2013).

Emmenegger, C. R. *et al.* Interaction of blood plasma with antifouling surfaces. *Langmuir* **25,** 6328–6333 (2009).

Ettelt, V. *et al.* Streptavidin-coated surfaces suppress bacterial colonization by inhibiting non-specific protein adsorption. *J. Biomed. Mater. Res. - Part A* **106,** 758–768 (2018).

Fadeeva, E., Schlie-Wolter, S., Chichkov, B.N., Paasche, G. and Lenarz, T., 2016. Structuring of biomaterial surfaces with ultrashort pulsed laser radiation. In *Laser Surface Modification of Biomaterials* (pp. 145-172). Woodhead Publishing.

Fantin, M., Isse, A. A., Gennaro, A. & Matyjaszewski, K. Understanding the Fundamentals of Aqueous ATRP and Defining Conditions for Better Control. *Macromolecules* **48,** 6862–6875 (2015).

Feng, W., Zhu, S., Ishihara, K. & Brash, J. L. Protein resistant surfaces: Comparison of acrylate graft polymers bearing oligo-ethylene oxide and phosphorylcholine side chains. *Biointerphases* **1,** 50–60 (2006).

Feng, W., Zhu, S., Ishihara, K. & Brash, J. L. Adsorption of fibrinogen and lysozyme on silicon grafted with poly(2-methacryloyloxyethyl phosphorylcholine) via surface-initiated atom transfer radical polymerization. *Langmuir* **21,** 5980–5987 (2005).

Flint, S. *et al.* Bacterial fouling in dairy processing. *International Dairy Journal* **101,** (2020).

Forooshani, P. K. & Lee, B. P. Recent approaches in designing bioadhesive materials inspired by mussel adhesive protein. *Journal of Polymer Science, Part A: Polymer Chemistry* **55,** 9–33 (2017).

Franz, S., Rammelt, S., Scharnweber, D. & Simon, J. C. Immune responses to implants - A review of the implications for the design of immunomodulatory biomaterials. *Biomaterials* **32,** 6692–6709 (2011).

Gerits, E. *et al.* Antibacterial activity of a new broad-spectrum antibiotic covalently bound to titanium surfaces. *J. Orthop. Res.* **34,** 2191–2198 (2016).

Ghaleh, H. *et al.* Biomimetic antifouling PDMS surface developed via well-defined polymer brushes for cardiovascular applications. *Eur. Polym. J.* **106,** 305–317 (2018).

Goh, S. C. *et al.* Polydopamine–polyethylene glycol–albumin antifouling coatings on multiple substrates. *J. Mater. Chem. B* 940–949 (2018). doi:10.1039/C7TB02636F

Gristina, A. G. *Biomaterial-Centered Infection: Microbial Adhesion Versus Tissue Integration*. *New Series* **237,** (1987).

Gu, Z. *et al.* Surface curvature relation to protein adsorption for carbon-based nanomaterials. *Sci. Rep.* **5,** (2015).

Guo, J., Suma, T., Richardson, J. J. & Ejima, H. Modular Assembly of Biomaterials Using Polyphenols as Building Blocks. *ACS Biomaterials Science and Engineering* **5,** 5578–5596 (2019).

Harding, J. L. & Reynolds, M. M. Combating medical device fouling. *Trends Biotechnol.* **32,** 140–146 (2014).

Hecker, M., Ting, M. S. H. & Malmström, J. Simple coatings to render polystyrene protein resistant. *Coatings* **8,** (2018).

Hirsh, S. L. *et al.* The Vroman effect: Competitive protein exchange with dynamic multilayer protein aggregates. *Colloids Surfaces B Biointerfaces* **103,** 395–404 (2013).

Hlady, V., Buijs, J. & Jennissen, H. P. *[26] Methods for Studying Protein Adsorption*. (1999).

Holländer, A. & Cosemans, P. Surface technology for additive manufacturing. *Plasma Process. Polym.* **17,** (2020).

Holmlin, R. E., Chen, X., Chapman, R. G., Takayama, S. & Whitesides, G. M. Zwitterionic SAMs that resist nonspecific adsorption of protein from aqueous buffer. *Langmuir* **17,** 2841–2850 (2001).

Hołysz, L., Mirosław, M., Terpiłowski, K. & Szcześ, A. Influence of relative humidity on the wettability of silicon wafer surfaces. *Ann. UMCS, Chem.* **63,** (2010).

Hong, D. *et al.* Achieving Ultralow Fouling under Ambient Conditions via Surface-Initiated ARGET ATRP of Carboxybetaine. *ACS Appl. Mater. Interfaces* **9,** 9255–9259 (2017).

Hong, S. H. *et al.* Sprayable Ultrafast Polydopamine Surface Modifications. *Adv. Mater. Interfaces* **3,** 1–6 (2016).

Hong, S. *et al.* Non-covalent self-assembly and covalent polymerization co-contribute to polydopamine formation. *Adv. Funct. Mater.* **22,** 4711–4717 (2012).

Howell, C., Grinthal, A., Sunny, S., Aizenberg, M. & Aizenberg, J. Designing Liquid-Infused Surfaces for Medical Applications: A Review. *Advanced Materials* **30,** (2018).

Hsu, L. *et al.* Development of a low-cost hemin-based dissolved oxygen sensor with anti-biofouling coating for water monitoring. *IEEE Sens. J.* **14,** 3400–3407 (2014).

Huang, C. J., Wang, L. C., Shyue, J. J. & Chang, Y. C. Developing antifouling biointerfaces based on bioinspired zwitterionic dopamine through pH-modulated assembly. *Langmuir* **30,** 12638–12646 (2014).

Huang, J. *et al.* A survey of design methods for material extrusion polymer 3D printing. *Virtual and Physical Prototyping* **15,** 148–162 (2020).

Huang, S., Liang, N., Hu, Y., Zhou, X. & Abidi, N. Polydopamine-Assisted Surface Modification for Bone Biosubstitutes. *BioMed Research International* **2016,** (2016).

Hynninen, V. *et al.* Improved antifouling properties and selective biofunctionalization of stainless steel by employing heterobifunctional silane-polyethylene glycol overlayers and avidin-biotin technology. *Sci. Rep.* **6,** (2016).

Inagaki, N., Tasaka, S., Horiuchi, T. & Suyama, R. *Surface Modification of Poly (aryl ether ether ketone) Film by Remote Oxygen Plasma*. *J Appl Polym Sci* **68,** (John Wiley & Sons, Inc, 1998).

Ishihara, K. *et al.* Hemocompatibility of human whole blood on polymers with a phospholipid polar group and its mechanism. *J. Biomed. Mater. Res.* **26,** 1543–1552 (1992).

Ishino, C., Reyssat, M., Reyssat, E., Okumura, K. & Quéré, D. Wicking within forests of micropillars. *EPL* **79,** (2007).

Jaffer, I. H. & Weitz, J. I. The blood compatibility challenge. Part 1: Blood-contacting medical devices: The scope of the problem. *Acta Biomaterialia* **94,** 2–10 (2019).

Jesmer, A. H., Huynh, V. & Wylie, R. G. Fabrication of low-fouling, high-loading polymeric surfaces through pH-controlled RAFT. *RSC Adv.* **10,** 20302–20312 (2020).

Jiang, C. *et al.* Antifouling Strategies for Selective in Vitro and in Vivo Sensing. *Chemical Reviews* **120,** 3852–3889 (2020).

Jiang, S. & Cao, Z. Ultralow-fouling, functionalizable, and hydrolyzable zwitterionic materials and their derivatives for biological applications. *Adv. Mater.* **22,** 920–932 (2010).

Jin, Q., Chen, Y., Wang, Y. & Ji, J. Zwitterionic drug nanocarriers: A biomimetic strategy for drug delivery. *Colloids Surfaces B Biointerfaces* **124,** 80–86 (2014).

Jo, S. & Park, K. Surface modification using silanated poly(ethylene glycol)s. *Biomaterials* **21,** 605–616 (2000).

Jun, K. H., Kwak, J. H. & Lim, K. S. *Simulation of depolarization effect by a rough surface for spectroscopic ellipsometry*. (2003).

Kang, H., Jeong, W. & Hong, D. Antifouling Surface Coating Using Droplet-Based SI-ARGET ATRP of Carboxybetaine under Open-Air Conditions. *Langmuir* **35,** 7744–7750 (2019).

Kang, S. M. *et al.* One-step multipurpose surface functionalization by adhesive catecholamine. *Adv. Funct. Mater.* **22,** 2949–2955 (2012).

Karimi, A., Karig, D., Kumar, A. & Ardekani, A. M. Interplay of physical mechanisms and biofilm processes: Review of microfluidic methods. *Lab on a Chip* **15,** 23–42 (2015).

Khalili, A. A. & Ahmad, M. R. A Review of cell adhesion studies for biomedical and biological applications. *International Journal of Molecular Sciences* **16,** 18149–18184 (2015).

Kijblinger, C. *et al. Comparison of the QCM and th'e SPR method for surface studies and immunological applications*. *Sensors and Actuators B* **262,** (1995).

Kingshott, P., Thissen, H. & Griesser, H. J. *Effects of cloud-point grafting, chain length, and density of PEG layers on competitive adsorption of ocular proteins*. *Biomaterials* **23,** (2002).

Kobayashi, M. *et al.* Wettability and antifouling behavior on the surfaces of superhydrophilic polymer brushes. *Langmuir* **28,** 7212–7222 (2012).

Kobayashi, M. *et al.* Structure and surface properties of high-density polyelectrolyte brushes at the interface of aqueous solution. *Macromol. Symp.* **279,** 79–87 (2009).

Kopac, T., Bozgeyik, K. & Yener, J. Effect of pH and temperature on the adsorption of bovine serum albumin onto titanium dioxide. *Colloids Surfaces A Physicochem. Eng. Asp.* **322,** 19–28 (2008).

Kortagere, S., Ekins, S. & Welsh, W. J. Halogenated ligands and their interactions with amino acids: Implications for structure-activity and structure-toxicity relationships. *J. Mol. Graph. Model.* **27,** 170–177 (2008).

Kostruba, A., Stetsyshyn, Y. & Vlokh, R. Method for determination of the parameters of transparent ultrathin films deposited on transparent substrates under conditions of low optical contrast. *Appl. Opt.* **54,** 6208 (2015).

Krause, J. E. *et al.* Photoiniferter-mediated polymerization of zwitterionic carboxybetaine monomers for low-fouling and functionalizable surface coatings. *Macromolecules* **44,** 9213–9220 (2011).

Kurzbaum, E. *et al.* From the Titanic and other shipwrecks to biofilm prevention: The interesting role of polyphenol-protein complexes in biofilm inhibition. *Science of the Total Environment* **658,** 1098–1105 (2019).

Laschewsky, A. Structures and synthesis of zwitterionic polymers. *Polymers* **6,** 1544–1601 (2014).

Lee, H., Scherer, N. F. & Messersmith, P. B. Single-molecule mechanics of mussel adhesion. *Proc. Natl. Acad. Sci.* **103,** 12999–13003 (2006).

Lee, H., Dellatore, S. M., Miller, W. M. & Messersmith, P. B. Mussel-Inspired Surface Chemistry for Multifunctional Coatings. *Science (80-.).* **318,** 426–430 (2007).

Lee, S., Kim, S., Park, J. & Lee, J. Y. Universal surface modification using dopamine-hyaluronic acid conjugates for anti-biofouling. *Int. J. Biol. Macromol.* **151,** 1314–1321 (2020).

Lehaitre, M. & Compere, C. *Real-Time Coastal Observing Systems for Marine Ecosystem Dynamics and Harmful Algal Blooms: Theory, instrumentation and modelling*. *Biofouling and Underwater Measurements* (Unesco publishing, 2008).

Leng, C. *et al.* Probing the Surface Hydration of Nonfouling Zwitterionic and PEG Materials in Contact with Proteins. *ACS Appl. Mater. Interfaces* **7,** 16881–16888 (2015).

Leng, C., Sun, S., Zhang, K., Jiang, S. & Chen, Z. Molecular level studies on interfacial hydration of zwitterionic and other antifouling polymers in situ. *Acta Biomaterialia* **40,** 6–15 (2016).

Leslie, D. C. *et al.* A bioinspired omniphobic surface coating on medical devices prevents thrombosis and biofouling. *Nat. Biotechnol.* **32,** 1134–1140 (2014).

Li, B., Yu, B., Ye, Q. & Zhou, F. Tapping the potential of polymer brushes through synthesis. *Acc. Chem. Res.* **48,** 229–237 (2015).

Li, B. *et al. Trimethylamine N-oxide-derived zwitterionic polymers: A new class of ultralow fouling bioinspired materials*. *Sci. Adv* **5,** (2019).

Li, B. *et al.* De novo design of functional zwitterionic biomimetic material for immunomodulation. *Sci. Adv.* **6,** (2020).

Li, Y., Xue, H., Song, Y. & Zwitter Technology LLC. Patent_Production_Purification_CB_Monomers. (2014).

Li, Z. & Guo, Z. Bioinspired surfaces with wettability for antifouling application. *Nanoscale* **11,** 22636–22663 (2019).

Lichtenberg, J. Y., Ling, Y. & Kim, S. Non-specific adsorption reduction methods in biosensing. *Sensors (Switzerland)* **19,** (2019).

Limoli, D. H., Jones, C. J. & Wozniak, D. J. Bacterial Extracellular Polysaccharides in Biofilm Formation and Function. *Microbiol. Spectr.* **3,** (2015).

Lin, W., Ma, G., Wu, J. & Chen, S. Different in vitro and in vivo behaviors between Poly(carboxybetaine methacrylate) and poly(sulfobetaine methacrylate). *Colloids Surfaces B Biointerfaces* **146,** 888–894 (2016).

Lopez-Mila, B. *et al.* Effect of shear stress on the reduction of bacterial adhesion to antifouling polymers. *Bioinspiration and Biomimetics* **13,** (2018).

Luan, Y. *et al.* 125I-radiolabeling, surface plasmon resonance, and quartz crystal microbalance with dissipation: Three tools to compare protein adsorption on surfaces of different wettability. *Langmuir* **30,** 1029–1035 (2014).

Malmsten, M., Emoto, K. & Van Alstine, J. M. *Effect of Chain Density on Inhibition of Protein Adsorption by Poly(ethylene glycol) Based Coatings*. *JOURNAL OF COLLOID AND INTERFACE SCIENCE* **202,** (1998).

Manna, U. & Lynn, D. M. Fabrication of liquid-infused surfaces using reactive polymer multilayers: Principles for manipulating the behaviors and mobilities of aqueous fluids on slippery liquid interfaces. *Adv. Mater.* **27,** 3007–3012 (2015).

Masotti, E. *et al.* Fluorinated vs. zwitterionic-polymer grafted surfaces for adhesion prevention of the fungal pathogen Candida albicans. *Polymers (Basel).* **12,** (2020).

Matsuda, Takehisa. "Photoiniferter-driven precision surface graft microarchitectures for biomedical applications." *Surface-Initiated Polymerization I*. Springer, Berlin, Heidelberg, 2006. 67-106.

Matyjaszewski, K., Hongchen, D., Jakubowski, W., Pietrasik, J. & Kusumo, A. Grafting from surfaces for 'everyone': ARGET ATRP in the presence of air. *Langmuir* **23,** 4528–4531 (2007).

Matyjaszewski, K. *et al. Diminishing catalyst concentration in atom transfer radical polymerization with reducing agents*. *PNAS October* **17,** (2006).

Matyjaszewski, K., Patten, T. E. & Xia, J. *Controlled/"Living" Radical Polymerization. Kinetics of the Homogeneous Atom Transfer Radical Polymerization of Styrene*. (1997).

Mcgovern, M. E., Kallury, K. M. R. & Thompson, M. *Role of Solvent on the Silanization of Glass with Octadecyltrichlorosilane*. *Langmuir* **10,** (1994).

Meissner, J., Prause, A., Bharti, B. & Findenegg, G. H. Characterization of protein adsorption onto silica nanoparticles: influence of pH and ionic strength. *Colloid Polym. Sci.* **293,** 3381–3391 (2015).

Miller, D. J. *et al.* Short-term adhesion and long-term biofouling testing of polydopamine and poly(ethylene glycol) surface modifications of membranes and feed spacers for biofouling control. *Water Res.* **46,** 3737–3753 (2012).

Motaman, S. A. H. *et al.* Optimal Design for Metal Additive Manufacturing: An Integrated Computational Materials Engineering (ICME) Approach. *JOM* **72,** 1092–1104 (2020).

Nishioka, S. *et al.* Facile design of plant-oil-infused fine surface asperity for transparent blood-repelling endoscope lens. *RSC Adv.* **6,** 47579–47587 (2016).

Noh, H. & Vogler, E. A. Volumetric interpretation of protein adsorption: Competition from mixtures and the Vroman effect. *Biomaterials* **28,** 405–422 (2007).

Occhiello, E., Guerrini, G. & Garbassi, F. *Adhesion properties of plasma-treated carbon/PEEK composites*.

Ohtani, K. *et al.* Surface treatment of flow channels in microfluidic devices fabricated by stereolithography. *Journal of Oleo Science* **63,** 93–96 (2014).

Okhrimenko, D. V. *et al.* Hydrolytic Stability of 3-Aminopropylsilane Coupling Agent on Silica and Silicate Surfaces at Elevated Temperatures. *ACS Appl. Mater. Interfaces* **9,** 8344–8353 (2017).

Ostuni, E., Chapman, R. G., Holmlin, R. E., Takayama, S. & Whitesides, G. M. A survey of structure-property relationships of surfaces that resist the adsorption of protein. *Langmuir* **17,** 5605–5620 (2001).

Oter, Z. C., Gencer, Y. & Tarakci, M. Microstructure evolution and surface quality of laser-sintered maraging steel parts produced on different building platform positions. *Optik (Stuttg).* **202,** (2020).

Pan, C. J., Hou, Y. H., Zhang, B. Bin, Dong, Y. X. & Ding, H. Y. Blood compatibility and interaction with endothelial cells of titanium modified by sequential immobilization of poly (ethylene glycol) and heparin. *J. Mater. Chem. B* **2,** 892–902 (2014).

Park, J. *et al.* Antimicrobial spray nanocoating of supramolecular Fe(III)-tannic acid metal-organic coordination complex: Applications to shoe insoles and fruits. *Sci. Rep.* **7,** (2017).

Pasche, S., Vo, J., Griesser, H. J., Spencer, N. D. & Textor, M. Effects of Ionic Strength and Surface Charge on Protein Adsorption at PEGylated Surfaces. (2005). doi:10.1021/jp050431

Pasternack, R. M., Amy, S. R. & Chabal, Y. J. Attachment of 3-(aminopropyl)triethoxysilane on silicon oxide surfaces: Dependence on solution temperature. *Langmuir* **24,** 12963–12971 (2008).

Peng, Z. *et al.* Dual effects and mechanism of TiO2 nanotube arrays in reducing bacterial colonization and enhancing C3H10T1/2 cell adhesion. *Int. J. Nanomedicine* **8,** 3093–3105 (2013).

Petroff, M. G., Garcia, E. A., Herrera-Alonso, M. & Bevan, M. A. Ionic Strength-Dependent Interactions and Dimensions of Adsorbed Zwitterionic Copolymers. *Langmuir* **35,** 4976–4985 (2019).

Pop-Georgievski, O. *et al.* Poly(ethylene oxide) layers grafted to dopamine-melanin anchoring layer: Stability and resistance to protein adsorption. *Biomacromolecules* **12,** 3232–3242 (2011).

Pranantyo, D. *et al.* Tea Stains-Inspired Initiator Primer for Surface Grafting of Antifouling and Antimicrobial Polymer Brush Coatings. *Biomacromolecules* **16,** 723–732 (2015).

Pujari, S. P., Scheres, L., Marcelis, A. T. M. & Zuilhof, H. Covalent surface modification of oxide surfaces. *Angewandte Chemie - International Edition* **53,** 6322–6356 (2014).

Rabe, M., Verdes, D. & Seeger, S. Understanding protein adsorption phenomena at solid surfaces. *Advances in Colloid and Interface Science* **162,** 87–106 (2011).

Rechendorff, K., Hovgaard, M. B., Foss, M., Zhdanov, V. P. & Besenbacher, F. Enhancement of protein adsorption induced by surface roughness. *Langmuir* **22,** 10885–10888 (2006).

Roach, P., Farrar, D. & Perry, C. C. Surface tailoring for controlled protein adsorption: Effect of topography at the nanometer scale and chemistry. *J. Am. Chem. Soc.* **128,** 3939–3945 (2006).

Roach, P., Farrar, D. & Perry, C. C. Interpretation of protein adsorption: Surface-induced conformational changes. *J. Am. Chem. Soc.* **127,** 8168–8173 (2005).

Rowley, A. T., Nagalla, R. R., Wang, S. W. & Liu, W. F. Extracellular Matrix-Based Strategies for Immunomodulatory Biomaterials Engineering. *Advanced Healthcare Materials* **8,** (2019).

Sakamaki, T. *et al.* Ion-Specific Hydration States of Zwitterionic Poly(sulfobetaine methacrylate) Brushes in Aqueous Solutions. *Langmuir* **35,** 1583–1589 (2019).

Schlenoff, J. B. Zwitteration: Coating surfaces with zwitterionic functionality to reduce nonspecific adsorption. *Langmuir* **30,** 9625–9636 (2014).

Scopelliti, P. E. *et al.* The effect of surface nanometre-scale morphology on protein adsorption. *PLoS One* **5,** (2010).

Seeliger, F. & Matyjaszewski, K. Temperature effect on activation rate constants in ATRP: New mechanistic insights into the activation process. *Macromolecules* **42,** 6050–6055 (2009).

Shao, Q., He, Y., White, A. D. & Jiang, S. Difference in hydration between carboxybetaine and sulfobetaine. *J. Phys. Chem. B* **114,** 16625–16631 (2010).

Shao, Q. & Jiang, S. Effect of carbon spacer length on zwitterionic carboxybetaines. *J. Phys. Chem. B* **117,** 1357–1366 (2013).

Sheng, W. *et al.* Brushing up from “anywhere” under sunlight: a universal surface-initiated polymerization from polydopamine-coated surfaces. *Chem. Sci.* **6,** 2068–2073 (2015).

Sileika, T. S., Barrett, D. G., Zhang, R., Lau, K. H. A. & Messersmith, P. B. Colorless multifunctional coatings inspired by polyphenols found in tea, chocolate, and wine. *Angew. Chemie - Int. Ed.* **52,** 10766–10770 (2013).

Simakova, A., Averick, S. E., Konkolewicz, D. & Matyjaszewski, K. Aqueous ARGET ATRP. *Macromolecules* **45,** 6371–6379 (2012).

Sin, M. C., Sun, Y. M. & Chang, Y. Zwitterionic-based stainless steel with well-defined polysulfobetaine brushes for general bioadhesive control. *ACS Appl. Mater. Interfaces* **6,** 861–873 (2014).

Sotiri, I., Overton, J. C., Waterhouse, A. & Howell, C. Immobilized liquid layers: A new approach to anti-adhesion surfaces for medical applications. *Exp. Biol. Med.* **241,** 909–918 (2016).

Sun, F. *et al.* Paper Sensor Coated with a Poly(carboxybetaine)-Multiple DOPA Conjugate via Dip-Coating for Biosensing in Complex Media. *Anal. Chem.* **89,** 10999–11004 (2017).

Sun, X. *et al.* Creation of antifouling microarrays by photopolymerization of zwitterionic compounds for protein assay and cell patterning. *Biosens. Bioelectron.* **102,** 63–69 (2018).

Tang, H. *et al.* Highly active copper-based catalyst for atom transfer radical polymerization. *J. Am. Chem. Soc.* **128,** 16277–16285 (2006).

Tang, W. *et al.* Understanding atom transfer radical polymerization: Effect of ligand and initiator structures on the equilibrium constants. *J. Am. Chem. Soc.* **130,** 10702–10713 (2008).

Tang, W. & Matyjaszewski, K. Effect of ligand structure on activation rate constants in ATRP. *Macromolecules* **39,** 4953–4959 (2006).

Tang, Y. P., Cai, T., Loh, D., O'Brien, G. S. & Chung, T. S. Construction of antifouling lumen surface on a poly(vinylidene fluoride) hollow fiber membrane via a zwitterionic graft copolymerization strategy. *Sep. Purif. Technol.* **176,** 294–305 (2017).

Tangpasuthadol, V., Pongchaisirikul, N. & Hoven, V. P. Surface modification of chitosan films. Effects of hydrophobicity on protein adsorption. *Carbohydr. Res.* **338,** 937–942 (2003).

Thompson, C. *et al.* Impact of Magnetic Stirring on Stainless Steel Integrity: Effect on Biopharmaceutical Processing. *J. Pharm. Sci.* **106,** 3280–3286 (2017).

Tilton, R. D., Channing, R. R. & Alice, P. Manipulation of Hydrophobic Interactions in Protein Adsorption. *Langmuir* **7,** 2710–2718 (1991).

Tonda-Turo, C., Carmagnola, I. & Ciardelli, G. Quartz crystal microbalance with dissipation monitoring: A powerful method to predict the in vivo behavior of bioengineered surfaces. *Frontiers in Bioengineering and Biotechnology* **6,** (2018).

Torstrick, F. B. *et al.* Impaction durability of porous polyether-ether-ketone (PEEK) and titanium-coated PEEK interbody fusion devices. *Spine J.* **18,** 857–865 (2018).

Tsarevsky, N. V., Pintauer, T. & Matyjaszewski, K. Deactivation efficiency and degree of control over polymerization in ATRP in protic solvents. *Macromolecules* **37,** 9768–9778 (2004).

Unsworth, L. D., Sheardown, H. & Brash, J. L. Protein-resistant polyethylene oxide-grafted surfaces: Chain density-dependent multiple mechanisms of action. *Langmuir* **24,** 1924–1929 (2008).

Ventura, C. *et al.* Marine antifouling performance of polymer coatings incorporating zwitterions. *Biofouling* **33,** 892–903 (2017).

Viefhues, M. *et al.* Physisorbed surface coatings for poly(dimethylsiloxane) and quartz microfluidic devices. *Anal. Bioanal. Chem.* **401,** 2113–2122 (2011).

Vilaseca, P., Dawson, K. A. & Franzese, G. Understanding and modulating the competitive surface-adsorption of proteins through coarse-grained molecular dynamics simulations. *Soft Matter* **9,** 6978–6985 (2013).

Visalakshan, R. M. *et al.* Biomaterial Surface Hydrophobicity-Mediated Serum Protein Adsorption and Immune Responses. *ACS Appl. Mater. Interfaces* **11,** 27615–27623 (2019).

Wang, F. *et al.* Review of the research on anti-protein fouling coatings materials. *Progress in Organic Coatings* **147,** (2020).

Wang, J.-S., Matyjaszewski, K. & Zanden, van. Controlled/“Living” Radical Polymerization. Atom Transfer Radical Polymerization in the Presence of Transition-Metal Complexes. *J. Am. Chem. Soc.* **117,** 5614–5615 (1995).

Wang, P. X., Dong, Y. S., Lu, X. W., Du, J. & Wu, Z. Q. Marrying mussel inspired chemistry with photoiniferters: A novel strategy for surface functionalization. *Polym. Chem.* **7,** 5563–5570 (2016).

Wang, P., Lu, Z. & Zhang, D. Slippery liquid-infused porous surfaces fabricated on aluminum as a barrier to corrosion induced by sulfate reducing bacteria. *Corros. Sci.* **93,** 159–166 (2015).

Wang, T., Wang, X., Long, Y., Liu, G. & Zhang, G. Ion-specific conformational behavior of polyzwitterionic brushes: Exploiting it for protein adsorption/desorption control. *Langmuir* **29,** 6588–6596 (2013).

Wang, Y., Shen, J. & Yuan, J. Design of hemocompatible and antifouling PET sheets with synergistic zwitterionic surfaces. *J. Colloid Interface Sci.* **480,** 205–217 (2016).

Wei, Q., Zhang, F., Li, J., Li, B. & Zhao, C. Oxidant-induced dopamine polymerization for multifunctional coatings. *Polym. Chem.* **1,** 1430–1433 (2010).

Wong, T. S. *et al.* Bioinspired self-repairing slippery surfaces with pressure-stable omniphobicity. *Nature* **477,** 443–447 (2011).

Wu, A., Gao, Y. & Zheng, L. Zwitterionic amphiphiles: Their aggregation behavior and applications. *Green Chemistry* **21,** 4290–4312 (2019).

Wu, H., Moser, C., Wang, H. Z., Høiby, N. & Song, Z. J. Strategies for combating bacterial biofilm infections. *International Journal of Oral Science* **7,** 1–7 (2015).

Wu, H. *et al.* One-pot synthesis of polydopamine-Zn complex antifouling coatings on membranes for ultrafiltration under harsh conditions. *RSC Adv.* **6,** 103390–103398 (2016).

Xie, Q., Pan, J., Ma, C. & Zhang, G. Dynamic surface antifouling: Mechanism and systems. *Soft Matter* **15,** 1087–1107 (2019).

Xu, G. *et al.* One-Step Anchoring of Tannic Acid-Scaffolded Bifunctional Coatings of Antifouling and Antimicrobial Polymer Brushes. *ACS Sustain. Chem. Eng.* **7,** 1786–1795 (2019).

Xu, L. Q., Neoh, K. G. & Kang, E. T. Natural polyphenols as versatile platforms for material engineering and surface functionalization. *Progress in Polymer Science* **87,** 165–196 (2018).

Xu, Z., Han, R., Liu, N., Gao, F. & Luo, X. Electrochemical biosensors for the detection of carcinoembryonic antigen with low fouling and high sensitivity based on copolymerized polydopamine and zwitterionic polymer. *Sensors Actuators, B Chem.* **319,** (2020).

Yadav, A. R., Sriram, R., Carter, J. A. & Miller, B. L. Comparative study of solution-phase and vapor-phase deposition of aminosilanes on silicon dioxide surfaces. *Mater. Sci. Eng. C* **35,** 283–290 (2014).

Yang, S., Zhang, S. P., Winnik, F. M., Mwale, F. & Gong, Y. K. Group reorientation and migration of amphiphilic polymer bearing phosphorylcholine functionalities on surface of cellular membrane mimicking coating. *J. Biomed. Mater. Res. - Part A* **84,** 837–841 (2008).

Yang, W. *et al.* Film thickness dependence of protein adsorption from blood serum and plasma onto poly(sulfobetaine)-grafted surfaces. *Langmuir* **24,** 9211–9214 (2008).

Yang, W., Xue, H., Li, W., And, J. Z. & Jiang, S. Pursuing 'zero' protein adsorption of poly(carboxybetaine) from undiluted blood serum and plasma. *Langmuir* **25,** 11911–11916 (2009).

Yang, Z., Saeki, D. & Matsuyama, H. Zwitterionic polymer modification of polyamide reverse-osmosis membranes via surface amination and atom transfer radical polymerization for anti-biofouling. *J. Memb. Sci.* **550,** 332–339 (2018).

Ye, Q., Zhou, F. & Liu, W. Bioinspired catecholic chemistry for surface modification. *Chem. Soc. Rev.* **40,** 4244 (2011).

Yu, B. Y. *et al.* Surface zwitterionization of titanium for a general bio-inert control of plasma proteins, blood cells, tissue cells, and bacteria. *Langmuir* **30,** 7502–7512 (2014).

Yu, Q., Zhang, Y., Wang, H., Brash, J. & Chen, H. Anti-fouling bioactive surfaces. *Acta Biomater.* **7,** 1550–1557 (2011).

Yuan, L., Yu, Q., Li, D. & Chen, H. Surface Modification to Control Protein/Surface Interactions. *Macromol. Biosci.* **11,** 1031–1040 (2011).

Zhan, K., Kim, C., Sung, K., Ejima, H. & Yoshie, N. Tunicate-Inspired Gallol Polymers for Underwater Adhesive: A Comparative Study of Catechol and Gallol. *Biomacromolecules* **18,** 2959–2966 (2017).

Zhang, A., Cheng, L., Hong, S., Yang, C. & Lin, Y. Preparation of anti-fouling silicone elastomers by covalent immobilization of carboxybetaine. *RSC Adv.* **5,** 88456–88463 (2015).

Zhang, H. & Chiao, M. Anti-fouling coatings of poly(dimethylsiloxane) devices for biological and biomedical applications. *Journal of Medical and Biological Engineering* **35,** 143–155 (2015).

Zhang, Y., Thingholm, B., Goldie, K. N., Ogaki, R. & Städler, B. Assembly of poly(dopamine) films mixed with a nonionic polymer. *Langmuir* **28,** 17585–17592 (2012).

Zhang, Y. *et al.* Fundamentals and applications of zwitterionic antifouling polymers. *J. Phys. D. Appl. Phys.* **52,** (2019).

Zhang, Y. *et al.* Additive Manufacturing of Metallic Materials: A Review. *Journal of Materials Engineering and Performance* **27,** (2018).

Zhang, Z., Chen, S., Chang, Y. & Jiang, S. Surface grafted sulfobetaine polymers via atom transfer radical polymerization as superlow fouling coatings. *J. Phys. Chem. B* **110,** 10799–10804 (2006).

Zhang, Z., Chen, S. & Jiang, S. Dual-functional biomimetic materials: Nonfouling poly(carboxybetaine) with active functional groups for protein immobilization. *Biomacromolecules* **7,** 3311–3315 (2006).

Zhang, Z. *et al.* Polysulfobetaine-grafted surfaces as environmentally benign ultralow fouling marine coatings. *Langmuir* **25,** 13516–13521 (2009).

Zhao, B. & Brittain, W. J. *Polymer brushes: surface-immobilized macromolecules*.

Zhao, C., Zhang, G., Xu, X., Yang, F. & Yang, Y. Rapidly self-assembled polydopamine coating membranes with polyhexamethylene guanidine: Formation, characterization and antifouling evaluation. *Colloids Surfaces A Physicochem. Eng. Asp.* **512,** 41–50 (2017).

Zhao, D. *et al.* Fouling-resistant behavior of liquid-infused porous slippery surfaces. *Chinese J. Polym. Sci. (English Ed.* **35,** 887–896 (2017).

Zhao, Y. *et al.* Fabrication of stable biomimetic coating on PDMS surface: Cooperativity of multivalent interactions. *Appl. Surf. Sci.* **469,** 720–730 (2019).

Zhu, M., Lerum, M. Z. & Chen, W. How to prepare reproducible, homogeneous, and hydrolytically stable aminosilane-derived layers on silica. *Langmuir* **28,** 416–423 (2012).

Zhu, Y. *et al.* Cellulose paper sensors modified with zwitterionic poly(carboxybetaine) for sensing and detection in complex media. *Anal. Chem.* **86,** 2871–2875 (2014).

Zoppe, J. O., Ataman, N.C., Mocny, P., Wang, J., Moaraes, J., Klok, H. Surface-Initiated Controlled Radical Polymerization: State-of-the-Art, Opportunities, and Challenges in Surface And Interface Engineering with Polymer Brushes. *Chem. Rev.* **117,** 1105-1318 (2017).

7.0 Appendix

7.1 Carboxybetaine Methacrylate Monomer Synthesis

Date: 11/02/2021
Revision No. 4
Created by: Colleen Chau

7.1.1 Purpose:

To synthesize carboxybetaine monomer (2-Carboxy-N,N-dimethyl-N-(2′ (methacryloyloxy)ethyl) ethanaminium *inner salt)*

7.1.2 Materials

Chemicals

- 2 – (Dimethylamino)ethyl methacrylate (DMAEMA)
- Acrylic Acid
- Anhydrous acetone
- Methanol
- Acetone
- Triethylamine
- Nitrogen
- Ice
- Basic alumina

Equipment

- Glovebox
- Fume hood
- Mechanical Stirrer
- Ice container
- Vacuum desiccator/oven
- Pasteur pipettes
- 250 mL round bottom flask
- 100 ml cylinder
- 250 ml beaker
- Thermometer
- Büchner funnel
- Whatman Grade 42 filter paper, ashless
- Büchner flask
- Rubber tubing
- Vacuum pump

7.1.3 Method

1. Fill a 5 ml or larger syringe with basic alumina
2. Place a bottle underneath the syringe to capture the inhibitor removed acrylic acid
3. Using the pasteur pipette, add the acrylic acid to the alumina column until the desired amount is reached
4. Cool round bottom flask using an ice bath down to 0°C (4ºC is acceptable but yield will be lower).
5. Under an inert atmosphere place 15 ml (0.09 mol) of DMAEMA into the cooled flask
6. Move the flask to a fume hood and place flask back onto the ice bath an cool to 0°C.
7. Add dropwise, 13 ml (0.18 mol) of acrylic acid within 30 min
8. Carry out reaction for another 30 min at 0°C
9. Carry out reaction at room temperature for 4h. The reaction should gradually become more viscous
10. Dilute solution with 12 ml of ethanol and stir overnight
11. Dilute the solution with 23 ml Methanol, 67 ml acetone, and 23 ml TEA under stirring
12. Stir for another 30 min a white solid precipitate will form
13. Place the filter paper in the Büchner funnel and wet the paper with acetone.
14. Filter off the solid using vacuum filtration.
15. Wash with dry acetone
16. Dry under vacuum
17. Verify synthesis of molecule using NMR
18. Store in a tightly closed container (airtight if possible) in the refrigerator between 2 – 8 ºC.

7.1.4 Hazard Identification and Risk of Exposure to Hazards:

- See below for chemical safety tables

7.1.5 Exposure Controls specific to Above Risk of Exposure:

- Wear appropriate PPE (cotton lab coat and cotton clothing when working with acrylic acid)
- Use fume hood for volatile chemicals such as DMAEMA and acrylic acid
- Opening and closing of DMAEMA must be done under inert atmosphere – glovebox
- Keep monomers solvents away from heat and static charge

7.1.6 Biological Waste Disposal Methods:

- Dispose of waste liquids and solvent in appropriate solvent disposal container (flammeables)
- DMAEMA is harmful to aquatic life

7.1.7 Spill Response Procedures:

For monomer spills, evacuate people in the surrounding area, confine spill and dispose in the hazardous waste. For solution and solvent spills, wipe up with paper towels and dispose in hazardous waste. Clean with a lot of water and dispose in hazardous waste.

7.1.8 References:

Li, Yuting; Xue, Hong; Song, Y. (2014). *US 20140275614A1*. United States: United States Patent Office.

Shachat, Norman; Haggard, Richard A.; Lewis, S. N. (1972). *3689470*. United States: United States Patent Office.

Chemical Safety Table

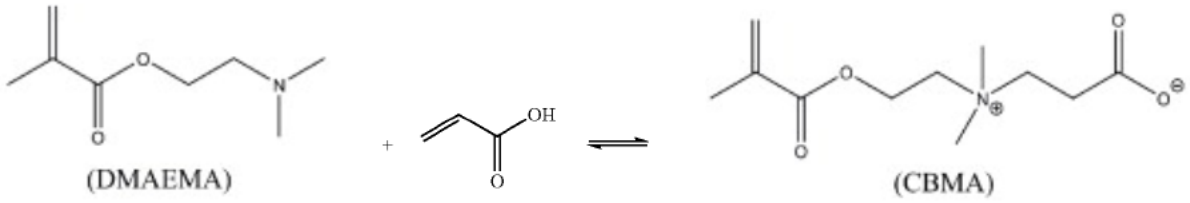

MW: 157. 21 g/mol MW: 72. 06 g/mol MW: 229.27

	EXPLOSIVE	FLAMMABLE	OXIDIZING	COMPRESSED GAS	CORROSIVE	TOXIC	CARCINOGENIC	ENVIRONMENTAL EFFECTS	INCOMPATIBILITY	STORAGE	SPECIAL PPE
2-(Dimethylamino) ethyl methacrylate					x	Oral Dermal Reproductive	x	x	Strong acids/bases Strong reducing/oxidizing agents	2 - 8 C. Moisture and light sensitive. Keep air tight, upright, and away from ignition	nitrile gloves (0.2 mm thickness) goggles/face shield fumehood
Acrylic Acid		x			x	Oral Inhalation Dermal Eye		x	Copper, nickel, mild steel, zinc	15 - 25C. Heat sensitive, decomposition in closed containers risk bursting	Nitrile gloves (0.4 mm thickness), >120 min breakthough time, fumehood
Anhydrous Ether		x				x					Fumehood

Acetone		x				x				Solvent Cabinet	Butyl Rubber Gloves, Fumehood
Methanol		x				Dermal/oral				Solvent Cabinet	Nitrile Rubber 0.4 mm thickness, 31 min breakthrough time, fumehood
Ethanol		x				Eye				Solvent Cabinet	
Triethylamine		x			x	X		x		keep container tightly closed	Nitrile Rubber 0.2 mm thickness, 49 min breakthrough time, fumehood

7.2 SI- ARGET – Carboxybetaine Modification of Planar Substrates

Date: 06/14/2018
Revision No. 3
Created by: Colleen Chau

7.2.1 Purpose:

To modify planar substrates with carboxybetaine

Chemicals

- (3-Trimethoxysilyl)propyl 2-bromo-2-methylpropionate
- Copper (II) bromide (99.0%)
- 2,2 – bipyridyl (bpy, >99%)
- L – ascorbic acid (> 99%)
- Ethanol
- Methanol
- MilliQ water
- Compressed air or N2

7.2.2 Equipment

- 3 Pyrex petri dishes
- Substrates
- Diamond tip silicon scribe
- Ruler
- Sonication bath
- Air or O2 plasma cleaner
- Stir bar
- Airtight, vial (reaction chamber)

7.2.3 Si Substrate Preparation

1. Clean glass petri dishes with alcohol under sonication and rinse with MilliQ water
2. Cut substrates into squares (7 mm x 7 mm) or in the case of PDMS, punch out 7 mm circles
3. Sonicate sequentially for 5 – 10 min each in acetone, isopropanol or ≥ 70% ethanol, MilliQ water
4. Dry over a nitrogen stream

7.2.4 Initiator Modification

1. Activate surfaces using O2 plasma at 50W, for 90 seconds
2. Make a 0.2 mM (3-Trimethoxysilyl) propyl 2-bromo-2-methylpropionate solution in ethanol (~6.58 mg or 5.3 ml in 100 ml).

3. Immediately immerse plasma activated surfaces into initiator solution and stir for 6h
4. Wash with ethanol 2x and water 1x
5. Place into well plates and cure for 15 min at 90C on top of hot plate.
6. Store in ethanol if not proceeding to next step right away

7.2.5 SI-ARGET-ARTP

1. In a glass vial, dissolve 0.046 mg of CuBr2, 0.193 mg of byp and 500 mg of CB monomer in MeOH and H2O (20:80 v/v) total volume = 3.2ml.
2. Add monomer solution into reaction chamber containing the silane-initiator surfaces
3. Dissolve 1.817 mg of ascorbic acid into 0.133 ml of MilliQ H2O
4. Add ascorbic acid solution into the reaction chamber
5. Seal reaction chamber and react for 3-5 h at room temperature
6. Wash surfaces with MeOH and water
7. Store surfaces in DI water

7.2.6 Hazard Identification and Risk of Exposure to Hazards:

- See below for chemical safety tables

7.2.7 Exposure Controls specific to Above Risk of Exposure:

- Wear appropriate PPE
- Use fume hood for volatile chemicals
- Keep solvents away from heat

7.2.8 Biological Waste Disposal Methods:

- Dispose of waste liquids and solvent in appropriate solvent disposal container
- Modified surfaces are disposed in biohazardous waste

7.2.9 Spill Response Procedures:

For monomer spills, evacuate people in the surrounding area, confine spill and dispose in the hazardous waste. For solution and solvent spills, wipe up with paper towels and dispose in biohazardous waste. Clean with a lot of water and dispose in biohazardous waste.

7.2.10 References:

Hong, D., Hung, H. C., Wu, K., Lin, X., Sun, F., Zhang, P., Jiang, S. (2017). Achieving Ultralow Fouling under Ambient Conditions via Surface-Initiated ARGET ATRP of Carboxybetaine. *ACS Applied Materials and Interfaces*, *9*(11), 9255–9259. https://doi.org/10.1021/acsami.7b01530

Zhang, Z., Chen, S., & Jiang, S. (2006). Dual-functional biomimetic materials: Nonfouling poly(carboxybetaine) with active functional groups for protein

immobilization. *Biomacromolecules*, *7*(12), 3311–3315. https://doi.org/10.1021/bm060750m

Li, Yuting; Xue, Hong; Song, Y. (2014). *US 20140275614A1*. United States: United States Patent Office.

Shachat, Norman; Haggard, Richard A.; Lewis, S. N. (1972). *3689470*. United States: United States Patent Office.

Chemical Safety Table

	EXPLOSIVE	FLAMMABLE	OXIDIZING	COMPRESSED GAS	CORROSIVE	TOXIC	CARCINOGENIC	ENVIRONMENTAL EFFECTS	INCOMPATIBILITY	STORAGE	SPECIAL PPE
Copper (II) Bromide, 99.999%					X	Oral/eye			Alkali metals	Avoid Moisture	Fumehood
2,2'-Bipyridine						skin/oral			Strong oxidizing agents		Fumehood
L - ascorbic acid									Strong oxidizing agents	Light Sensitive	
(3-trimethoxysilyl) propyl 2-bromo-2-methylpropionate					X	skin/eye			Oxidizing agents	Moisture sensitive	
Anhydrous Ether		x				x					Fumehood
Acetone		x				x				Solvent Cabinet	Butyl Rubber Gloves, Fumehood
Methanol		x				Dermal/oral				Solvent Cabinet	Nitrile Rubber 0.4 mm thickness, 31 min breakthrough time, fumehood
Ethanol		x				Eye				Solvent Cabinet	
Triethylamine		x			X	X		x		keep container tightly closed	Nitrile Rubber 0.2 mm thickness, 49 min breakthrough time, fumehood

(3-Aminopropyl) triethoxysilane		x			x	Dermal Oral, Eye			Strong oxidizing agents, Acids	Store in inert gas, Moisture sensitive	
Toluene		x			x	Dermal Reproductive CNS Inhalation Bladder/Liver/ kidney/Brain		x			Fluorinated Rubber 0.7 mm thickness, 480 min breakthrough time, Fumehood